OCS Study
MMS 91-0061

Numerical Modeling Studies of the Gulf of Mexico and the Caribbean Sea Using the Bryan-Cox Model

MMS
U.S. Department of the Interior
Minerals Management Service
Gulf of Mexico OCS Region

OCS Study
MMS 91-0061

Numerical Modeling Studies of the Gulf of Mexico and the Caribbean Sea Using the Bryan-Cox Model

Authors

W. Sturges
Florida State University

S. Welsh
Louisiana State University

Prepared under MMS Contract
14-12-0001-30363
by
Florida State University
Department of Oceanography
Tallahassee, Florida 32306-3048

Published by

U.S. Department of the Interior
Minerals Management Service
Gulf of Mexico OCS Region

New Orleans
December 1991

DISCLAIMER

This report was prepared under contract between the Minerals Management Service (MMS) and Florida State University. This report has been technically reviewed by the MMS and approved for publication. Approval does not signify that contents necessarily reflect the views and policies of the Service, nor does mention of trade names or commercial products constitute endorsement or recommendation for use. It is, however, exempt from review and compliance with MMS editorial standards.

REPORT AVAILABILITY

Extra copies of the report may be obtained from the Public Information Unit (MS 5034) at the following address:

U.S. Department of the Interior
Minerals Management Service
Gulf of Mexico OCS Regional Office
1201 Elmwood Park Boulevard
New Orleans, Louisiana 70123-2394

Attention: Public Information Unit (MS 5034)

Telephone Number: (504) 736-2519

CITATION

This study should be cited as:

Sturges, W. and S. Welsh. 1991. Numerical modeling studies of the Gulf of Mexico and the Caribbean Sea using the Bryan-Cox model. OCS Study/MMS 91-0061. U.S. Department of the Interior, Minerals Management Service, Gulf of Mexico OCS Regional Office, New Orleans, La. 77 pp.

ABSTRACT

A numerical model of the Gulf Stream formation region has been developed, based on the Bryan-Cox-Semtner, or "GFDL" primitive equation formulation. It is fully nonlinear with 12 levels and has realistic topography in each level. It includes the western north Atlantic from the mid-Atlantic ridge into the Caribbean Sea, the Gulf of Mexico, and the east coast of the United States to Cape Hatteras. A new feature of the model is the manner of forcing along the boundary. The vertical shear is set by the historical (observed) mean density field at the eastern boundary, and the total transport by the curl of the wind stress, extending previous work of Holland.

The model was initialized with the mean density field and is forced by mean winds. It was spun up for 4 model years at 1° resolution and for an additional 7 yr at 1/4° resolution during which minor adjustments were made in the model. The following 7 years of model runs are the basis of the work reported here, when the model appears to have reached statistical equilibrium, and the flow in the Straits of Florida is no longer increasing.

There are several interesting results. Although the model at this stage of its development is forced by constant mean winds, the outflow at the Straits of Florida and the inflow at the Straits of Yucatan have variability that is associated with the cycle of ring separations. Loop Current rings form with a mean time between separations of roughly 30 weeks, although some separation times were as long as 64 weeks.

We show in detail the separation of a typical anticyclonic ring. The most striking feature is that the separation is not a single catastrophic process but a long gradual one, considerably at variance with the "rope-like" conceptual model held by many oceanographers. The model flow has speeds that are less than those observed. Nevertheless, most of the features of the model currents are remarkably similar to recent observations.

At depths greater than approximately 1300 m, the flow is quite different from the upper circulation pattern. A rich field of deep motions is found. These appear to be weak vortex-like features, having horizontal scales smaller than the upper-layer warm core rings and speeds typical of topographic Rossby waves. They travel to the west essentially in company with the upper warm core rings, but move about relative to the rings and travel slightly faster.

We find that in the deepest part of Yucatan Channel the flow is sometimes to the north, but usually to the south. A very suggestive feature of the flow there is that the deep southerly currents appear to be driven directly by a southerly-flowing portion of the Loop Current. When the Loop Current penetrates farther to the north and northeast, the southerly portion of the intense surface layer current is no longer over the deepest parts of Yucatan Channel, and no deep flow is forced. Observations to document this behavior appear consistent with it but are not adequate to confirm the idea unambiguously.

The modelled flow in the Florida Current is too weak, and this is attributed to lack of sufficiently energetic boundary forcing as well as from the use of steady winds; these deficiencies are being addressed in a newer implementation of the model.

TABLE OF CONTENTS

LIST OF FIGURES

LIST OF TABLES

LIST OF ACRONYMS AND ABBREVIATIONS

The following acronyms and abbreviations may be used throughout this Report:

COTR	Contracting Officer's Technical Representative
FSU	Florida State University
GFDL	Geophysical Fluid Dynamics Laboratory
I-R	Infra-red
MMS	Minerals Management Service
NCAR	National Center for Atmospheric Research
NOAA	National Oceanic and Atmospheric Administration
SAIC	Science Applications International Corporation
SCRI	Supercomputer Computations Research Institute
Sv	Sverdrup, = 10^6 m^3/s
TRW	Topographic Rossby Wave

ACKNOWLEDGEMENTS

This work has been a cooperative venture that has depended heavily on the efforts of J.C. Evans, Univ. of South Carolina, Columbia, and W.R. Holland, NCAR, Boulder, Colorado. The program was begun with help from the Visitors Program of the Supercomputer Computations Research Institute at FSU. The FSU and SCRI have generously provided matching computer time on the Cyber 205, the ETA 10, and the Cray Y-MP. The MMS has provided support through this contract, without which this program would not have gone forward, and for which we are most grateful. We thank our colleague W. Dewar of FSU who has provided many helpful discussions; we thank E. Waddell and P. Hamilton of SAIC Raleigh, N.C., for many things, including providing tapes of current meter data. We thank Dana Thompson and Harley Hurlburt for providing candid and helpful comments at several stages of this work. We note with great sadness the death of Mike Cox, who was generous with suggestions and friendly advice. We thank Pat Klein for her skill in preparing and revising manuscripts, and Paula Tammadoni-Jahromi for preparation of many figures. We also wish to acknowledge support of NSF OCE 8416458. And, finally, we wish to acknowledge the helpfulness, competence, and general good humor of our COTR, Dr. Murray Brown.

I. INTRODUCTION AND GENERAL MODEL DESCRIPTION

When oceanographers discuss numerical modelling of the Gulf of Mexico, the remarkably successful work of Hurlburt and Thompson (e.g., Hurlburt and Thompson 1980, 1982 and later) is the point of reference. Their two-layer model, and others that have been based on it, are numerically very efficient and physically effective. It was our desire to construct a "next-step" numerical model capable of coupling the deep water circulation to the currents on the continental shelf, that had improved vertical resolution, and that coupled the Gulf to the flow in the Gulf Stream system. A model that allows these features is the so-called Bryan-Cox-Semtner GFDL model (Bryan and Cox, 1968; Cox, 1970, 1975, 1984, 1987). For a comprehensive summary, the reader is referred to the review by Evans *et al.* (1987). A general description of the development of the model is given in papers by Semtner, (1986a, 1986b).

The numerical model we have chosen is in use by many other investigators; it is an established model and its abilities and shortcomings are well known. The use of this model provides the improved vertical resolution and the coupling with the open Atlantic that we sought, but at significantly higher cost in computer resources than for previous models. The model is based on the primitive equations with thermodynamics and has topography and realistic geometry. The implementation of the eastern boundary forcing is new. It is an extension of the technique of pumps and baffles used earlier in a quasi-geostrophic model by W. Holland. (This technique is discussed later.)

The discussion in this report will center on the Gulf of Mexico, because of MMS interests, whereas our purpose was to model the whole region. It seems worthwhile to point out, however, that a fully reliable numerical model of the Gulf of Mexico may require the rest of the region we have included, at a minimum, to be modelled. In order not to over-constrain the Loop Current, the inflow at Yucatan and the outflow through the Straits of Florida must be modeled carefully. This point will be discussed later. The choice of where to place the boundaries is not trivial. Our choice was based on economic considerations, such as model run time. An increase in model domain of approximately 25% would allow inclusion of the full east coast of the U.S., but this was not one of our primary objectives. The model was implemented at FSU by a collaborative effort between the authors, together with Dr. William Holland (NCAR), and Dr. J.C. Evans (U. South Carolina). It was initially implemented on the Cyber 205 then at FSU. It has been run on the ETA-10 and the Cray Y-MP at FSU, on the Cray at NCAR, and on other platforms.

The original objective of this study was to develop a high resolution numerical model of the Gulf of Mexico, the Caribbean Sea, the adjacent Atlantic Ocean — the Gulf Stream formation region — with detailed geometry and substantially better vertical resolution than previous models. We believe use of this model at high resolution allows us to gain a better understanding of the mechanisms of a variety of circulation problems.

Initially the model has been forced with the Hellerman and Rosenstein (1983) mean winds. The density field was initialized with time-averaged temperature and salinity (the so-called Levitus data) to minimize spin-up time. There are plans for later implementation to add time-varying winds and to increase the horizontal resolution.

The model described here is presently being run by Prof. J.C. Evans and his co-workers at the University of South Carolina, on a variety of computing platforms. His implementation has been modified from the one described in this report to include a significant amount of additional inflow ($6 \times 10^6 m^3/s$) at the southern part of the eastern boundary. The existence of that component of the flow was unknown to us when we began this program (e.g., see Schmitz and Richardson, 1991). The addition of that extra flow adds significantly to the model velocities.

The velocities observed in the model results reported here are somewhat less than observed (as described in detail in a later section). We suspected initially that this deficiency was caused mainly by the forcing by constant mean winds rather than by the more energetic time-dependent wind field. In the more recent runs, Evans (pers. comm.) has found that using time-dependent winds has also increased the model velocities.

It is also very likely that higher numerical model resolution would be an improvement. Decreasing the grid size from 1/4° to 1/8° would allow use of smaller horizontal eddy friction. Use of a 1/4° grid means that there are approximately 14 grid points across an anticyclonic eddy 350 km in diameter, which is generally believed to be adequate. In the narrow passages, however, such as the Straits of Yucatan or the Straits of Florida, this resolution becomes much less than we would prefer. Increasing resolution by a factor of 2 requires an increase in computer runtime by a factor of 8, and the availability of computer time was our limiting resource.

Semtner and Chervin (1988) have had success using coarser grid resolution for a savings of computer time, but were forced to use higher-order horizontal eddy viscosity. By contrast, Hurlburt and Thompson (pers. comm.) are using models that have finer grid resolution by a factor of three than we have used here; they (and others) find that the use of higher resolution improves model results. The decision of our group was to use the simplest form of eddy viscosity so as not to add additional physical uncertainty to the model. The controversy is not over what is best, but what is economically feasible, and it continues. Our primary (initial) choice was to make the grid resolution 1/4°; the size of the available core storage in the Cyber 205 then placed constraints on the total domain size. The resolution places some constraints, of course, on the magnitude of horizontal eddy viscosity, as discussed in detail later.

The model was first run on a relatively coarse grid (1°) for a four-year spin-up. The resolution was then increased to 1/4° for an additional 7 years of initialization and model tuning. We experimented with small variations in the magnitude of horizontal eddy viscosity, to achieve the minimum friction consistent with reliable operation. We have tended to make conservative choices; a slightly higher viscosity seemed an acceptable trade-off in exchange for improved numerical stability. At the end of the 6th year of 1/4° runs, the widths of the important narrow channels (Yucatan, Straits of Florida, etc.) were widened slightly. This was a correction to the original topography made necessary by the details of the way the velocity calculations are performed in the model. We report here the results of the full program, but our main results are based on the final 7 model years. Thus we have run the model for four years at 1° resolution and 14 years at 1/4° resolution. The times shown in each figure (e.g., week 362) are counted after the first 11 years of model spinup. The flow appears to have come into statistical equilibrium as evidenced by the fact that the transport

through the Straits of Florida (shown later) has been stable for the last part of the runs described here. Although many of the results seem to be quite realistic, it is not at all certain that the statistical properties of the flow will not change. It was our original expectation that ~25 years of model time would be required for equilibrium. The model spin-up is thus essentially completed in the upper part of the flow. The deeper layers may take longer to reach equilibrium, and modeling experience does not offer clear and unambiguous guidelines.

Figure 1 shows the area included in the model, by showing the streamfunction (the total vertically integrated transport) at two times in the model's later output.

The method used here has artificial solid boundaries at the northern and eastern walls, resulting in unrealistic flows in those regions. A 6° (~650 km) wide buffer region is used at the eastern wall, using a modification of Holland's technique of pumps and baffles. The vertical shear there is set by the computed mean geostrophic shear using the Levitus data (Levitus, S., 1982). The magnitude of the total flow in the eastern buffer is set by integrating the curl of the wind stress (Hellerman and Rosenstein, 1983) over the Atlantic Ocean from the African coast to the boundary of the model. This flow is forced out of the buffer region, west of the mid-Atlantic ridge.

The flow along the east coast of the United States approaches Cape Hatteras, where in the model it meets the artificial boundary at 36° N. In the initial stages of setting up the model there was some concern whether perhaps special care might be needed along the northern wall to insure that the flow would return gracefully into the buffer region along the eastern edge. As it developed, the flow goes in a seemingly reasonable way from Cape Hatteras into the buffer region; nothing extra was needed. A higher horizontal viscosity is used in the region east of the Antilles, ramping up smoothly to the buffer region. However, the model is forced by observed mean wind stress and the input conditions of observed mean ocean density field; nothing is arbitrarily added to enhance the apparent plausibility of the results; our intent was to keep the physics as clean as possible.

During the initial phases of the work it was understood that the model would be forced by steady winds. Nevertheless, an important basic question must be addressed in regard to sampling the currents in the model. We need to determine what frequency bands are likely to have energetic currents in the model, in order to sample them adequately.

It is well known that near-shore coastal currents are driven largely by coastal winds. Coastal oceanographers refer to a range of periods of about 4 to 10 days as "wind-driven". However, it is known (e.g. SAIC, 1986) that there is a substantial amount of wind energy at periods as long as 40 days. Thus while a model driven by steady winds might not be expected to produce currents in the 4 to 10 day band, we should recognize *a priori* that there may be energy at periods of approximately several weeks in which the primary forcing could be wind-generated, could arise from inherent instabilities in the flow, or could be a manifestation of topographic Rossby waves. Therefore we examined the data from the long records on the west Florida shelf taken in the MMS program (SAIC, 1986).

From these studies we concluded that the highest important periods to resolve in sampling the numerical model are at periods of roughly two to three weeks. On this basis, we concluded that (for the model forced by steady winds) a weekly

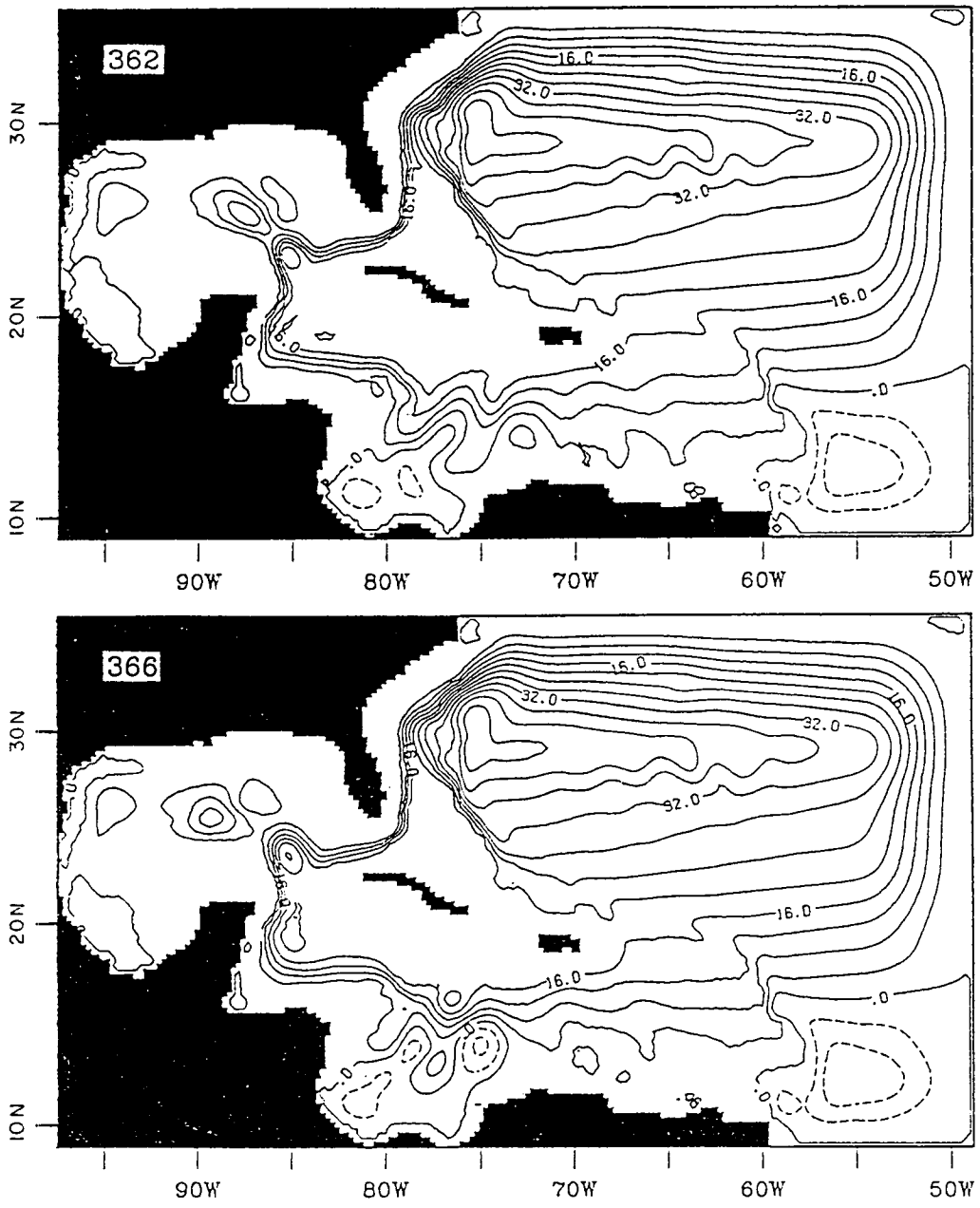

Figure 1. Streamfunction maps of the whole domain of the model. The times shown (*e.g.*, 362) are in weeks since an 11-yr spin-up (see text). During this interval no adjustments were made in the model. The (vertically integrated) transport values are in Sverdrups (10^6 m^3/sec). The model has solid boundaries at the northern and eastern walls so the flows there are completely unrealistic.

sampling of the model results would provide a data set not significantly aliased by higher-frequency motions. To be safe, therefore, we have generally sampled the model once every 2 days; at a few selected regions we sampled daily for limited test periods. Results obtained more recently (e.g., Hamilton, 1990) have shown that the most energetic motions in the deep water at shorter periods are likely to be topographic Rossby waves having periods of ~30 days, which is consistent with our early choice.

It should be clear that any numerical modeling work in the Gulf of Mexico will be compared with the work of Hurlburt and Thompson. We have tried here to avoid any unnecessary comparisons with their work, however. This is because such comparisons, to be quantitatively meaningful, require a great deal of additional effort (which we believe would not be fruitful), but moreso because we have intended to concentrate on those aspects of the work in which comparisons would be ambiguous at best. There are three major ways in which this modeling work differs from theirs. First, we decided not to specify the vertical distribution of velocity near the Straits of Yucatan. Second, the model contains twelve levels of density stratification rather than two, to permit greater vertical resolution. And third, the geographic domain of the model is roughly five times the size of theirs. Thus the major differences in our results lie in areas in which the two models are not meaningfully comparable.

II. STREAMFUNCTION MAPS

Figure 1 shows a pair of streamfunction maps; this quantity is for some purposes similar to maps of velocity vectors in the upper layer flow. Because the streamfunction is a scalar quantity, it is often easier to interpret than vector plots. The transport is parallel to the streamfunction contours; the magnitude of the net transport at any location is the difference between the contour values at two adjacent points. One must remember, however, that the streamfunction maps represent the full vertical integral of the flow. In regions of strong flow, such as in the Straits of Yucatan, or the Straits of Florida, where the flow is largely unidirectional, there is no problem with the interpretation. Where the flow is weak, and particularly where the deep flow runs counter to the surface flow, one must keep in mind that the streamfunction maps are not equivalent to maps of horizontal velocity at a selected depth. Later in this report, such maps will be used to describe the flow and show the differences between the flow in the upper versus deeper levels.

As can be seen in Figure 1, the flow through the Straits of Yucatan extends into the Gulf of Mexico forming a large loop (hence, the name "Loop Current") before the flow leaves to become the Gulf Stream. A Loop-Current ring has formed and appears to be ready to separate at week 362. By week 366, in the lower part of the figure, the ring appears to have separated completely. The streamfunction contours in the Atlantic show numerical values in Sverdrups (Sv = $10^6 m^3/s$); the maximum value is ~44 Sv off the coast of the Carolinas. This is approximately 85% of the value observed in nature, and much more than is forced by the buffer region at the eastern boundary.

In the central Gulf of Mexico, Figure 1b shows an anticyclonic ring that is drifting to the west. The discussion of the behavior of rings during and after they have separated from the Loop Current is included in Chapter IV.

In the southern Caribbean Sea, large wave-like or eddy-like features are seen in the strong flow through the Caribbean. While this flow is not documented so well as the Loop Current motions, these eddy-like motions are consistent with observations; e.g., see Molinari et al. (1981). These maps (Figure 1) are instantaneous "snapshots" produced 4 weeks apart. There is no averaging involved. A series of maps is included in Appendix A, and these also are spaced 4 weeks apart. The set of maps in the appendix is included to show the rich amount of detail contained in the model's flow and to document its initial progress.

One interesting and important characteristic of a model such as this is its spin-up behavior. Figure 2 shows the transport through the Straits of Florida during the initial few years of model runs; the transport doubles (from 9 Sv to 18 Sv) in ~140 weeks.

By examining the entire set of output, one can see when model rings separate from the Loop Current as a time series. The times (in these "data") for the formation of rings is typically 25-35 weeks. The ring was identified as having separated if the streamfunction lines were closed entirely around the ring. The separation of a ring is described in detail in a later section.

A striking feature is the wide variability of the time between ring separations. Many of these events occur at delays of ~30 weeks, yet the delay has been as long as 64 weeks — roughly twice the usual period. It should be abundantly clear that the

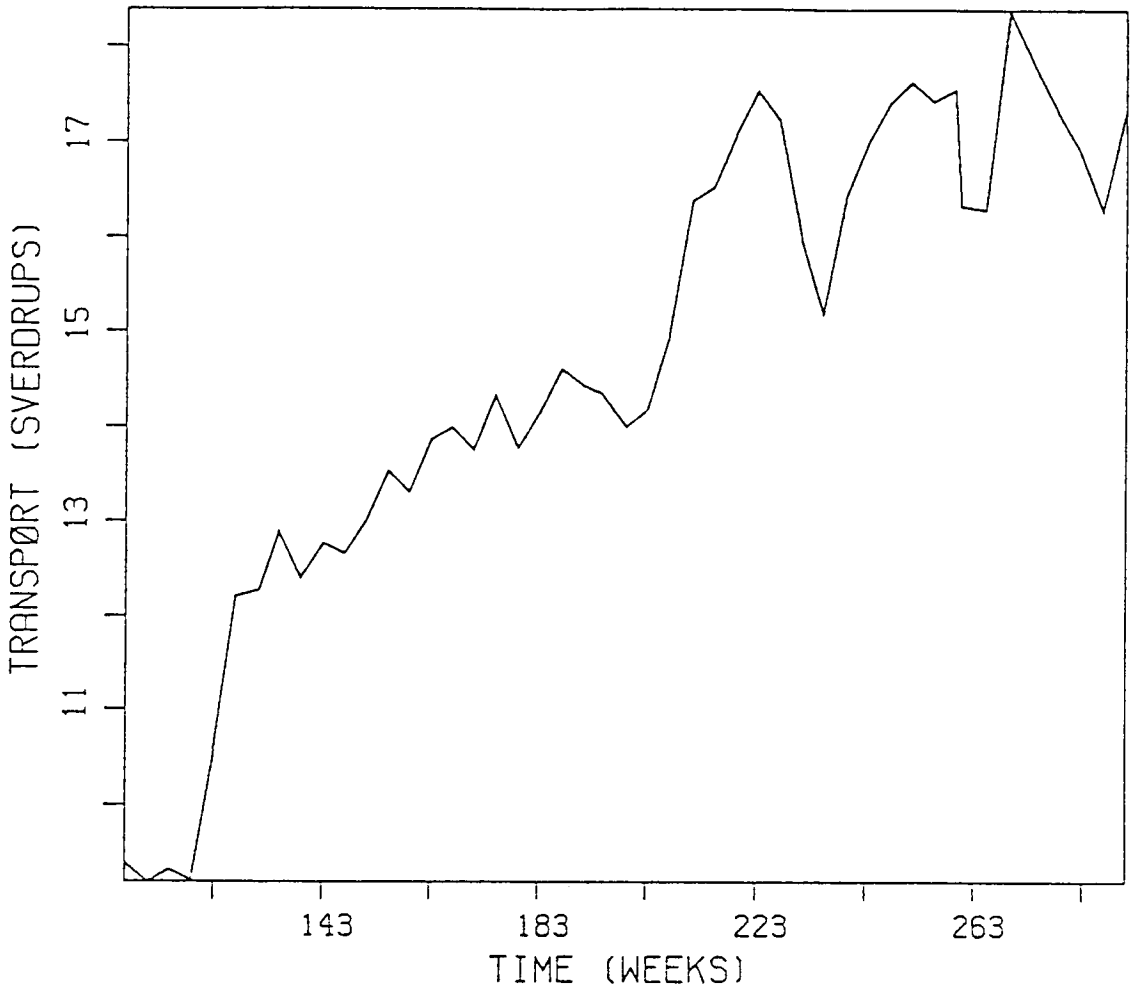

Figure 2. Transport through the Straits of Florida during the initial model spin-up. Times shown here begin after the initial 4-year coarse resolution spin-up. During this interval adjustments were made in the model, so this time scale is intentionally left separate from time values shown in the other figures.

periodicities in the model are determined by the internal dynamics of the flow — not by the wind forcing, which is steady. This result is consistent with that of Hurlburt and Thompson who were able to model relatively realistic mean ring separation times with steady forcing.

III. STRUCTURE OF THE MODEL

The model has 12 discrete horizontal levels, as sketched in Figure 3. The specific depths are listed in Table 1. In a later section of this report, model output velocities will be shown at various levels. For the most part Level 3 will be used to describe the near-surface flows. Level 9, whose center is near 1300 m, will usually be typical of the deeper flow.

Level 6 is the deepest one that is continuous through the Straits of Florida past Miami. Level 10 is the deepest one that is continuous through the Straits of Yucatan.

The operating manual for the model contains a list of variables; it extends to 10 pages, single spaced. It does not seem appropriate to include that list here, but the parameters which seem most relevant are: coefficient of horizontal mixing for momentum, 5×10^6 cgs; for temperature, 3×10^6 cgs; for vertical mixing of momentum, 1 cgs; time step, 30 minutes; grid resolution, 0.25 degrees. there is no explicit bottom friction in this implementation.

Table 1

Depths of Levels in Model (meters)

Level	Box Height	Depth at middle	Depth at bottom
1	40	20	40
2	40	60	80
3	100	130	180
4	160	260	340
5	160	420	500
6	160	580	660
7	160	740	820
8	300	970	1120
9	350	1295	1470
10	350	1645	1820
11	900	2270	2720
12	900	3170	3620

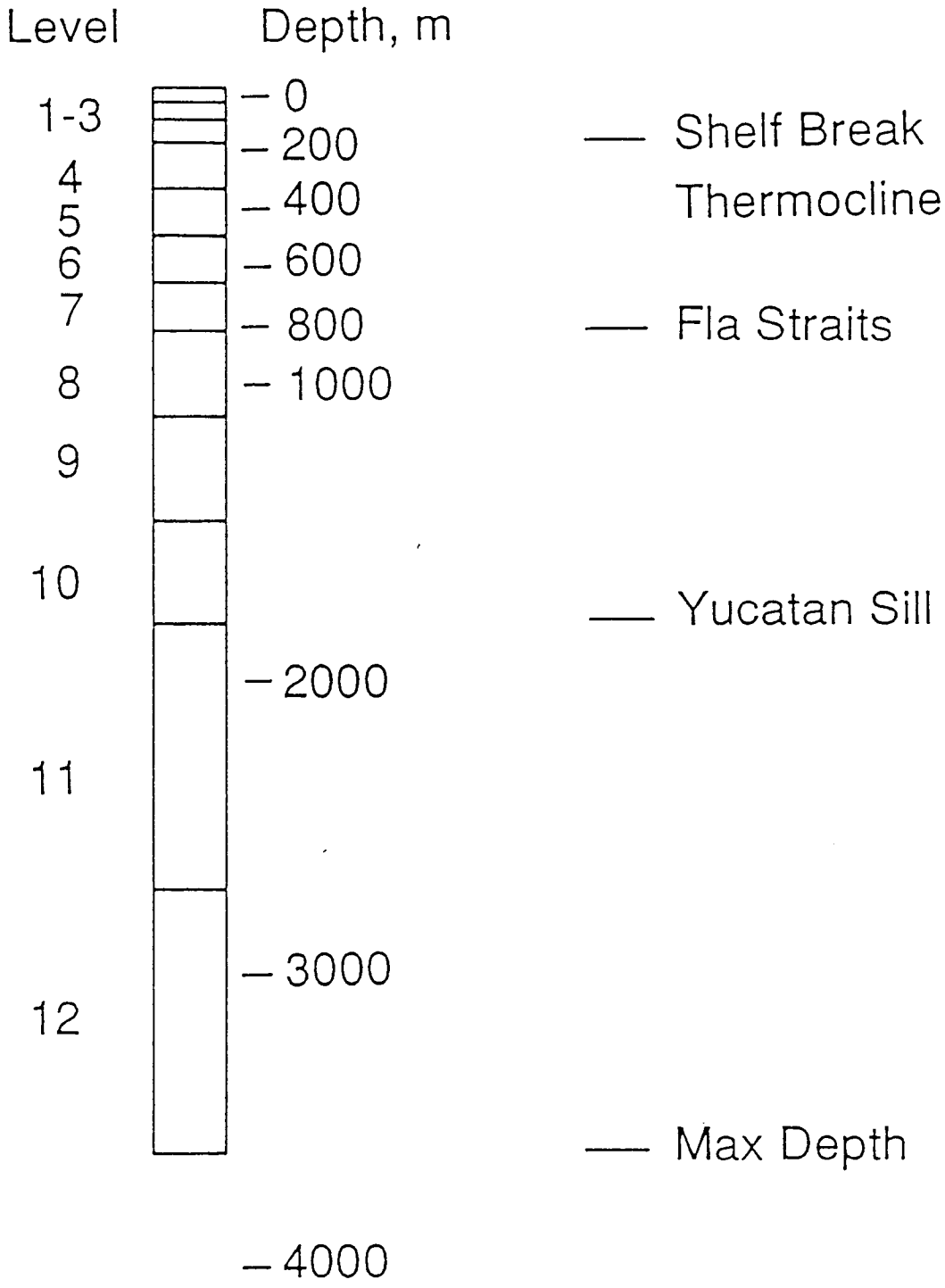

Figure 3. A diagram of the depths and thicknesses of the levels in the model, also showing the major topographic features.

IV. THE MECHANISM OF SEPARATION OF ANTICYCLONIC RINGS

When we think about a complex physical process, it is often helpful to form a simple conceptual model. During the late 1960's a conceptual model of the separation of Gulf Stream rings came to be known as "Fuglister's Rope." Figure 4 (from Richardson, 1980) shows the basic idea. There was a widely held belief that the process of ring separation was an abrupt, energetic, perhaps even spectacular, event (e.g., Csanady, 1979; Fofonoff, 1981).

This separation process has been called the oceanographic equivalent of a "big bang." The reason that this rope-like model has remained influential, of course, is that it is a good representation of some parts of what is observed. Figure 5 shows a pair of diagrams made from I-R data from the Gulf of Mexico. In the bottom panel of Figure 5 the ring has nearly completed the "necking-down" process that is so essential to ring formation (e.g., Pratt & Stern, 1986).

We are naturally curious about what the kinematic steps are in order for a ring that appears not yet to have separated, as in Figure 5 (26 Apr), to be transformed into an apparently detached ring only a few weeks later; *i.e.*, how is it that "the rope is cut?" Or, perhaps, is this analogy misleading in some respects? Therefore this section has two major purposes. The first is to present in detail maps of our model's velocity field during the time of ring formation and separation. It should be clear that this model does not duplicate the ocean to extremely high accuracy; we assume that the reader is aware of such limitations. However, the results of this model, as represented by the horizontal flow field, are so different from a rope-like model as to deserve emphasis. These results form the basis for a different conceptual view.

The second major point of this section is to present a description of deep circulation patterns associated with seemingly "isolated" upper-layer warm core rings. Many studies have suggested that upper-layer warm core rings do not travel "in isolation." Because of the enormous observational problems, we do not have clear pictures of the deep velocity patterns associated with upper-layer ring studies in the ocean. We find in the model that each large warm core ring has associated with it a characteristic family of deep motions.

The model velocities shown here are not as vigorous as observed in the ocean, so the flow induced in the deeper layers is also too weak; for the present purposes we do not consider this a crucial issue. We suggest that the rich field of deep velocities associated with the upper layer rings is an important part of the flow associated with rings. Because this flow is so much more difficult to observe than, for example, the upper-layer I-R maps of ring motion, these initial results may provide insights into the processes by which rings separate. Because the model has not yet been made as realistic as is possible, it does not seem appropriate to make extensive comparisons between model results and observations; nevertheless, we will make a few comparisons to show that in some ways the results shown here are consistent with observations.

We have made the assumption that the fundamental processes that govern the way a ring separates from the main flow are only weakly dependent on the local flow parameters. Thus, learning about the separation of an anticyclonic ring in the Gulf of

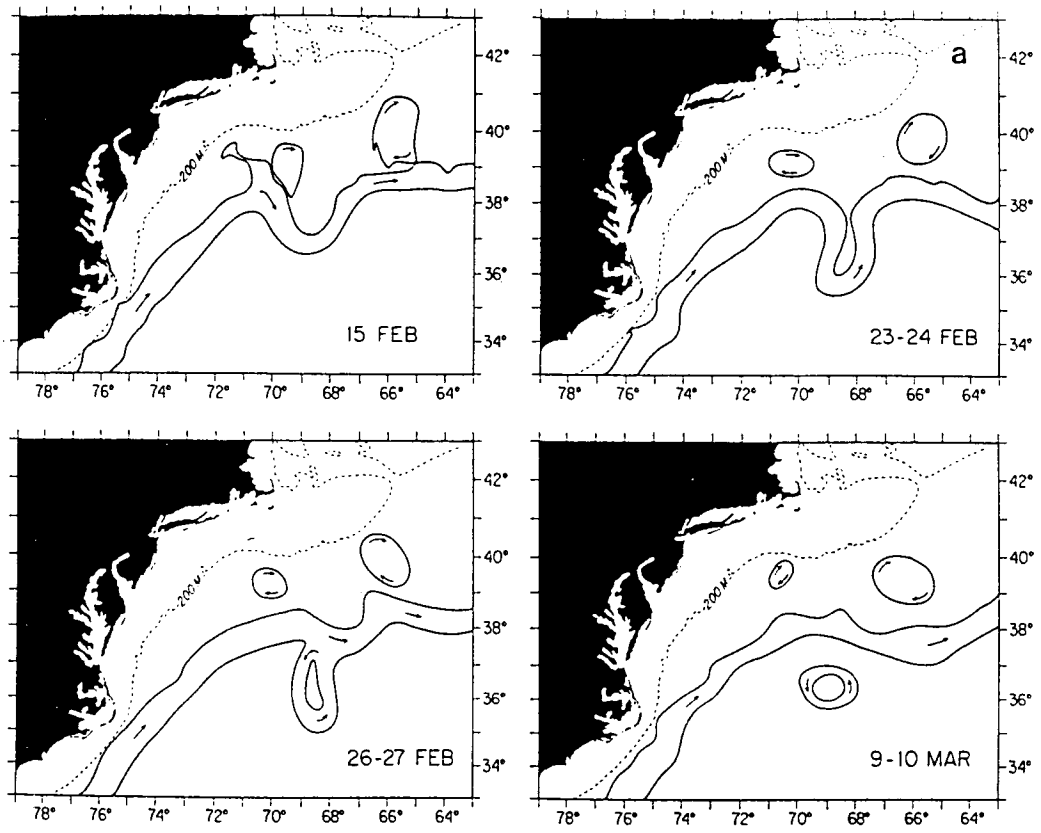

Figure 4. A schematic of the flow field during the formation of a ring. Adapted with permission from Richardson (1980, his Figure 1a).

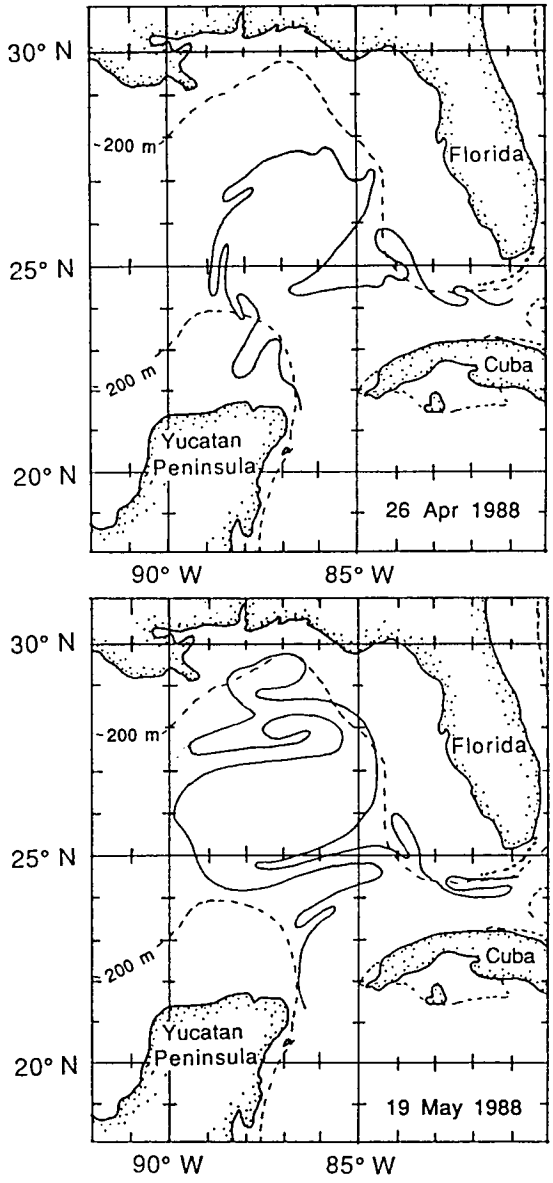

Figure 5. A sequence of paths of the Loop Current from NOAA maps of satellite IR imagery. Many details have been omitted in order to emphasize the transition from a large meander to an anticyclonic ring.

Mexico should be instructive about separations from the Kuroshio or in the Gulf Stream. We refer the reader to the impressive regime diagram of Hurlburt and Thompson (1982) which serves as an example for numerical work, particularly as it relates to models of the Gulf of Mexico. Analytical studies of instability mechanisms (e.g., Killworth *et al.*, 1984, Pratt and Stern, 1986) are suggestive and are presumably applicable to the flow here in the Loop Current. Although the flow field in the Gulf of Mexico is similar to that farther downsteam, there are important differences. The direction of the flows into and out of the Gulf of Mexico are strongly constrained by topography. Auer (1987) has shown that the diameters of warm core rings in the Gulf of Mexico tend to be larger than in the Gulf Stream past Cape Hatteras. In the 200-400 km sizes there is a great deal of similarity, and the life spans are similar, but Auer found no warm core rings in the Gulf of Mexico with initial diameters under 150 km. More recently, smaller diameter rings have been observed in the Gulf of Mexico (J. Hawkins, *pers. comm*). Auer reported (his table 4) that the normalized surface diameter decay rates were identical in the comparison of warm core rings from the Gulf Stream and from the Loop Current. Kraus et al. (1990) have shown that there is a general tendency for eddy scales to decrease toward higher latitudes, in keeping with the tendency for the internal radius of deformation to decrease. Whether the constraints on inflow and outflow direction are relevant to the existence of larger rings in the Gulf of Mexico is a topic for later explorations. The large diameter is fortunate, however, from a modeling point of view. The grid spacing in the runs discussed below is 1/4°, which clearly gives better resolution in a 350 km ring than in a 150 km one.

Observational studies on rings in the Gulf have been discussed by Elliott (1982), Maul (1977), Vukovich and Crissman (1986) and many others. The observations of ring separation reported by Lewis and Kirwan (1987) are perhaps the most relevant, and their results seem quite consistent with our model results. The work of Hamilton (1990) is the most comprehensive analysis of deep velocity observations in the Gulf of Mexico of which we are aware, and it, too, is nicely consistent with our findings. The process of ring separation has been studied by, e.g., Ikeda and Apel (1981), by Pratt and Stern (1986), and others.

In a later chapter, we will make more detailed comparisons between observations at moorings and simulated moorings in the model. One of the shortcomings of the model results shown here is the velocities are somewhat too low. A typical peak velocity in the model is ~145 cm/s, or less than 3 knots in the upper level, in the high velocity region just to the east of the Yucatan Peninsula, and ~100 cm/s in the free flow in the Loop Current to the north. Observed velocities, however, are sometimes found to be as much as 50% greater. The flow fields shown here as representative of the upper layers are in the third level (80 - 180m), where the velocity is somewhat less than at the sea surface. Lewis and Kirwan (1987) observed no ring swirl velocities larger than ~85 cm/s, and found that they were rarely above 75 cm/s. Because the swirl velocities in our results tend to be below 70 cm/s, we believe that our model velocities are too low.

A vertical cross section of the instantaneous model velocity in the Straits of Yucatan resembles, generally, any one of the observed sections in the Florida Current (e.g., Schott *et al.*, 1988) or in the Straits of Yucatan (Maul *et al.*, 1985). The maximum speeds are concentrated toward the western side, the speeds decay to very small values

near the bottom, and there is often flow to the south near the bottom. Because the forcing of the model is not yet fully developed, it does not seem appropriate to describe these features in detail. For completeness, however, a vertical cross section of the model velocities at week 370 is included in Appendix C.

As mentioned earlier, in the runs with steady forcing, the rings have separated from the Loop Current at a rate that is, typically ~30 weeks. Sturges (1991) has found in the spectrum of Loop Current variability a primary peak near 8.5 months (37 weeks), which is attributed to the basic ring-shedding cycle, in the absence of other forcing variability such as the annual cycles of most oceanographic variables. It seems to us that the rate at which rings are shed is one of the fundamental observables of the system. The approximate agreement between the ring shedding cycle in the model and the ocean, with no arbitrary tuning to accomplish it, is a most encouraging result.

A Ring Separation Cycle

Figure 6 shows a map of horizontal velocities at level 3 in a limited region of the model. (The bottom of level 3 is at the edge of the continental shelf.) We see the flow into the Gulf of Mexico and out again between Cuba and the southern tip of Florida. Just north of the Yucatan Peninsula a large anticyclonic ring has formed but is still attached to the main flow.

Three features seem important here. First, a substantial part of the inflow on the western side of the Yucatan Channel continues to flow to the north around the anticyclonic ring. Much of the flow out of the Gulf of Mexico seems to be involved in the flow along the eastern edge of the nascent ring. Second, although the ring has not yet separated from the Loop Current, there is a significant amount of recirculation in the interior of the anticyclone.

The third interesting feature of Figure 6, related to the idea just discussed, is that in the southern part of the Loop Current between the Yucatan Peninsula and Cuba, at a latitude of ~23°N, a significant amount of recirculation is already taking place, even while the large anticyclone to the north is still attached. This feature is consistent with inferences from hydrographic data. Nowlin (1972) shows that the dynamic height inside the Loop Current (e.g. his Figs. 1-29, p. 37) is significantly greater than one would expect based on the external flow field alone; see also Molinari *et al.* (1977). Even more importantly, direct observations of the surface flow by drifters (Lewis and Kirwan 1987) seem to support each of these three aspects of the results. Their discussion of the separation cycle (e.g., p. 11,736) clearly anticipates (and supports) the model results presented here.

In the lower right hand part of Figure 6 the outflow from the Caribbean Sea approaching Yucatan Straits is surprisingly concentrated in a westward flow. Comparing this with Figure 1, however, we see that this flow is not constrained by a model boundary but is well within the interior of the model. This flow seems to be consistent with the deep topography and follows the approximately ~2400 m contour, as will be discussed later.

We have chosen Figure 6 as the starting point for our description of a ring shedding cycle, but this starting time is arbitrary. Figures 7A-D show the long gradual process by which the ring moves away. Over roughly the next 20 weeks we see the

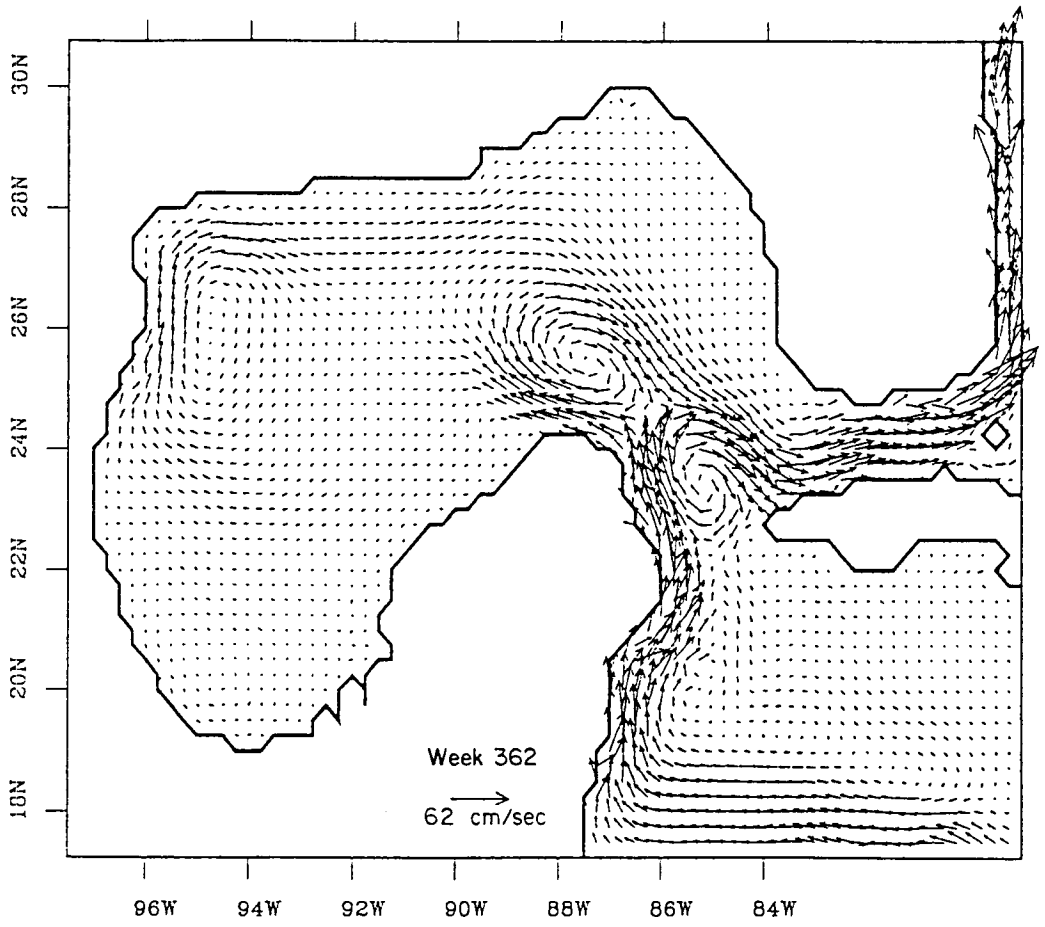

Figure 6. A snapshot of the flow in level 3 (80-180 m depth), which is typical of the upper levels of the model. (Note that the southern and eastern boundaries of the figure are not the boundaries of the model.) Week 362 is measured from an initial 11-year spin-up. The outline of the bottom topography shown is the 180 m contour.

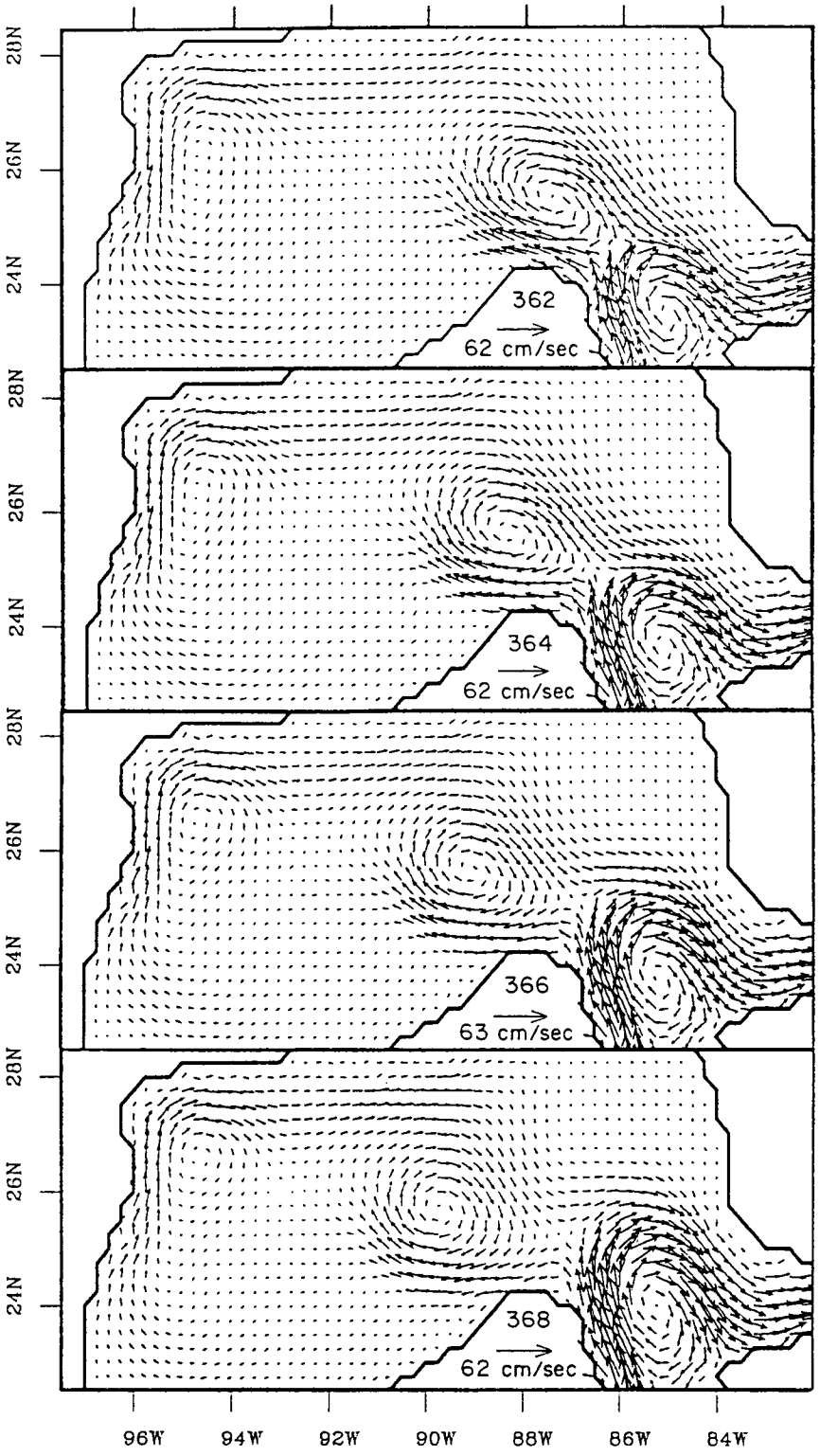

Figure 7A. A sequence of snapshots of the flow in level 3 (as in Figure 6) every 2 weeks, showing the motion of the anticyclonic ring as it drifts to the west, (continued).

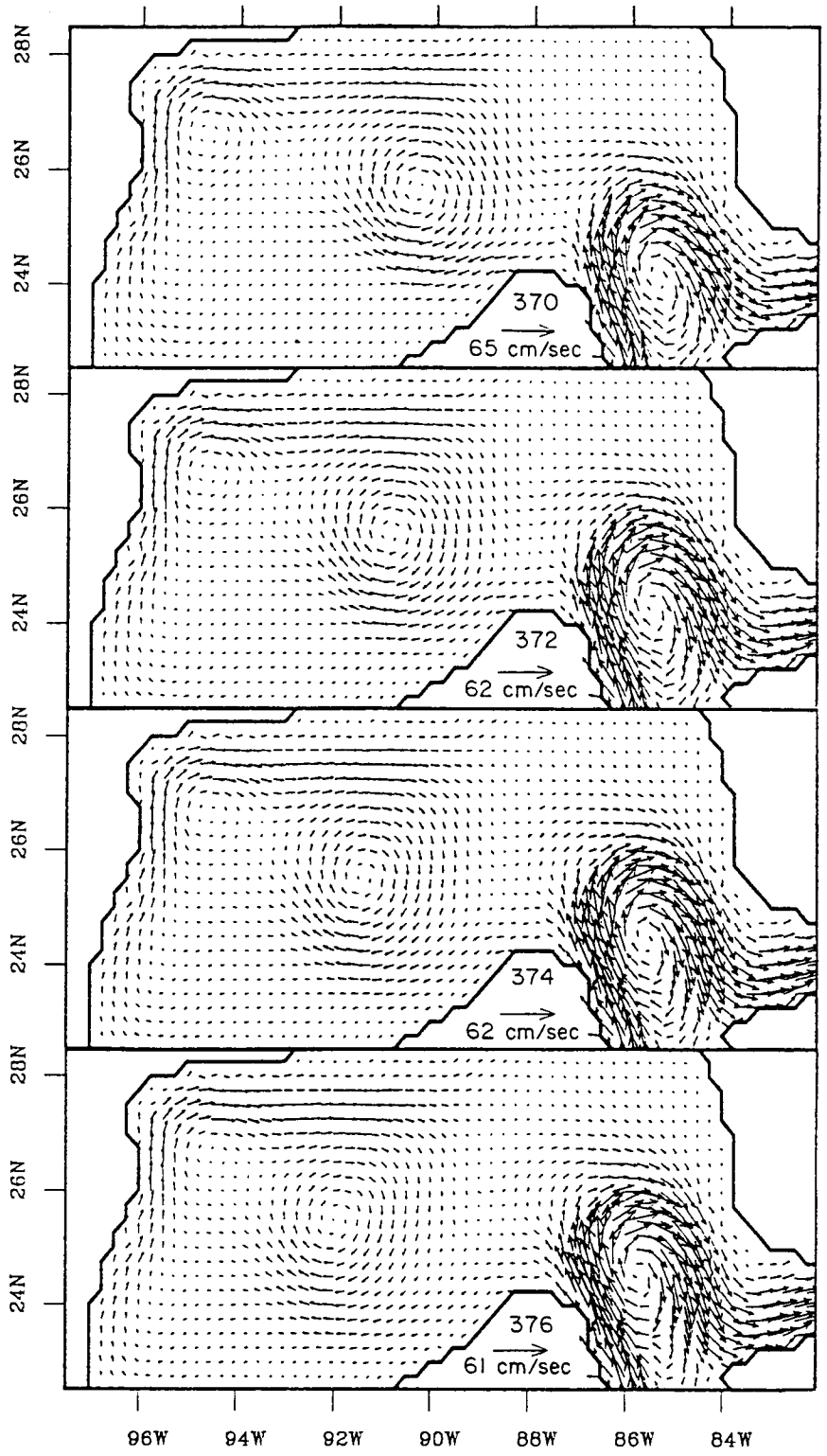

Figure 7B. A sequence of snapshots of the flow in level 3 (as in Figure 6) every 2 weeks, showing the motion of the anticyclonic ring as it drifts to the west, (continued).

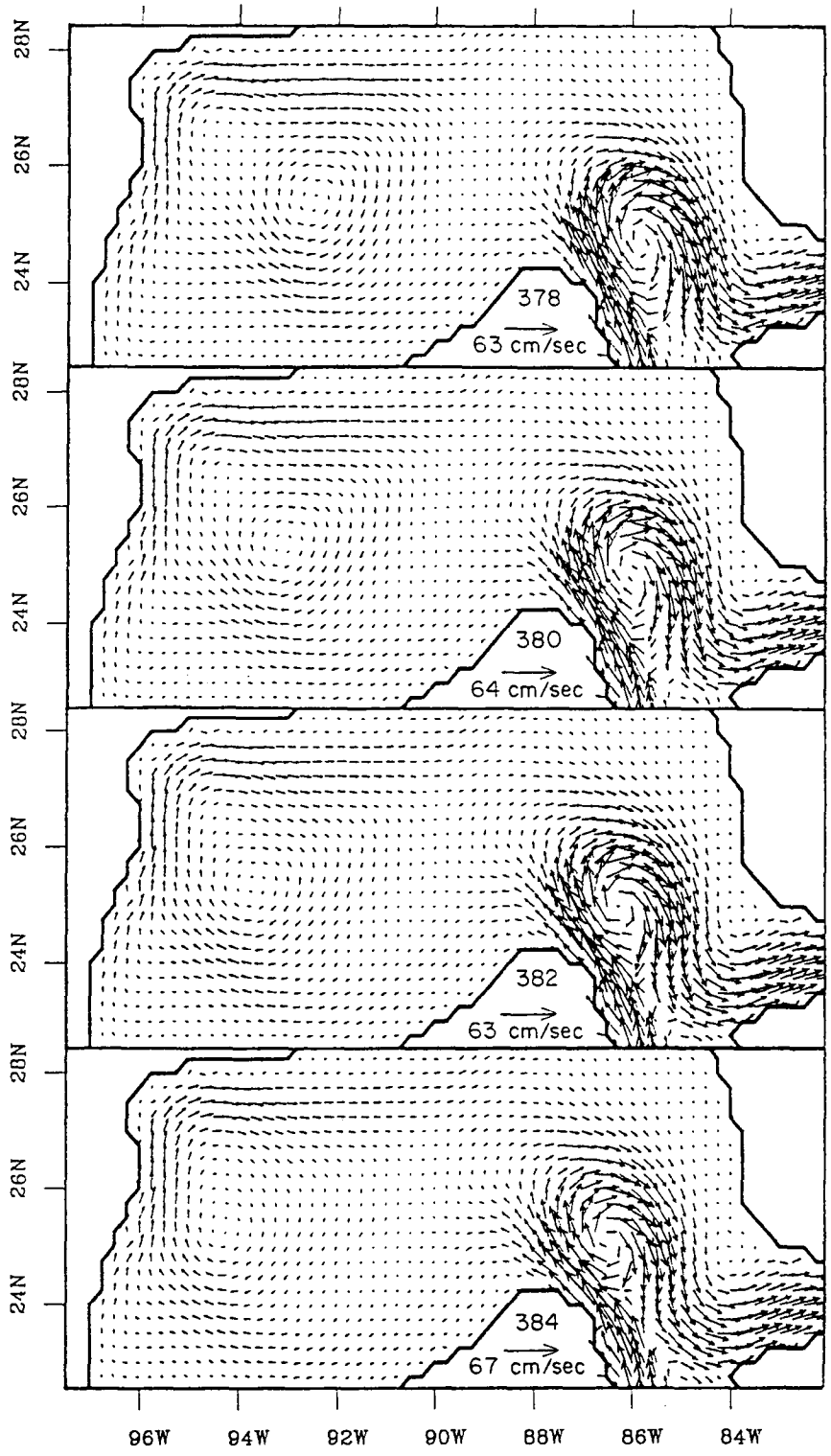

Figure 7C. A sequence of snapshots of the flow in level 3 (as in Figure 6) every 2 weeks, showing the motion of the anticyclonic ring as it drifts to the west, (continued).

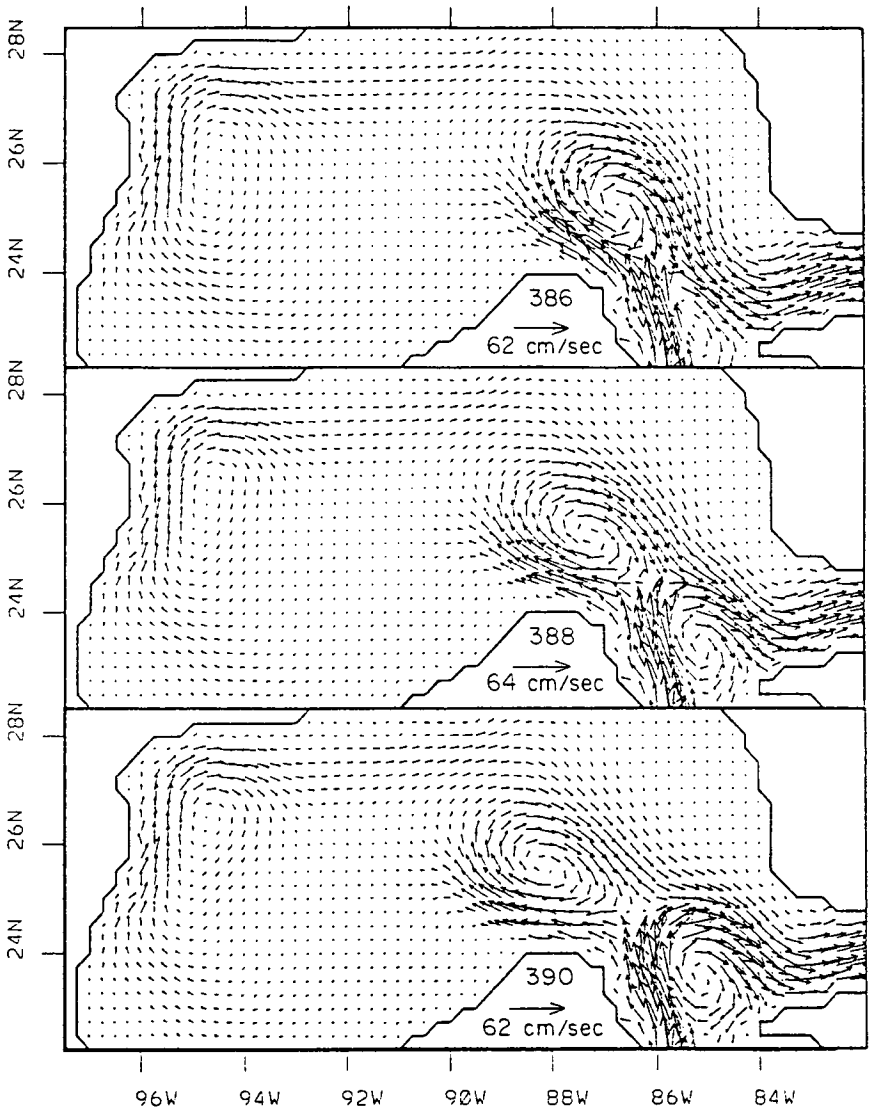

Figure 7D. A sequence of snapshots of the flow in level 3 (as in Figure 6) every 2 weeks, showing the motion of the anticyclonic ring as it drifts to the west.

ring propagating until it combines with the anticyclonic gyre already present in the western Gulf of Mexico. At week 366 the map of mass transport streamfunction for this whole water column (Figure 1) suggests that the ring has separated. The velocity distribution in Figure 7, however, still shows that at week 366, much of the northward flow in the Straits of Yucatan is flowing around the anticyclone, then around the eastward cell of the Loop Current and finally out of the Straits of Florida. Many weeks later (depending on the size of the figures and the reader's visual acuity) after the streamfunction map would have suggested the separation of the ring, many of the horizontal velocity vectors in Figure 7 still show that there is a remnant of the flow field that connects the flow on the western side of the Loop Current with the southern portion of the anticyclone now in the center of the Gulf of Mexico.

By week 376-380, the connections involving eastward flow between the anticyclone and the Loop Current are difficult to discern in Figure 7C. The center of the anticyclonic gyre, by week 380, is at approximately 93°W. To the south of the ring's center, between it and the Mexican coast, the flow is all to the west. At this point it is difficult to see any distinction between the anticyclone reaching the western Gulf and the large anticyclonic flow field that was originally present. Figure 7D shows that by week 388 or 390 the cycle is starting over. There are a number of details that show that the cycle does not repeat exactly, but the gross features of the separation cycle are quite similar. Our choice of horizontal eddy viscosity in these runs is slightly high, which will accentuate the interconnecting velocity fields between the detached ring and the main flow. However, we also point out that the induced interconnecting flow is also completely consistent with ideas of turbulent entrainment and vorticity dynamics. That is, the velocity induced near the ring from the far field of the Loop Current would be of the sign to bring fluid toward the Loop Current.

The most striking feature of this sequence of patterns is that although it was clear at the beginning of this sequence that the ring had not yet separated, it is difficult to point to any specific time and state that the ring has now "just separated." It is true, of course, that other properties are relevant to the question of ring separation. One naturally asks whether fluid is transported within the ring (see Nof, 1983; Flierl, 1984; Davey and Killworth 1984), etc. We wish to emphasize here primarily the distinction between ring separation as "catastrophic event" and the gradual process depicted in Figure 7.

The Deep Velocity Field

It is well known that the flow in the surface layer of the Loop Current continues out through the Straits of Florida at depths approaching 800 meters (e.g., Richardson *et al.*, 1969). The flow in the upper layer of the Loop Current and in the large anticyclonic rings appears to be highly coherent throughout this upper part of the water column. Figure 8 shows the model flow at three representative deeper levels. The position of the upper ring is shown by the dot. Level 7 is a transition level. In the regions of strong flow, such as in the Straits of Yucatan, the flow in level 7 appears consistent with the upper flow. In the open Gulf, however, the flow in level 7 appears consistent with that in the deeper water and not with that of the surface waters. This

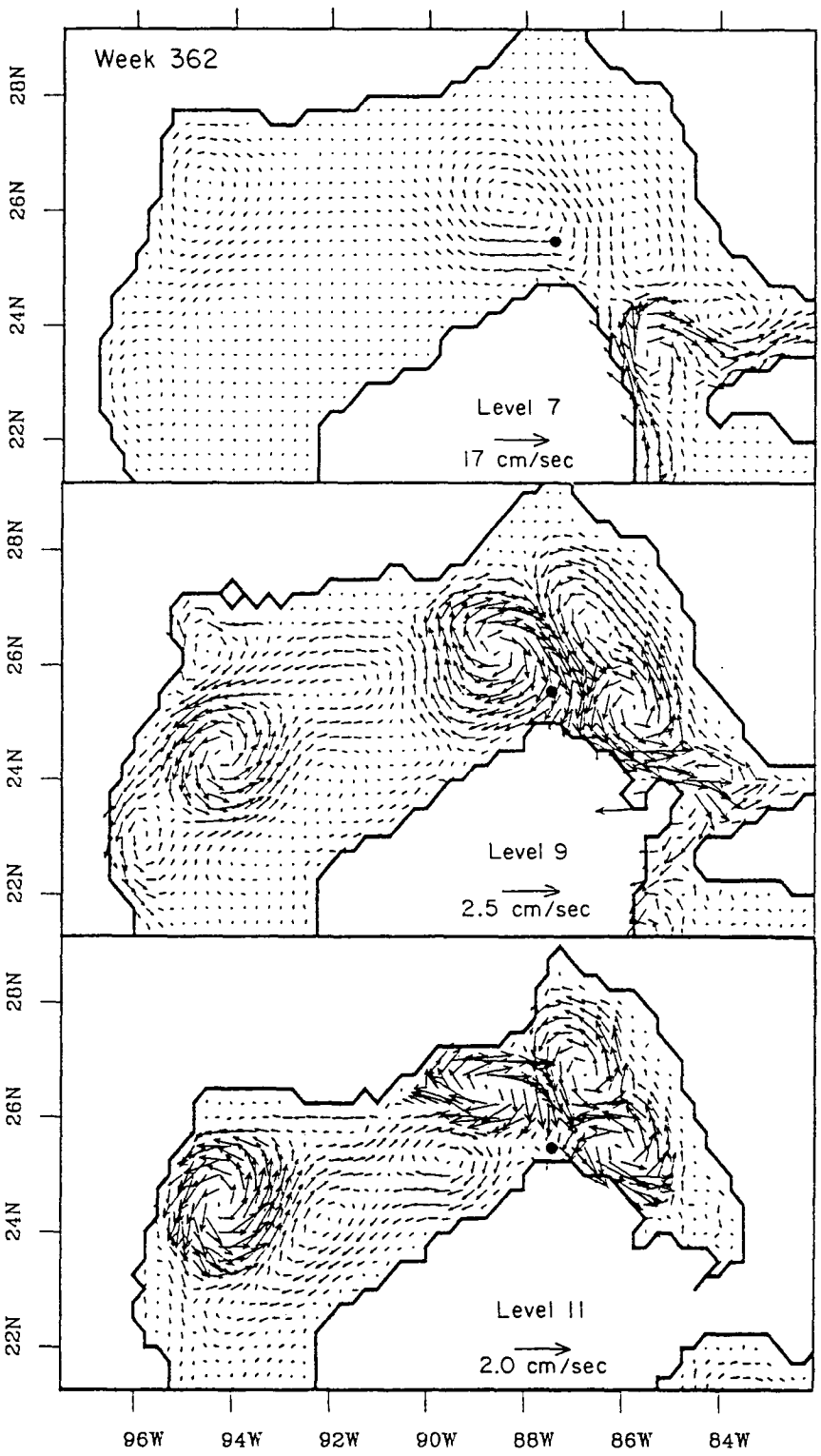

Figure 8. Snapshots of the flow in levels 7, 9, and 11 at week 362. Their depth ranges are: level 7, 660-820 m; level 9, 1120-1470 m; level 11, 1620-2720 m (see also Figure 3). The black dot in each diagram shows the position of the center of the upper ring at that time step. The outline of bottom topography is the contour of the maximum depth at that level.

remark introduces the notion that we find a deep flow field that is quite distinct form that seen near the surface.

Level 9 represents a level in which the flow is continuous between the deep Gulf of Mexico and the Carribean Sea through Yucatan Straits, and level 11 represents the deepest flow. The major differences in the appearance of these levels in this figure arises from the differences in scaling of the vectors — which is based upon the maximum velocities. The maximum velocity in level 7 is found in the flow near the Straits of Florida; the large apparent difference between levels 7 and 9 is an artifact of this scaling. In these levels, which represent the deep flow in the model, a family of deep vortex-like motions stands out. These features (in our model) are not isolated, highly nonlinear vortices of the type found in the upper ocean. Because the velocities here are ~2-5 cm/s, these features can not be nonlinear but can be assumed to be topographic Rossby waves as described by Hamilton (1990). The flow shown here in level 9 is surprisingly similar to the flow at the sill in the Yucatan Channel reported by Maul et al. (1985).

Figure 8 shows that beneath the upper anticyclone, but offset to the northwest, there is a deep anticyclonic feature. To the east of it we see a long peanut-shaped, nearly double cyclonic vortex; a number of additional smaller highs and lows are apparent. In level 9 the noticeable cyclonic feature in the western part of the basin almost obscures a weaker feature of similar sign to its southwest. The anticyclonic feature in the upper northwest corner of level 7 can barely be seen at level 9; the topography is different at that level. When looking at many sets of figures of this type one sees that the flow in the deep motions is vertically consistent throughout all levels in the deep water. Figure 9 shows a series of maps using level 9 to represent the flow in the deeper part of the model. One can follow the motion of the deep velocity field in Figure 9 and trace the motion of each individual high and low feature. The two primary vortex-like features in the center of the pattern are quite distorted, however, as they move to the west.

An unexpected change in the deep flow field takes place during weeks 370-376 (see Figure 9B); the cyclonic feature originally in the east propagates to the west, but interacts with the southern boundary; it travels between the anticyclonic feature and the boundary. Thus by weeks 386-390, the pattern of flow in the western Gulf is remarkably similar to the set of highs and lows that had been there at week 362, although the progression of events shown in Figure 9 tells us that each feature has been replaced by a new member of the family. It is clear that the pattern of the deep flows moves about, slightly, relative to the upper ring. Although we have shown only a single ring separation cycle, the process is similar in other cycles.

In this sequence, we saw that the deep motions, usually described as topographic Rossby waves, travel faster than the upper-layer anticyclone. This result is consistent with the findings reported by Hamilton (1990); the patterns will appear similar in all levels (they are barotropic) but are obscured in the upper levels by the high-velocity rings.

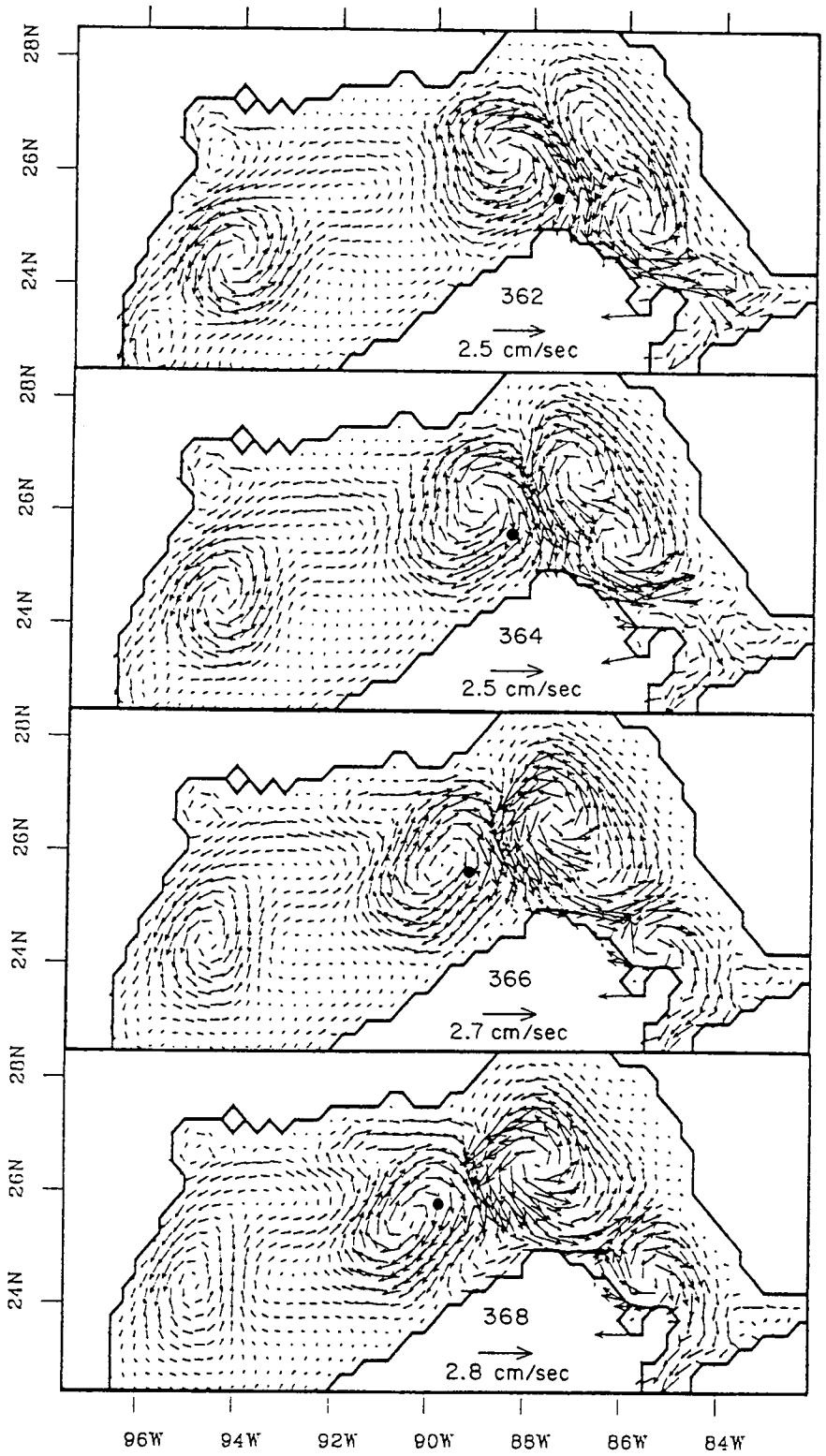

Figure 9A. A sequence of snapshots of the flow in level 9 every 2 weeks, which is typical of the deeper levels of the model. The black dot at each time step shows the position of the upper ring (see Figure 6 for comparison). Week 362 is measured from an initial 11-yr. spin-up. This level extends from 1120-1470 m; the outline of the bottom topography shown is the 1470 m contour, continued.

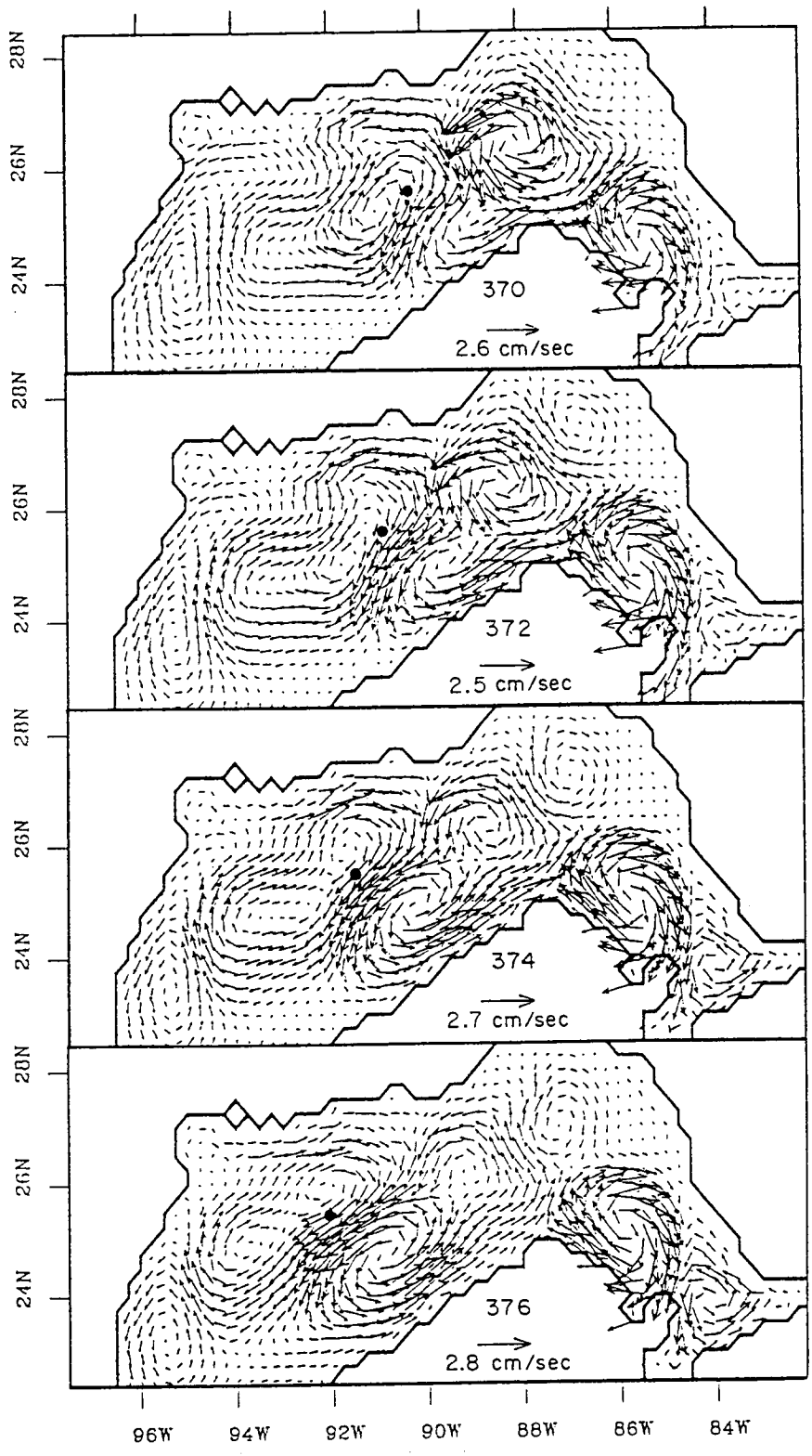

Figure 9B. A sequence of snapshots of the flow in level 9 every 2 weeks, which is typical of the deeper levels of the model. The black dot at each time step shows the position of the upper ring (see Figure 6 for comparison). Week 362 is measured from an initial 11-yr. spin-up. This level extends from 1120-1470 m; the outline of the bottom topography shown is the 1470 m contour, continued.

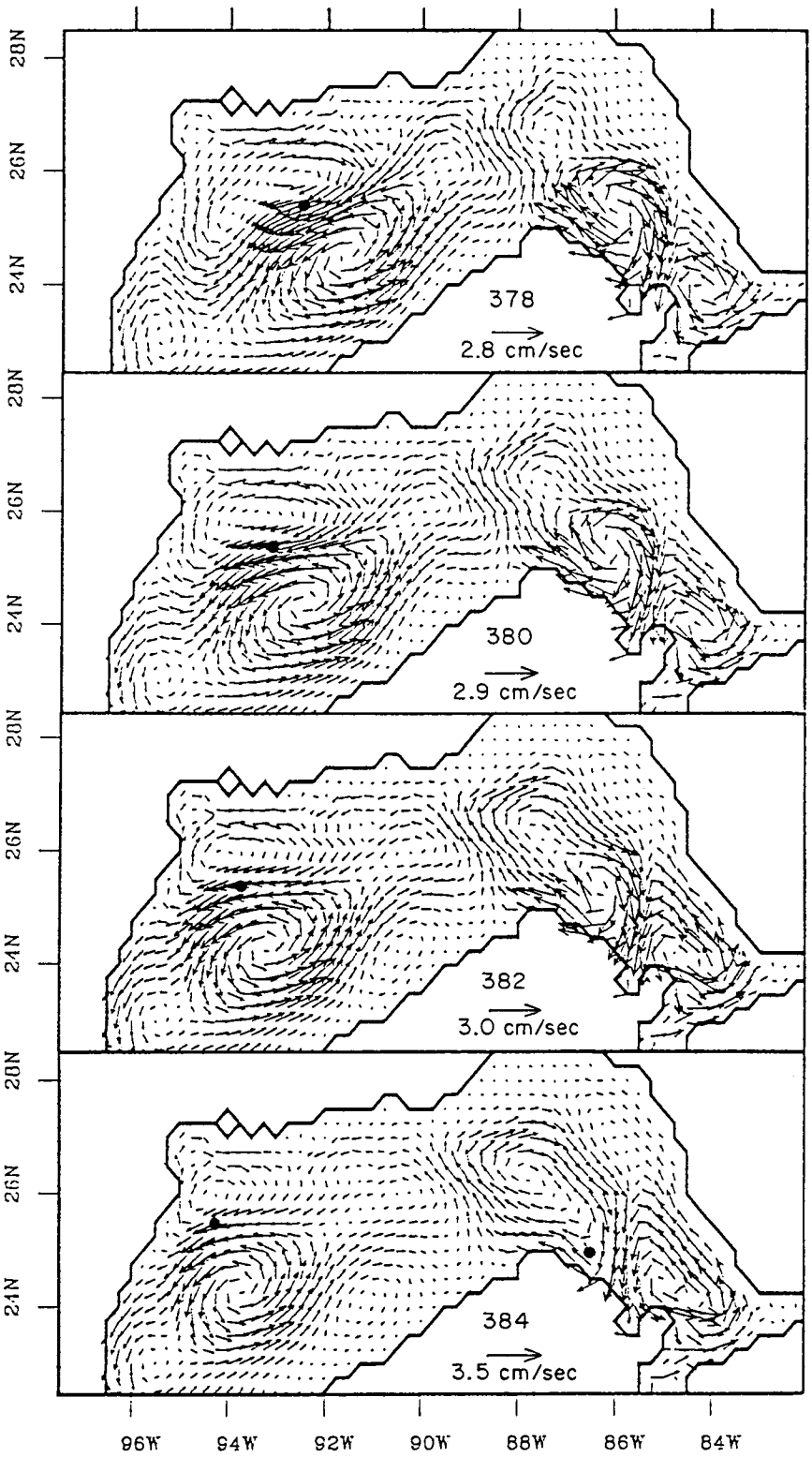

Figure 9c. A sequence of snapshots of the flow in level 9 every 2 weeks, which is typical of the deeper levels of the model. The black dot at each time step shows the position of the upper ring (see Figure 6 for comparison). Week 362 is measured from an initial 11-yr. spin-up. This level extends from 1120-1470 m; the outline of the bottom topography shown is the 1470 m contour, continued.

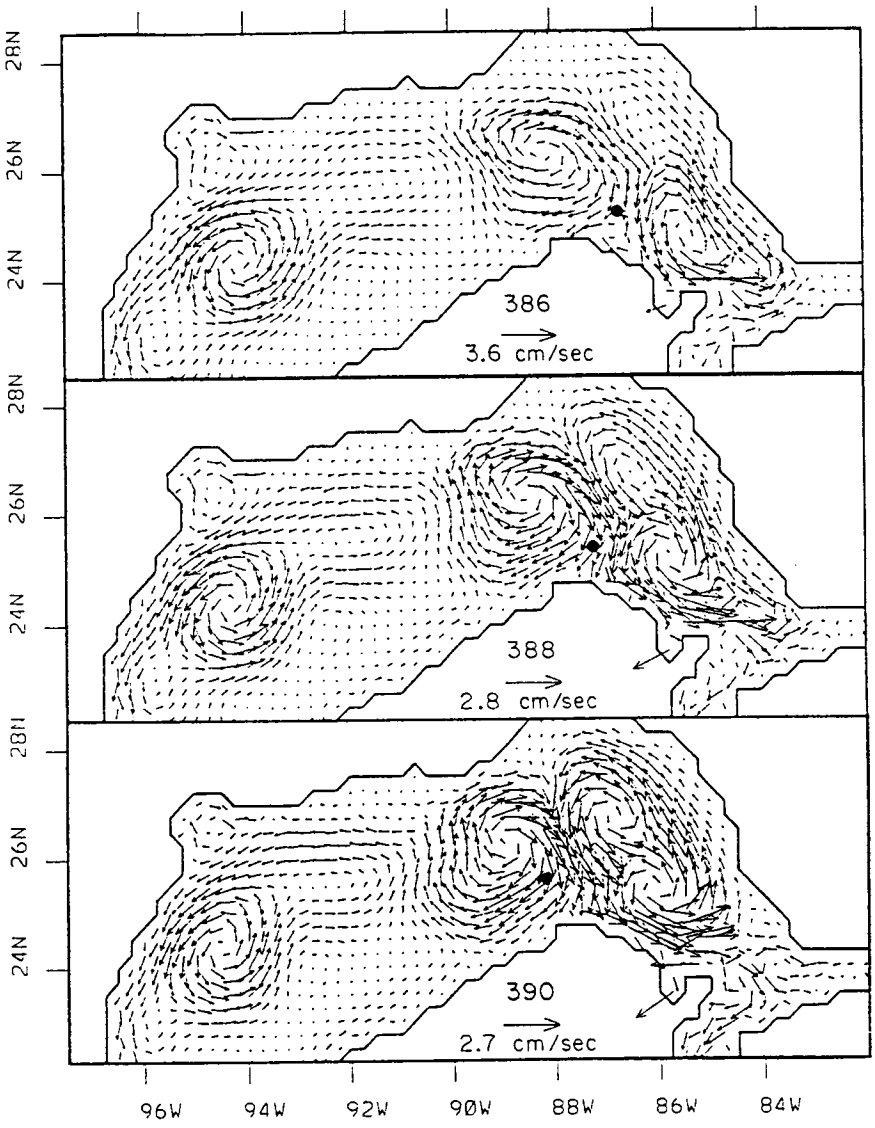

Figure 9D. A sequence of snapshots of the flow in level 9 every 2 weeks, which is typical of the deeper levels of the model. The black dot at each time step shows the position of the upper ring (see Figure 6 for comparison). Week 362 is measured from an initial 11-yr. spin-up. This level extends from 1120-1470 m; the outline of the bottom topography shown is the 1470 m contour.

Discussion

Some interesting, if speculative, generalizations can be drawn from these results. If we think of this full sequence in Figure 7 as representative of one cycle, we can examine the central times, weeks 374 or 376, as the out-of-phase center part of the cycle. It is clear that in many areas of the basin the flow reverses, so that the net flow would be expected to be small. In some parts of the basin, however, the flow does not reverse. Along the western boundary from ~21°N to ~ 25°N the flow is southward at all times in the deeper levels. No one should expect an exact correspondence between the model and the ocean in the details of the flow field. Nevertheless, it seems instructive that there are regions in the model in which the flow does not reverse at any stage of a ring cycle and these regions can be explored for first-order mean flows.

Another striking feature of the flow in level 9 (Figure 9) is that there is southward deep flow through Yucatan Channel except for a brief interval near week ~382. This topic is explored in the next section.

At the western boundary, in the upper levels of the flow, Figure 7 shows that throughout the cycle, the flow at the western boundary is to the north; farther offshore (~94°W) the flow is to the south. This flow farther offshore is reversed by week 378 as the ring goes by, suggesting weak mean flow. At the western boundary, however, the flow is uniformly to the north at all times. This would suggest the existence of a mean flow of the same order but modulated by the arrivals of anticyclonic rings. We emphasize that these are general remarks that may give us only broad insights about the real flow fields.

The physical mechanisms by which the new ring merges with the old ring already present in the western Gulf are clearly not fully realistic in the model. It is known that the merging process is often accompanied by the presence of filaments extending beyond the edges of each ring (e.g., Cushman-Roisin, 1989; Nof, 1988). The horizontal resolution of the model (1/4°) is inadequate by an order of magnitude to allow such features to be realistically included.

A remarkable feature of Figures 9B, 9C is that the upper ring center lies just above what could be called a weak jet. The deep velocities here are only ~3 cm/s, but this is <u>not</u> small in comparison with the westward translation of a ring. Thus we suspect that the 5 cm/s westward motion of the upper ring could be enhanced substantially by the deep flow.

We have shown here that the ring does not become separated from the Loop Current in a single event; nevertheless, there is a stage at which the motion of the anticyclone begins to be mainly westward, and significantly different from the usual northward motion of the Loop Current. An observer examining the figures from the model output can, with little ambiguity, identify the time at which the ring begins the separation process as evidenced by its westward translation. By examining the weekly streamfunction maps, we found that these times coincided with the times of maximum transport between Florida and Cuba.

A possible mechanism to explain this phase relation is as follows. While a ring is growing, some transport must be extracted from the main flow to supply the ring growth. In this model with constant forcing, we may conclude that at the point when

the ring separates from the main flow and is no longer robbing it, the main flow should attain its maximum value.

Figure 10A (upper) shows the positions of the centers of the anticyclonic ring in Figures 7 A-D (the dots) and of the new anticyclone forming within the Loop Current (pluses). We see that the motion of the centers is mainly to the north until the ring begins to self-advect to the west. Figure 10B (lower) shows a plot of ring positions versus time; we see that the drift to the west is ~5 cm/s. This value is remarkably consistent with the speeds observed. Vukovich (in SAIC, 1986) found a range of ~1 to 8 cm/s with a mean of 5 cm/s. It is reassuring to find such agreement, especially taking into account that no parameters of the model are tuned to achieve it.

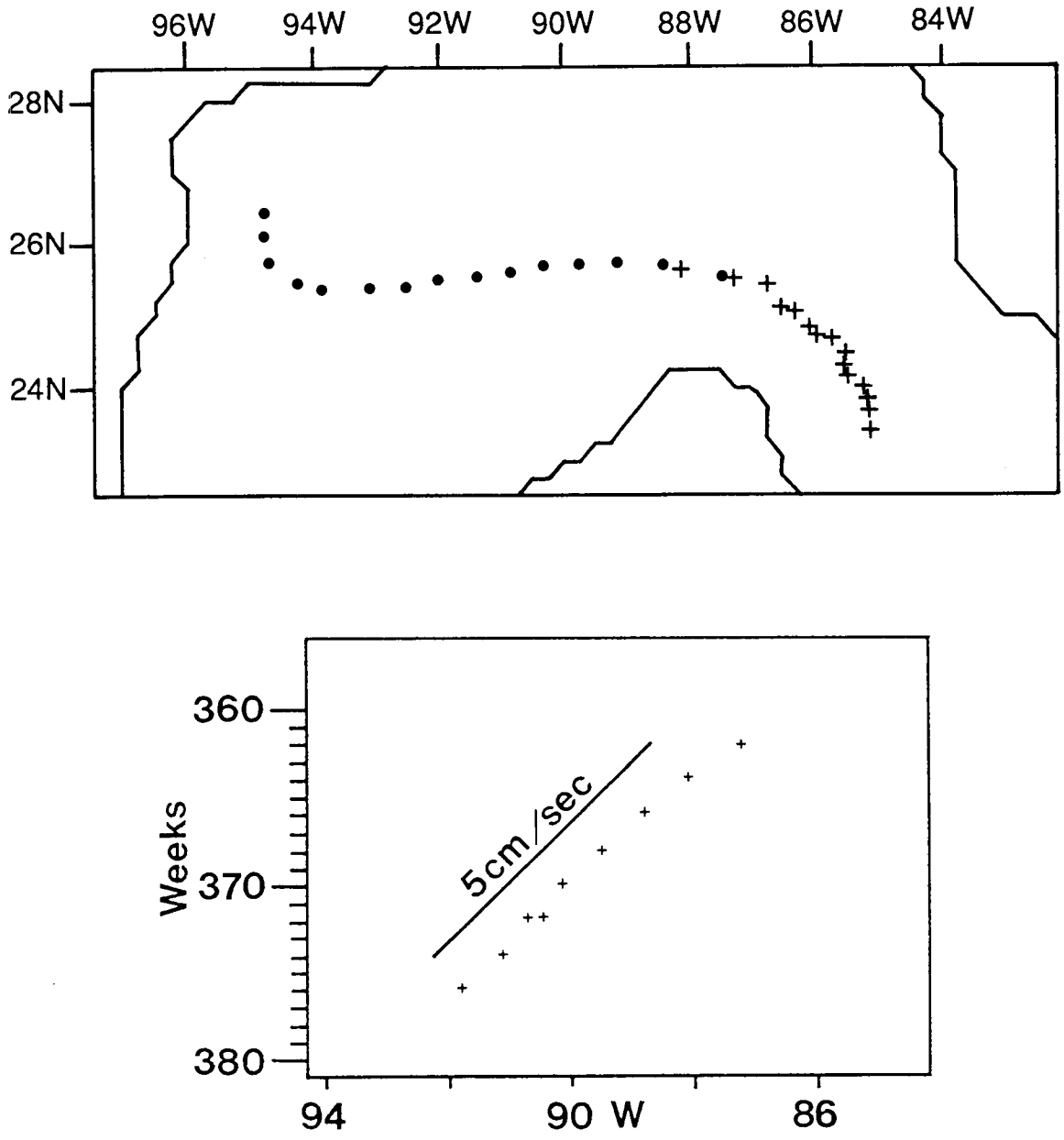

Figure 10. Part a, upper panel, shows the positions of the centers of the anticyclonic ring, taken from Figure 7, (dots) and of the new anticyclone forming within the Loop Current (pluses). Part b, lower panel, shows a plot of the ring position (longitude only) versus time. The straight line shows a speed of 5 cm/s.

V. DEEP FLOW IN THE STRAITS OF YUCATAN

Figure 9 suggests that the model flow in level 9 is usually to the south in Yucatan Channel.* Only near weeks 382-384 does the flow reverse. To explore this important aspect of the deep circulation, Figures 11 and 12 show the flow near times of extremes in the nature of the flow fields in levels 7 and 9.

In level 7 (which extends to 820 m) the flow usually "looks like" the strongest part of the flow in the upper waters. For completeness Figure 13 shows the flow in level 1. It is clear that the position of the strong flow in the Loop Current extends straight down into level 7. Comparison with the flow in level 9 reveals what we suspect is an important feature.

At week 366, the anticyclonic ring is just detaching; the new anticyclonic feature that has been forming in the fresh portion of the Loop Current is far to the south. Near 24° N, 84°W, the flow to the southeast is positioned over the deep part of Yucatan Channel. This flow is therefore able to impart momentum all the way down into level 9.

At the other extreme of this cycle, the center of the anticyclonic flow in the Loop Current has moved farther to the north; by week 382 the south or southeasterly flow in the upper water is no longer over the deepest part of the channel. That flow is now over a peculiar feature of the bottom topography, and momentum to the south cannot be put into level 9. A portion of the northeast edge of Yucatan Peninsula juts out into the deep part of Yucatan Channel, as seen on the figures that portray level 9. This obstruction to the deep flow extends up to the depths of the ~1200 m isobath, whereas Yucatan Channel is ~2000 m deep.

There are some insights that may be drawn from this series of figures. The motion of the real Loop Current, forced by mechanisms not contained in our model, moves about in an obviously more complex way than the simple cycle shown here. When the southeasterly flowing portion is over the deeper parts of the channel we might expect to find southerly flow there, and conversely. The deep flows observed in the longest records (e.g. Maul *et al.*, 1985) have persistent speeds of ~5 cm/s, and this is consistent with the speeds in the model. We are not aware that the fluctuations in the flow have been compared with the variations of position of the Loop Current, however, in a manner consistent with the ideas put forward here; the variations of the flow observed by Maul et al. appear consistent with this idea by cursory examination (e.g., see their Fig. 3) but the data are adequate for only a limited comparison.

We note in passing that in Figure 12 the flow in the northern Caribbean Sea appears to have a very strong topographic constraint. The flow in level 7 is obviously blocked by the bottom topography; when one looks at the flow in level 3, that constraint is not so apparent.

---

*Maps showing surface features use the term Straits of Yucatan; maps showing deep topographic features refer to this area as the Yucatan Channel. The context should make the distinction clear.

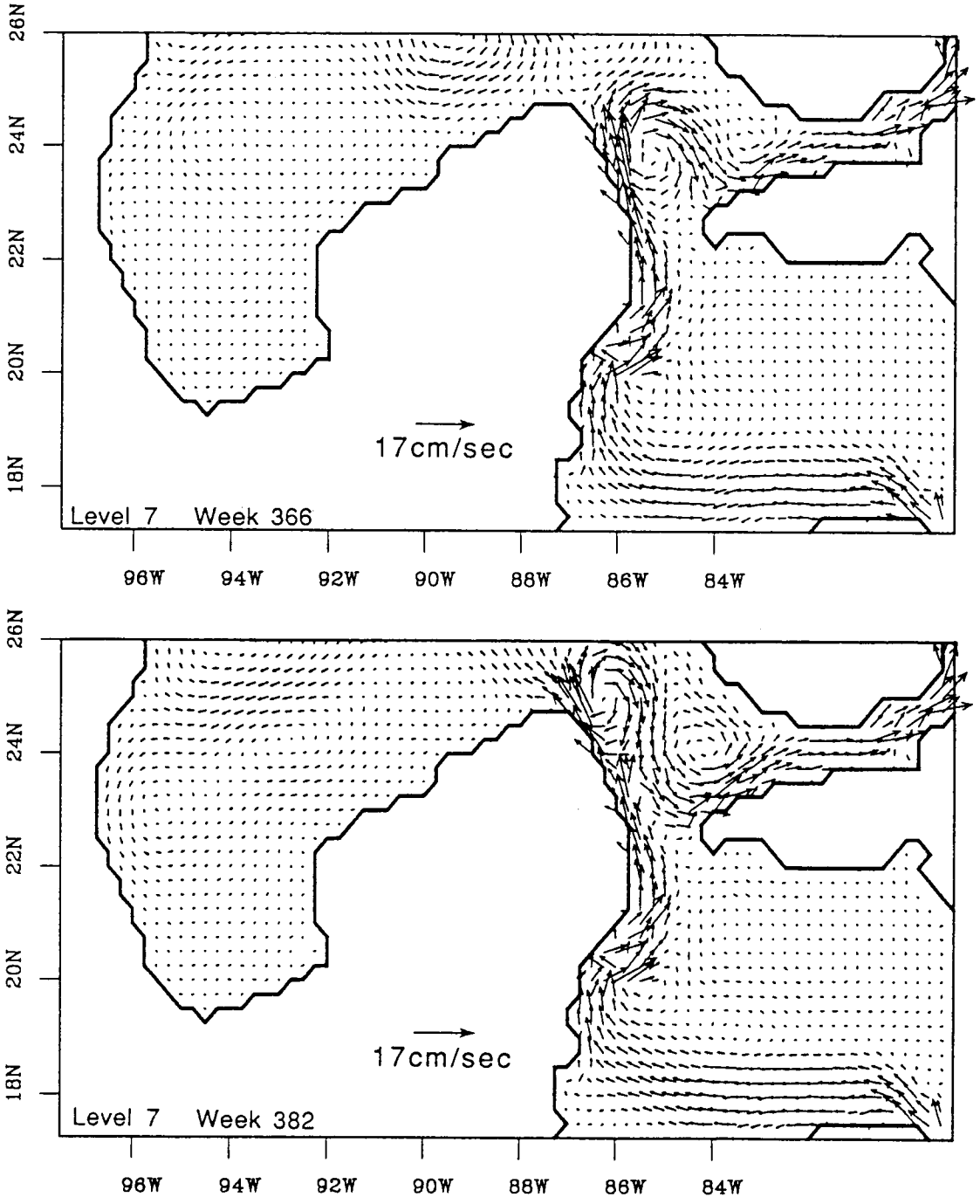

Figure 11. Snapshots of the flow in level 7 at weeks 366 and 382. (See also Figure 8). The times are consistent with Figures 6-9.

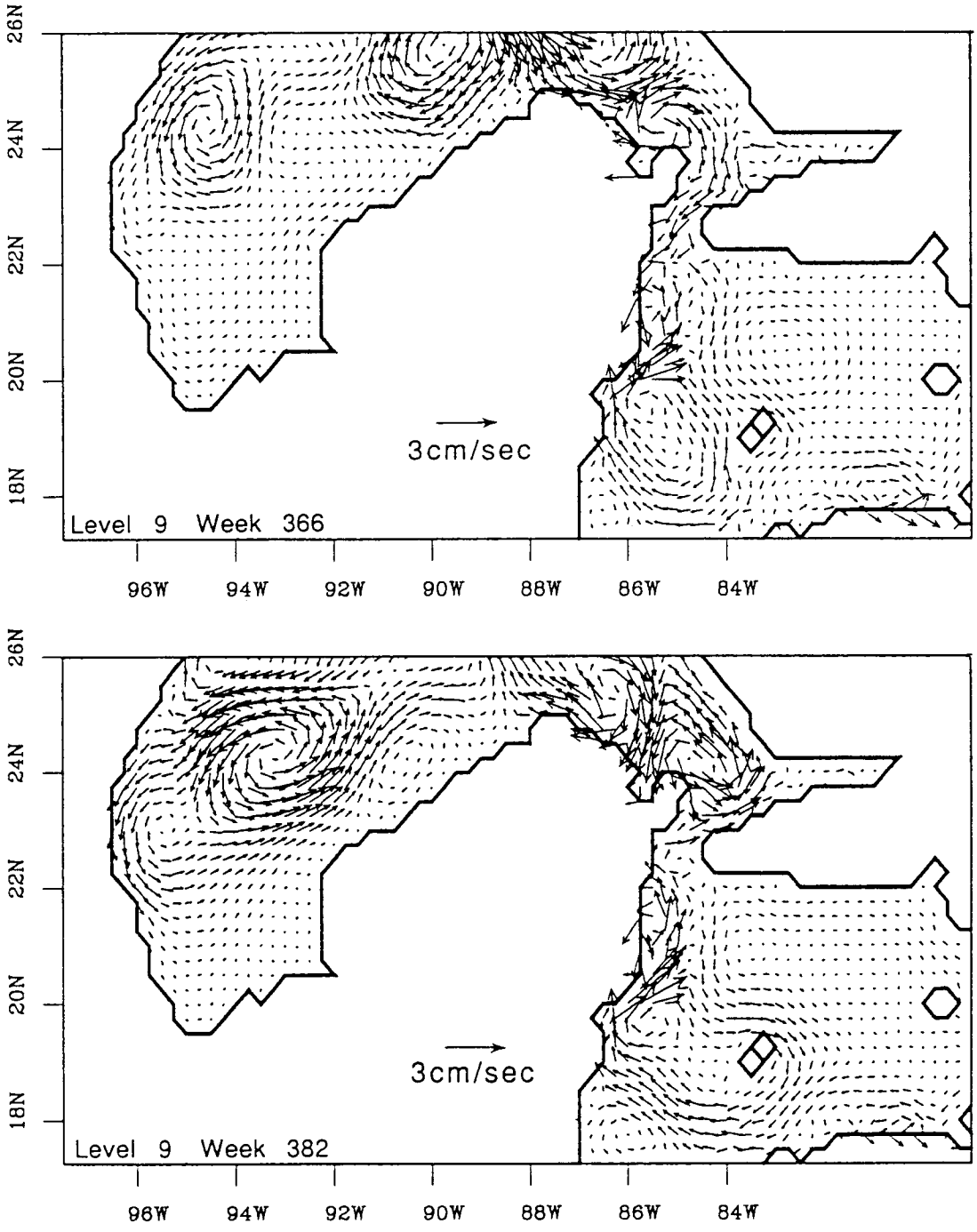

Figure 12. Snapshots of the flow in level 9 at weeks 366 and 382 (see Figure 11 for comparison).

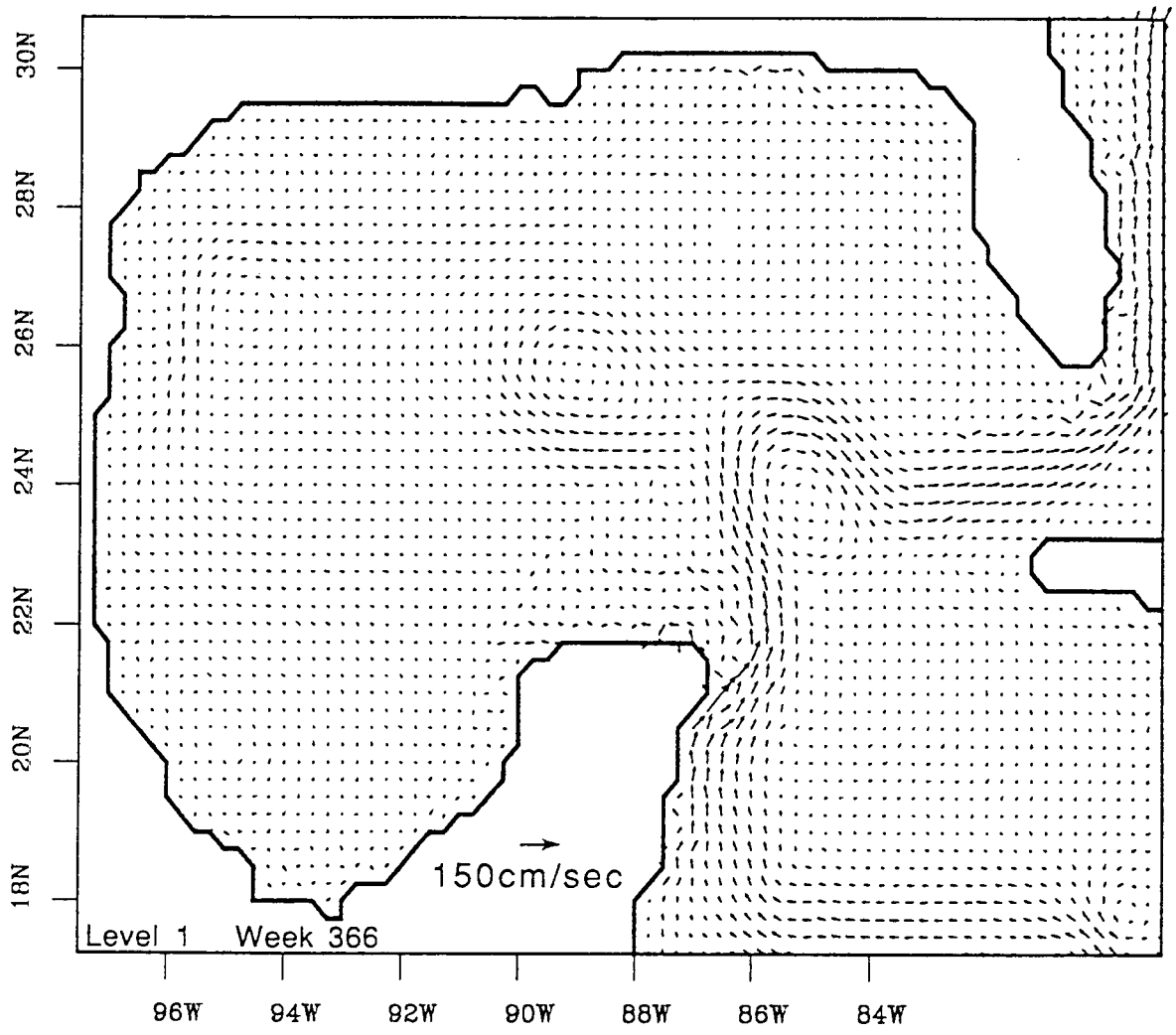

Figure 13. Snapshot of the flow in level 1 of the model at week 366 (see Figure 11 for comparison).

VI. COMPARISONS BETWEEN MODEL-SIMULATED CURRENTS AND THOSE MEASURED AT MOORINGS

Comparisons in the Eastern Gulf

Near Mooring C. To compare observed currents with model results, many locations were selected within the model and time series of velocity data were archived by sampling every 2 days at every model level. The first "virtual current meter mooring" is at Mooring C, in 180 m of water at the edge of the shelf near 26°N, as indicated on Figure 14. The second is at Mooring A, farther offshore; the third is slightly to the southeast of mooring G.

The model currents near Mooring C show that the largest velocities are associated with approaches of the Loop Current. However, the velocities are so small (~4 cm/s) that they are completely unrealistic and hence are not shown. It is generally believed that the major sources of energy for coastal currents are from wind forcing at periods shorter than 3 weeks (e.g., SAIC 1986) and from eddy-like motions on the shelf. Since these energy sources are not yet implemented in the model, it is to be expected that the coastal currents would not be modeled realistically.

Near Mooring A. Figure 15 shows the model currents at a sampling location farther offshore, at Mooring A. For a number of reasons, particularly the lack of variable forcing, the motions of the Loop Current in the model are slow and regular. There is no interaction between the Loop Current and the edge of the shelf. Without these interactions, two classes of motions are not produced: topographic Rossby waves in the 30-day band, as described by Hamilton (1990) and eddy interactions near the shelf edge. It is not (necessarily) that the model is "wrong," but that these motions are simply not forced. A direct comparison would not be meaningful, but Hamilton (1990) shows that the peak speeds observed at depth (1100-1600 m) are ~10-12 cm/s. For convenience, Appendix B shows a set of velocity plots, adapted from those shown by Hamilton, at all the relevant moorings. The speeds at "A," in the model, reach only ~23 cm/s at the surface, and ~8 cm/sec in level 6. Thus the model speeds here are somewhat less than those observed in the ocean — by 20-30%; the major source of variation in the model is associated with the ring shedding cycle.

Near Mooring G. Figure 16 shows model velocities extracted from levels 1,3, 5, 9 and 11 at a location near Mooring G (Fig. 14). The most complete records obtained from Mooring G are at the deeper levels, 1565 m - 3174 m, which correspond to model levels 10-12. Hamilton (1990) showed (his Fig. 3; see also Fig. B.1) that the observed currents were uniform at the deeper levels. We find the same result in the model; in Figure 16 the currents at level 11 can hardly be distinguished from the plotted curve for level 9.

The peak surface speeds in the model near "G" are slightly above 60 cm/s; the observations (at ~400 m) are similar, although the frequency distributions are quite different. At depths of 1500-3000 m, observed velocities reach ~20-25 cm/s. The model values (Fig. 16) reach peaks near 12-15 cm/s, which is obviously much less.

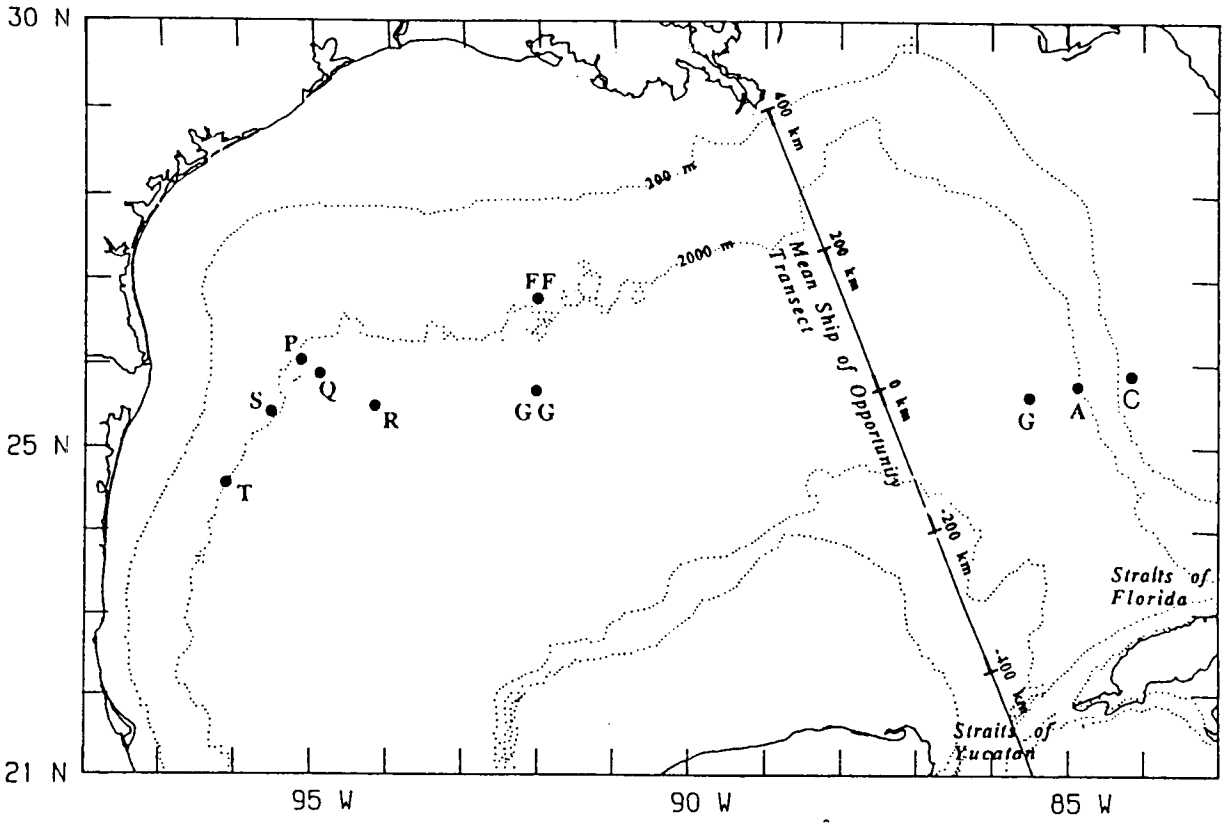

Figure 14. Map of the Gulf of Mexico showing current-meter mooring locations from the MMS program (SAIC 1986, 1987). The Ship of Opportunity transect line shows the location of frequent XBT sampling. Figure adapted from Hamilton (1990), with permission of the author.

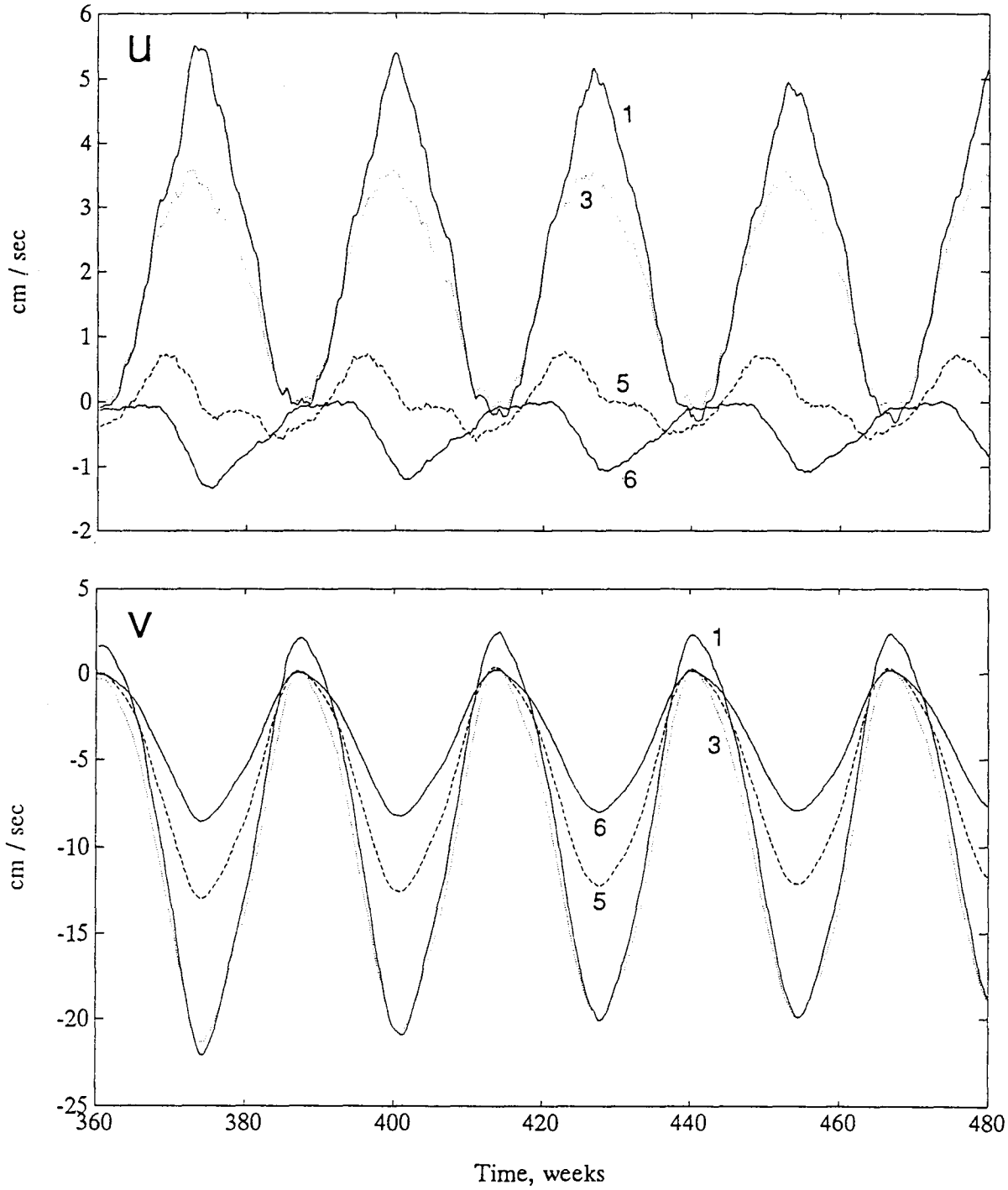

Figure 15. Model currents from a location just to the east of Mooring A (see Figure 14). The E-W component is above, the N-S component is below. These are shown for levels 1, 3, 5, and 6 (see Table 1); the depth extends only to level 6, or 660 m at this location. The time axis, based on the final 7 years of model runs, coincides with the earlier figures of velocity plots during the ring separation cycle.

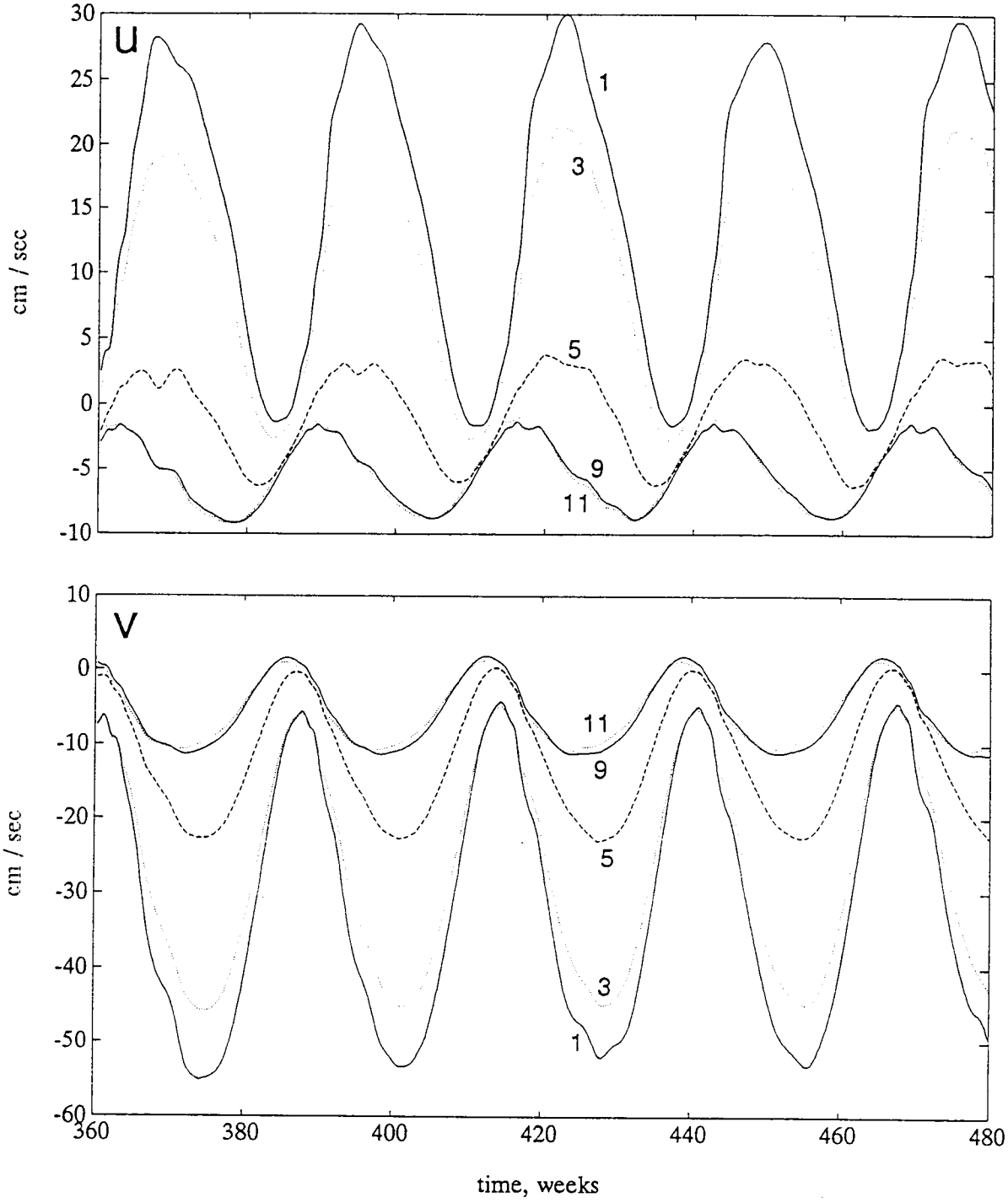

Figure 16. Model currents from a location just to the southeast of Mooring G (see Figure 14). The E-W component is above, the N-S component is below. These are shown for levels 1, 3, 5, 9 and 11. The time axis, based on the final 7 years of model runs, coincides with the earlier figures of velocity plots during the ring separation cycle.

What is far simpler to observe in the model, however, is the topographic Rossby wave (TRW) behavior in the deeper part of the basin. Hamilton was able to decipher these motions by skillful analysis. By examining the output from the model (e.g., Figures 8-9) it is immediately obvious that a set of coherent deep motions is propagating from east to west. These TRW's behave essentially as deduced by Hamilton. He noticed that the deep TRW's propagated somewhat faster to the west than the upper anticyclone. This feature is seen in the figures here as well. The fact that the deep velocities in the model are less than observed will not significantly affect linear wave behavior.

Comparisons in the Central Gulf

Near Mooring GG. Figure 14 shows the position of Mooring GG near 92°W, in 3000 m depth. Hamilton (1990) has analyzed the currents there, and shows (his Fig. 7; see also Fig. B-2) that the currents are similar at the 1650 m and 2500 m instruments. Figure 17 shows the observed currents at 305 m and 1650 m at mooring GG. The largest speeds at the deeper instrument (approaching ~20 cm/s) are associated with the passage of rings. The remarkable feature is that the large speeds at 305 m occur at a time when weak speeds are observed at the lower instrument. Figure 18 shows model currents as the deep motions go past simulated current meters; level 9 has a central depth at 1470 m and seems appropriate for comparison. The observed currents have peak speeds of ~20 cm/s. Those in the model are much weaker, reaching ~25 cm/s in the upper levels and less than 6 cm/s at level 9.

As discussed previously the deep motions in the model, as in the ocean, travel across the Gulf as topographic Rossby Waves. The properties of these waves will not change substantially, whether their amplitude is 6 or 20, because the behavior of these (linear) waves depends little on amplitude. We note that there is substantial vertical shear between the near surface (level 1) flow and that in levels 3, 5, and 9. There is very little shear below level 9, however, and in this character the model is in accord with the observations.

An obvious reason for the low speeds is that the inflow in the model at Yucatan is not strong enough. An additional reason, however, may be associated with the way the model treats bottom topography. The model has discrete jumps in depth between each level. Since topographic waves depend critically on bottom slope, it is possible that finer depth resolution in the model, by inclusion of more levels, would improve the behavior of the TRW's.

It is not easy to determine from figures such as these, but Hamilton was able to make a very interesting observation from the current meter data: he detected that the near-bottom waves had an apparent westward propagation velocity faster than that of the upper-layer warm core rings. As was shown in Chapter IV, this behavior is also found in the deep motions of the model. With the aid of the figures here, however, the analysis is aided enormously because we are able to examine figures using data at every grid point.

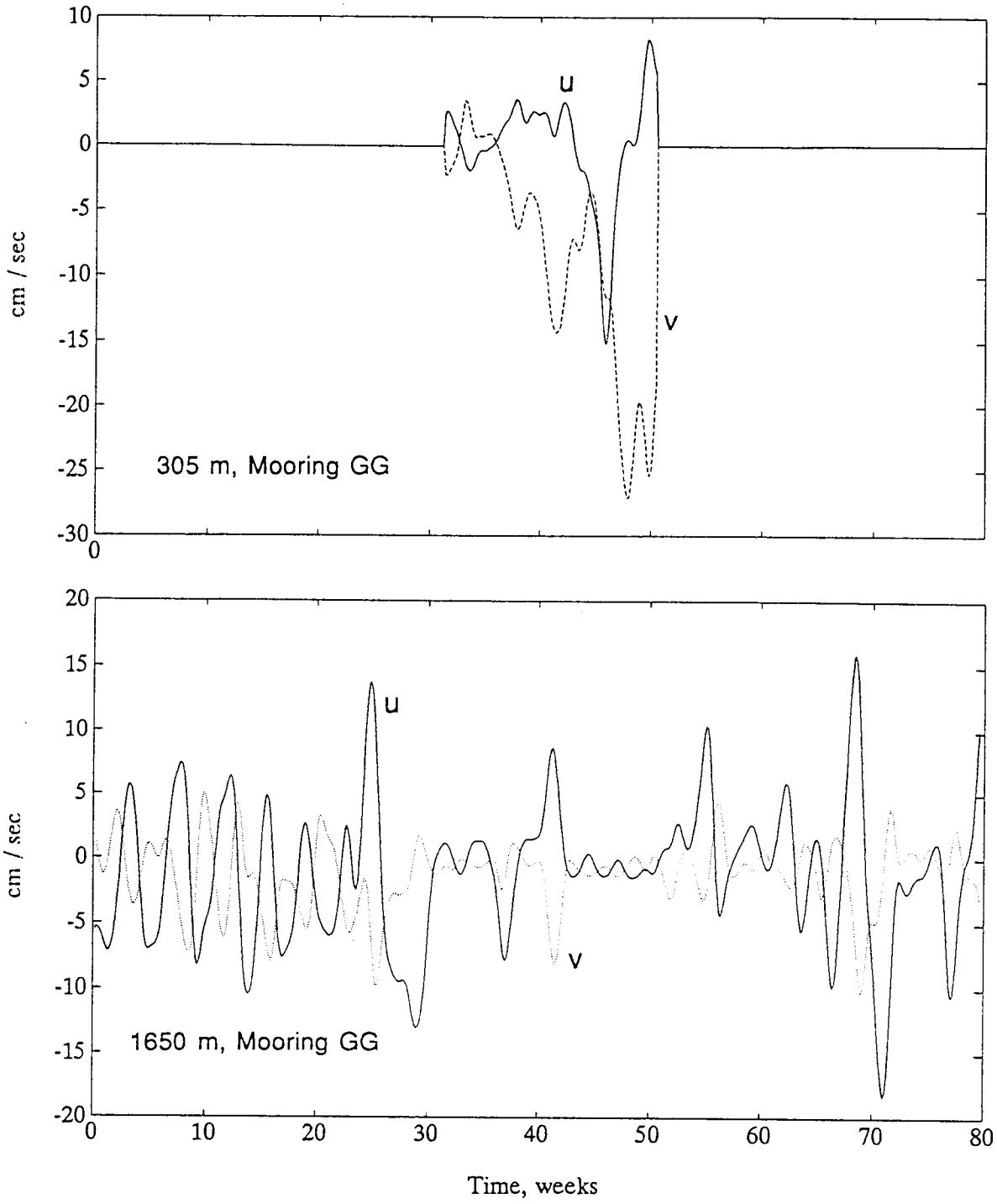

Figure 17. Observed currents at Mooring GG, in the central Gulf. Data are shown for two depths. These data have been low-pass filtered to suppress all fluctuations having periods shorter than 8 days. The filtered data at 1650 m start on 14 Apr 1987; at 305 m, 18 Nov 1987.

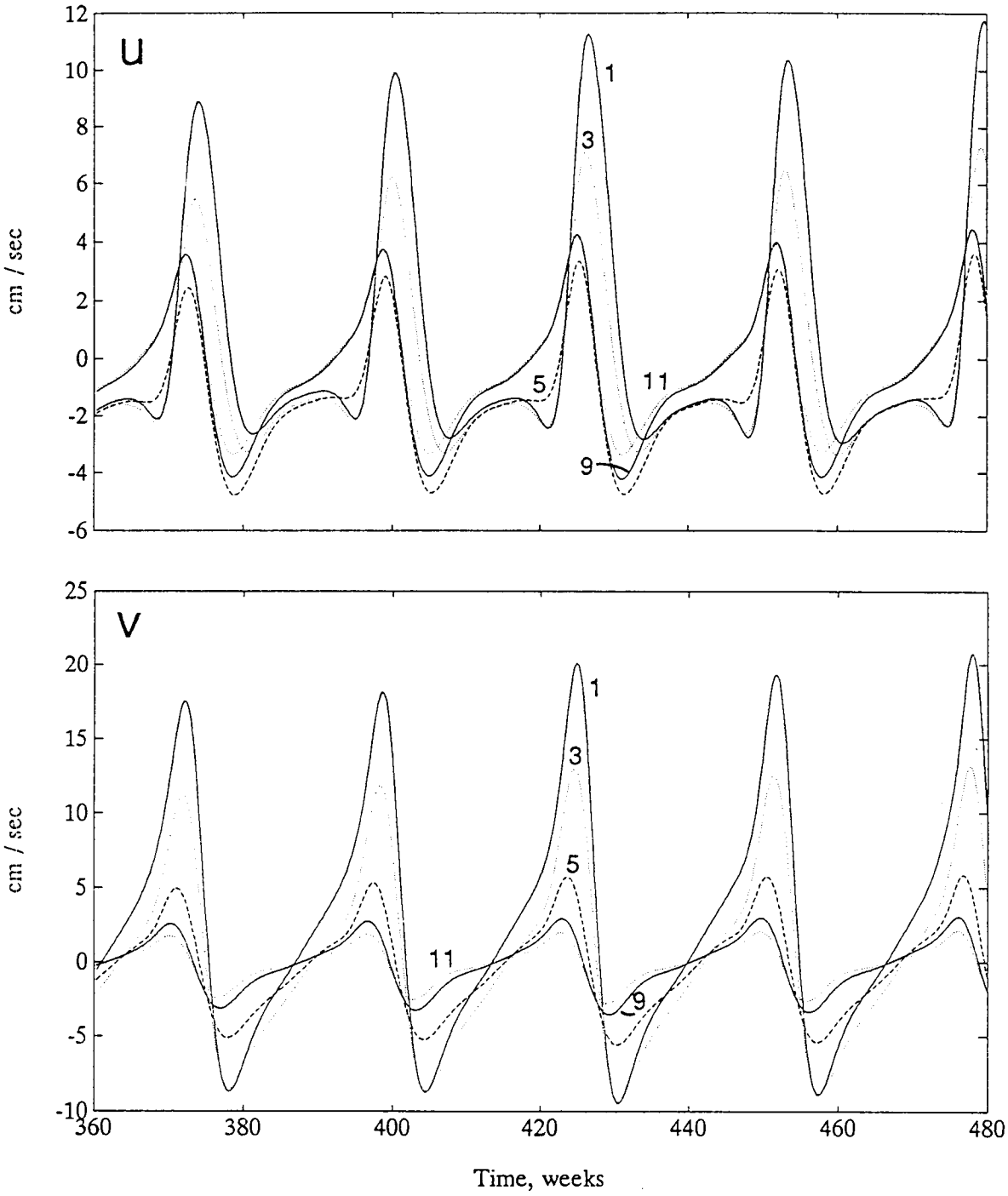

Figure 18. Model currents from the location of Mooring GG (see Figure 14). The E-W component is above, the N-S component is below. These are shown for levels 1, 3, 5, 9 and 11. The time axis, based on the final 7 years of model runs, coincides with the earlier figures of velocity plots during the ring separation cycle.

Comparisons in the Western Gulf

Near Mooring P. Figure 19 shows the observed currents at Mooring P. For comparison, Figure 20 shows currents extracted from the model at a location very near P. We see that speeds of ~10 cm/s are observed as deep as 1500 m. By contrast, the model velocities are, at best, approximately half that value. This remains consistent with the smaller values found in the model at GG. To get a more comprehensive understanding of the flow field, however, the figures in Section IV offer full horizontal maps from which these plots are a subsample.

Near the western Boundary. Figure 21 presents the model flow in the "western boundary current" at 26°N, 96°W, somewhat inshore of mooring P. The northward velocity component reaches ~45 cm/s near the surface. The northward velocity extends to the bottom here. The speeds in Figure 21 are strongly modulated by the addition of each new ring. The flow here is strong because of a western boundary current that results from the combined effects of ring accumulations and of the large-scale wind curl forcing (Elliott 1982; Sturges and Blaha, 1976). A wind-driven western boundary current develops in the model even before rings form, as is well known. We do not yet understand the relative importance of wind curl forcing and of ring forcing. A series of experiments is planned to shed light on this question.

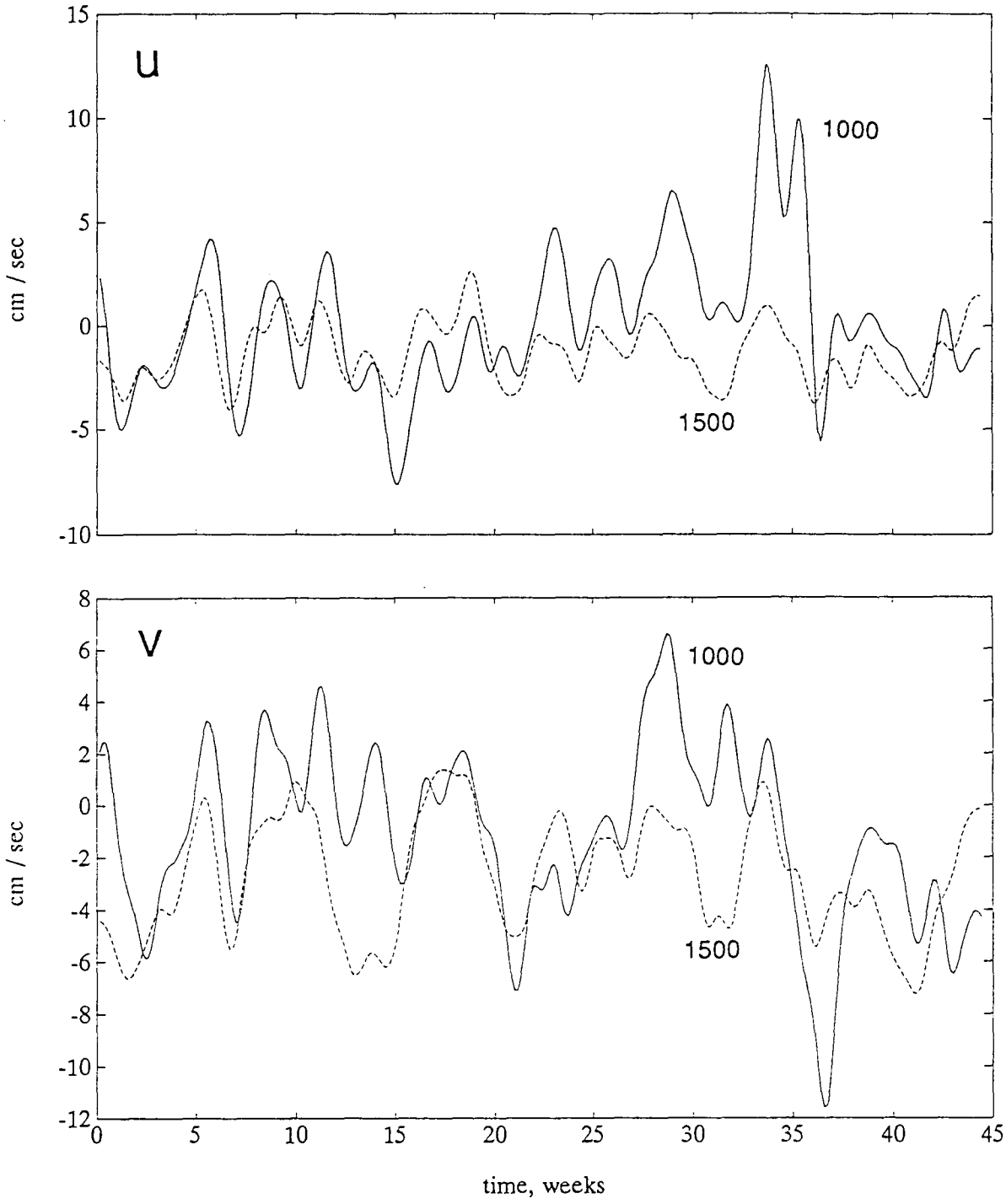

Figure 19. Observed currents at Mooring P, in the western Gulf. Data are shown for two depths; these data have been low-pass filtered to suppress all fluctuations having periods shorter than 8 days. The filtered data start on June 19th, 1985; 311 daily values. There is no correspondence between these data (calendar) times and model time, except for frequency.

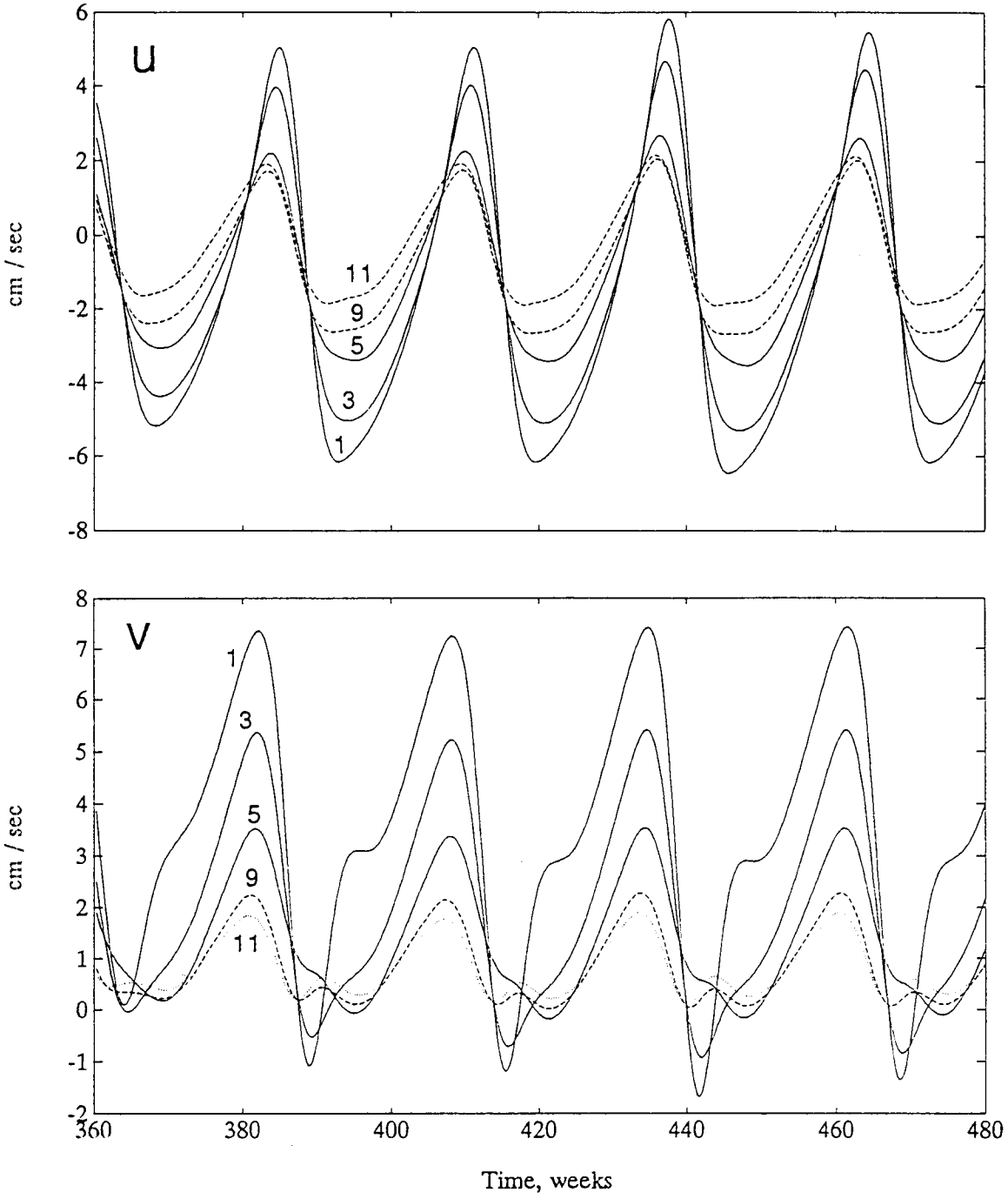

Figure 20. Model currents from a location a few km to the east of Mooring P (see Figure 14). The E-W component is above, the N-S component is below. These are shown for levels 1, 3, 5, 9 and 11. The time axis, based on the final 7 years of model runs, coincides with the earlier figures of velocity plots during the ring separation cycle.

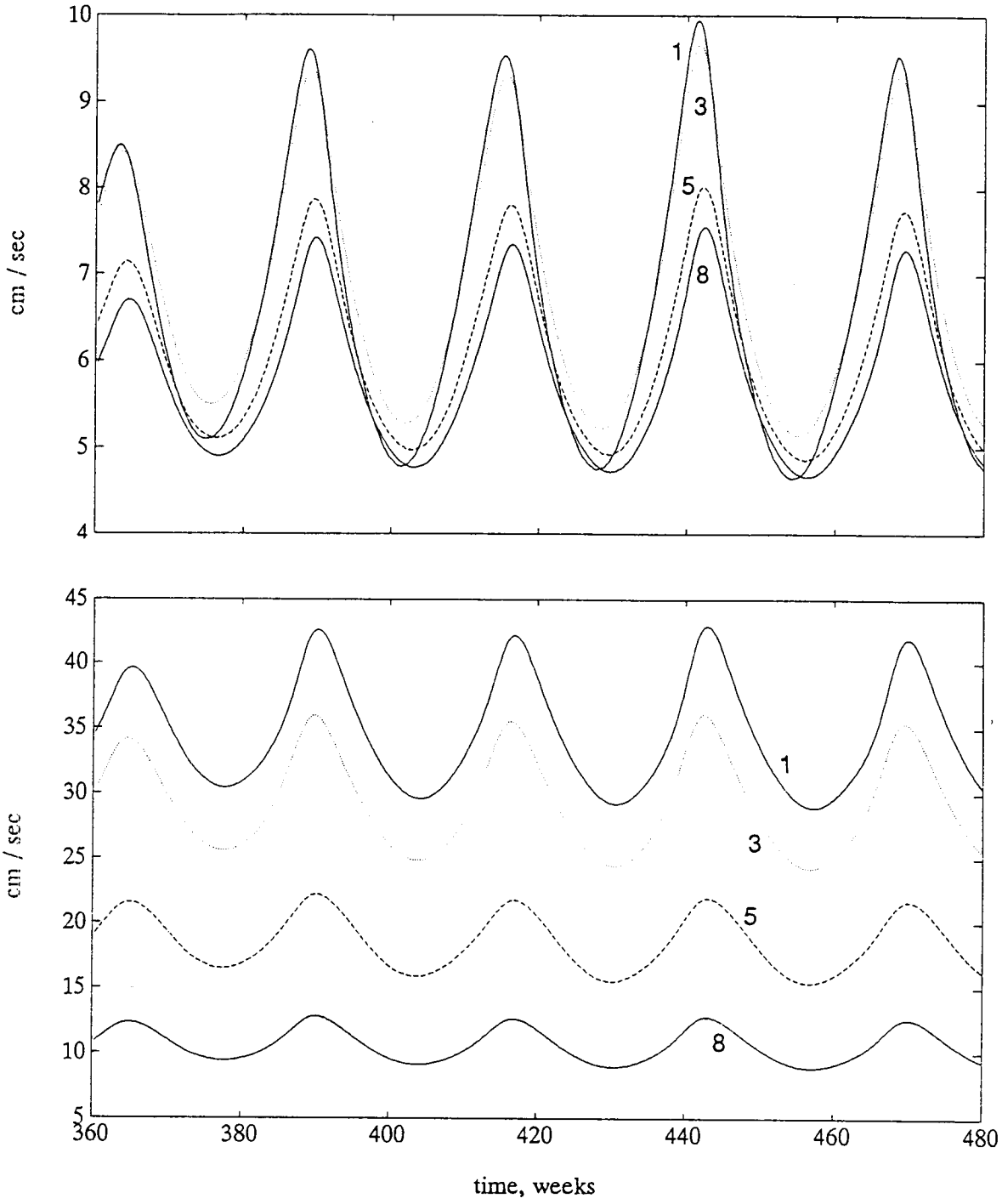

Figure 21. Model currents from a location near the western boundary of the Gulf, at 26°N, 96°W, 90 km to the west of Mooring P (Figure 14). The E-W component is above, N-S is below. These are shown for levels 1, 3, 5, and 8, as the model extends only to that level (1120 m) here. The time axis, based on the final 7 years of model runs, coincides with the earlier figures during the ring separation cycle.

VII. CONCLUSIONS

We have developed a numerical model of the Gulf of Mexico. In order to separate the inflow at the Straits of Yucatan from the direct forcing of the model, we moved the eastern boundary to the mid- Atlantic ridge. Thus the model includes the Caribbean Sea and the Gulf Stream formation region. The model is based on the Bryan-Cox, GFDL model that is well known in the modeling community. It is fully nonlinear, and the inclusion of 12 levels was intended to provide greater vertical resolution than any previous model of this part of the ocean.

Several realistic results were obtained; without any "tweaking" the model gives reassuringly good results. The major fluctuations have approximately the correct frequency content; rings separate from the Loop Current at periods of roughly 30 weeks and longer, even though the model is forced by steady winds.

The most obvious weakness in the present model is that the forcing results in currents that are weaker than observed and several classes of motion are therefore not found in the model as would be expected. Comparison between the model results and observations at moorings, and with the published interpretations of Lewis and Kirwan (1987) and of Hamilton (1990) show remarkably good physical agreement except for the speeds' being too weak.

The improved vertical resolution of this model has allowed us to examine in detail the kinematics of the process by which a warm-core ring separates from the Loop Current. These results have therefore provided insights into a dominant oceanic process. From examining the ring separation process in detail we can see that the old analogy of a "rope-like" ring growth and separation is misleading. The ring separation process is long and gradual, and it is difficult to point to any time in the cycle and say precisely that "the ring just separated." The answer to the question, "in the ocean, just how does the rope get cut?" is that the rope-like model is simply inadequate.

In the deep part of the model we find a rich field of eddy-like motions; these are topographic Rossby waves, not the highly nonlinear type of behavior associated with the major anticyclonic rings. These motions are forced by the upper rings, but travel slightly faster and are not phase locked to them.

A most interesting model observation is associated with southerly flow in the deep part of Yucatan Channel. This flow occurs when the Loop Current is positioned so that the southerly-flowing portion of the current is directly above the deep part of Yucatan Channel. It appears that the southerly-flowing portion of the Loop Current is able to transfer momentum downward to the bottom flow over some parts of the Loop Current cycle. When the Loop Current (in the model) moves father to the north, the southerly flowing part of the high speed current is no longer above the deep channel, and the deepest flow is then to the north.

The model is being modified (by our colleague J.C. Evans) to increase the inflow at the eastern boundary, in keeping with the recent discovery that there is northward flow along the coast of South America. That part of the inflow was not accounted for by our wind-curl-only forcing.

The next step is to add time-varying winds. It seems prudent to increase the degree of complexity slowly, to allow us to analyze the results from the least complex forcing as well as possible in order to understand the energetic mechanisms operating

in the model. Furthermore, the model has not yet been forced with winds having energy in the 3-10 day band typically associated with coastal currents, so this general class of motion is, of course, not in the present results.

While we are generally delighted with the model results, in some ways it is very frustrating to note that the basic limitation in this work is not the physics contained in the model but the cost to implement it, both in computer time and in human resources. The present so-called "high resolution" model uses a 1/4° grid. It is extremely desirable to perform experiments with higher resolution, as it is well known that 1/4 ° is a severe compromise between resolution and cost.

BIBLIOGRAPHY

Auer, S. J. 1987. Five-year climatological survey of the Gulf Stream system and its associated rings. Jour. Geophys. Res. 92: 11,709-11,726.

Bryan, K., and M. D. Cox. 1968. A nonlinear model of an ocean driven by wind and differential heating: Parts I and II. J. Atmos. Sci. 25:945-978.

Cox, M. D. 1970. A mathematical model of the Indian Ocean. Deep-Sea Res. 17:47-75.

Cox, M. D. 1975. A baroclinic numerical model of the world ocean: preliminary results. Numerical Models of Ocean Circulation, Nat. Acad. of Sciences. Washington, D.C. pp. 107-120.

Cox, M. D. 1984. A primitive equation three-dimensional model of the ocean. GFDL Ocean Group Tech. Rept. No. 1, GFDL/NOAA, Princeton University, Princeton, 250 pp.

Cox, M. D. 1985. An eddy resolving numerical model of the ventilated thermocline, J. Phys. Oceanog. 15:1312-1324.

Cox, M. D. 1987. An eddy resolving model of the ventilated thermocline: time dependence. J. Phys. Oceanogr. 17:1044-1056

Csanady, G. T. 1979. The birth and death of a warm core ring. J. Geophys. Res. 84:777-780.

Cushman-Roisin, B. 1989. On the role of filamentation in merging of anticyclonic lenses. J. Phys. Oceanogr. 19:253-258.

Davey, M. K., and P. D. Killworth. 1984. Isolated waves and eddies in a shallow water model. J. Phys. Oceanogr. 14:1047-1064.

Elliot, B. A. 1982. Anticyclonic rings in the Gulf of Mexico. J. Phys. Oceanogr. 12(11):1292-1309.

Evans, J. C., D. B. Haidvogel, and W. R. Holland. 1987. A review of numerical ocean modeling (1983-1986): mid-latitude mesoscale and gyre-scale. R. Geophys. 25(2):235-244.

Flierl, G. R. 1984. Rossby wave radiation from a strongly nonlinear warm eddy, J. Phys. Oceanogr. 14:47-58.

Fofonoff, N. P. 1981. The Gulf Stream system, pp. 112-139. In Evolution of Physical Oceanography. B.A. Warren and Carl Wunsch, Eds. MIT Press, Cambridge, Mass.

Hamilton, P. 1990. Deep currents in the Gulf of Mexico. J. Phys. Ocean. 20:1087-1104.

Hellerman, S., and M. Rosenstein, 1983. Normal monthly wind stress over the world ocean with error estimates, J. Phys. Oceanogr., 13, 1093-1104.

Hurlburt, H.E., and J.D. Thompson. 1980. A numerical study of Loop Current intrustions and eddy shedding, J. Phys. Oceanogr. 10:1611-1651.

Hurlburt, H. E., and J. D. Thompson. 1982. The dynamics of the Loop Current and shed eddies in a numerical model of the Gulf of Mexico, pp. 243-298. In Hydrodynamics of Semi-enclosed Seas. J.C.J. Nihoul (Ed.) Elsevier, New York,.

Ikeda, M., and J. R. Apel. 1981. Mesoscale eddies detached from spatially growing meanders in an eastward flowing oceanic jet using a two-layer quasi-geostrophic model, J. Phys. Oceanogr. 11:1638-1661.

Killworth, P. D., N. Paldor, and M. E. Stern. 1984. Wave propagation and growth on a surface front in a two-layer geostrophic current, J. Marine Res. 42:761-785.

Krauss, W., R. Doscher, A. Lehmann, and T. Viehoff. 1990. On eddy scales in the eastern and northern North Atlantic Ocean as a function of latitude. J. Geophys. Res. 95:18,049-18,056.

Levitus, S., 1982. Climatological Atlas of the World Ocean. NOAA Professional Paper 13. U.S. Dept. of Comm., Rockville, Md. 173 pp.

Lewis, J. K., and A. D. Kirwan. 1987. Genesis of a Gulf of Mexico ring as determined from kinematic analysis. J. Geophys. Res. 92:11,727-11,740.

Maul, G. A. 1977. The annual cycle of the Gulf Loop Current, Part I: Observations during a one-year time series, J. Mar. Res. 35(1):29-47.

Maul, G. A., D. A. Mayer, and S. R. Baig. 1985. Comparison between a continuous three-year current meter observation at the sill of the Yucatan Strait, satellite measurements of Gulf Loop Current area, and regional sea level. J. Geophys. Res. 90:9089-9096.

Molinari, R. L., S. Baig, D. Behringer, G. Maul, and R. Legeckis. 1977. Winter intrusions of the Loop Current, Science 198:505-507.

Molinari, R. L., M. Spillane, I. Brooks, D. Atwood, and C. Duckett, 1981. Surface currents in the Caribbean Sea as deduced from Lagrangian observations. J. Geophys. Res., 86: 6537-6542.

Nof, D. 1983. On the migration of isolated eddies with application to Gulf Stream rings, J. Mar. Res. 41:399-425.

Nof, D., 1988. The fusion of isolated nonlinear eddies, J. Phys. Oceanogr. 18:887-905.

Nowlin, W. D., Jr. 1972. Winter circulation patterns and property distributions. In Contributions on the Physical Oceanography of the Gulf of Mexico. L.R. A. Capurro and J.L. Reid, Eds. Texas A & M Oceanographic Studies, Gulf Publ. Co., Houston, Tx. pp 3-53.

Pratt, L. J., and M. E. Stern. 1986. Dynamics of potential vorticity fronts and eddy detachment, J. Phys. Oceanogr., 16:1099-1118.

Richardson, P. L. 1980. Gulf Stream ring trajectories, J. Phys. Oceanogr. 10:90-104.

Richardson, W. S., W. J. Schmitz, Jr., and P. P. Niiler. 1969. The velocity structure of the Florida current from the Straits of Florida to Cape Fear. Deep-Sea Res. 15(Suppl.):225-231.

Schmitz, Jr., W. J., and P. L. Richardson. 1991. On the sources of the Florida Current. Deep-Sea Res. 38(Suppl.1):S379-S409.

Schott, F. A., T. N. Lee, and R. Zantopp. 1988. Variability of structure and transport of the Florida Current in the period range of days to seasonal. J. Phys. Oceanogr. 18:1209-1230.

Semtner, A. J. 1986a. Finite-difference formulation of a world ocean model. Proceedings of the NATO Advanced Study Institute on Advanced Physical Oceanographic Numerical Modelling. D. Reidel Publishing Co., Dordrecht.

Semtner, A. J. 1986b. History and methodology of modelling the circulation of the world ocean. Proceedings of the NATO Advanced Study Institute on Advanced Physical Oceanographic Numerical Modelling. D. Reidel Publishing Co., Dordrecht.

Semtner, A. J., Jr., and R. M. Chervin. 1988. A simulation of the Global Ocean Circulation with Resolved Eddies. J. Geophys. Res. 93:15,502-15,522.

Sturges, W. 1991. An Estimate of the Spectrum of Loop Current Variability from Gappy Data. J. Phys. Oceanogr. In press.

Sturges, W., and J. P. Blaha. 1976. A western boundary current in the Gulf of Mexico. Science 192:367-369.

SAIC. 1986. Gulf of Mexico physical oceanography program, year 4, volume II: Technical Report. Science Applications International Corporation/MMS 87-0007, U.S. Dept. of the Interior, Minerals Mgmt. Service, Gulf of Mexico OCS Regional Office, New Orleans, La.

SAIC. 1987. Gulf of Mexico physical oceanography program, years 1 and 2, volume II: Technical Report. Science Applications International Corporation/ MMS 85-0094. U.S. Dept. of the Interior, Minerals Mgmt. Service, Gulf of Mexico OCS Regional Office, New Orleans, La.

Vukovich, F. M., and B. W. Crissman. 1986. Aspects of warm rings in the Gulf of Mexico. J. Geophys. Res., 91(C2):2645-2660.

APPENDIX A

STREAMFUNCTION MAPS FROM MODEL RUN

The following figures show maps of the streamfunction every 4 weeks, from week 148-179 and week 216-304. There is a change in the appearance of the plots at week 215, at which point we were able to make the plots at FSU. Prior to those, the plots were made at NCAR. The difficulty was not with producing the maps, but in the very large amount of data transfer necessary. In the early model runs, output tapes were mailed to NCAR and the plots made there. The break between weeks 179 and 215 is the result of an apparent loss of one tape in the mail. Except for this break, the model output is saved at weekly steps, even though the plots shown here are nominally every 4 weeks.

Figures A-1 - A-33: Streamfunction maps from model run. The time steps shown (e.g. week 148.) are measured during runs made after the initial 4 year spinup at coarse resolution.

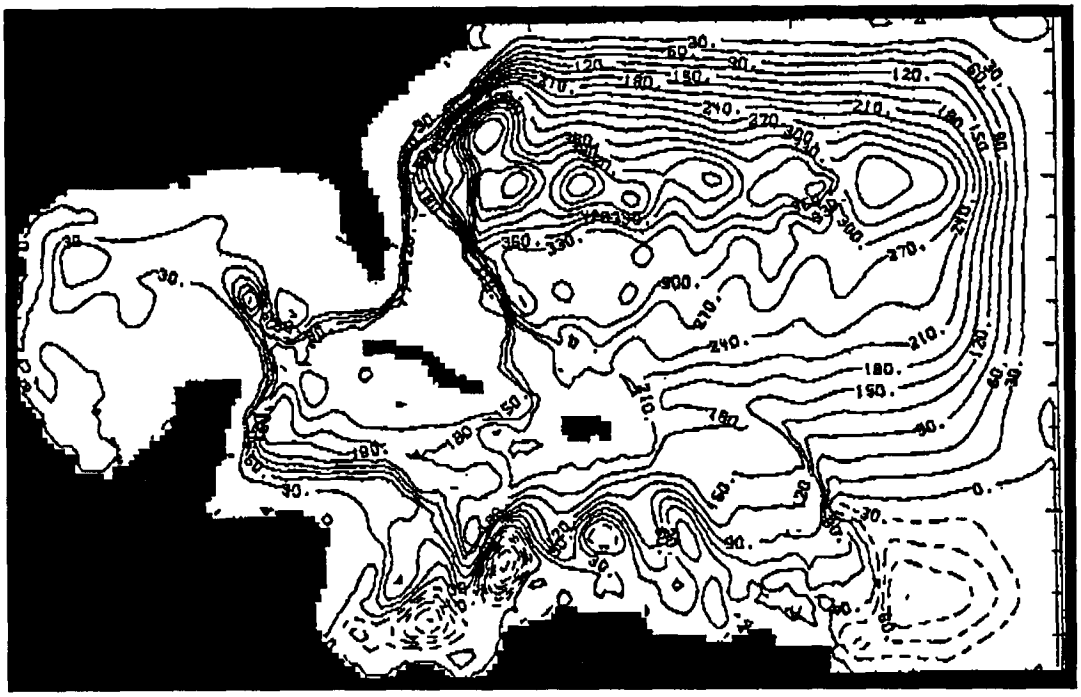

148 weeks

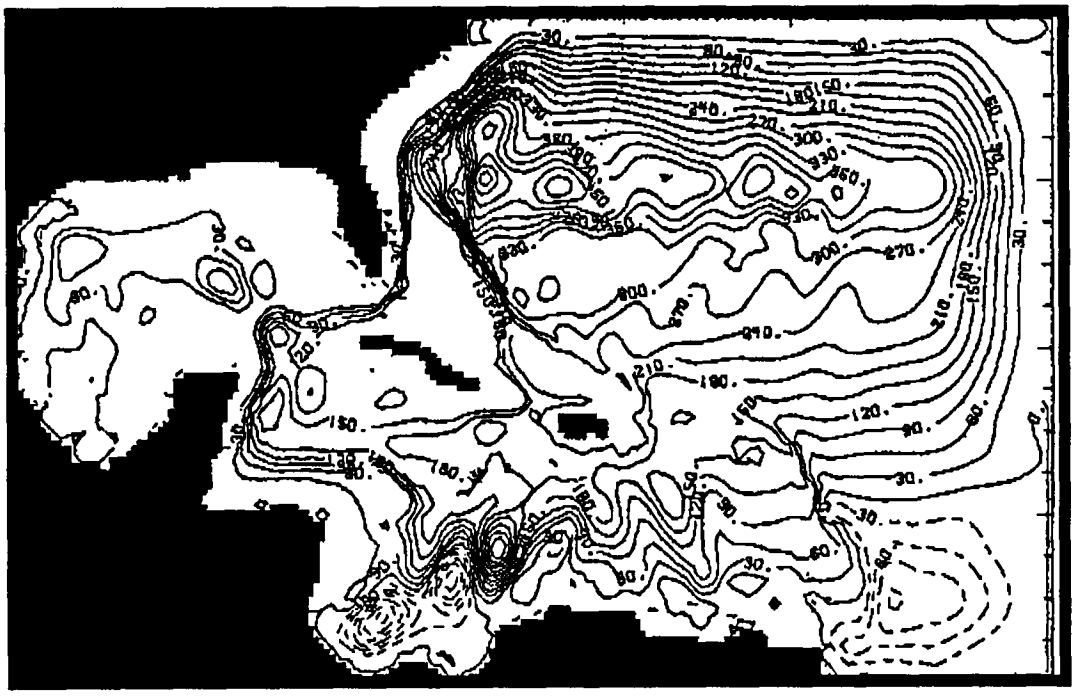

152 weeks

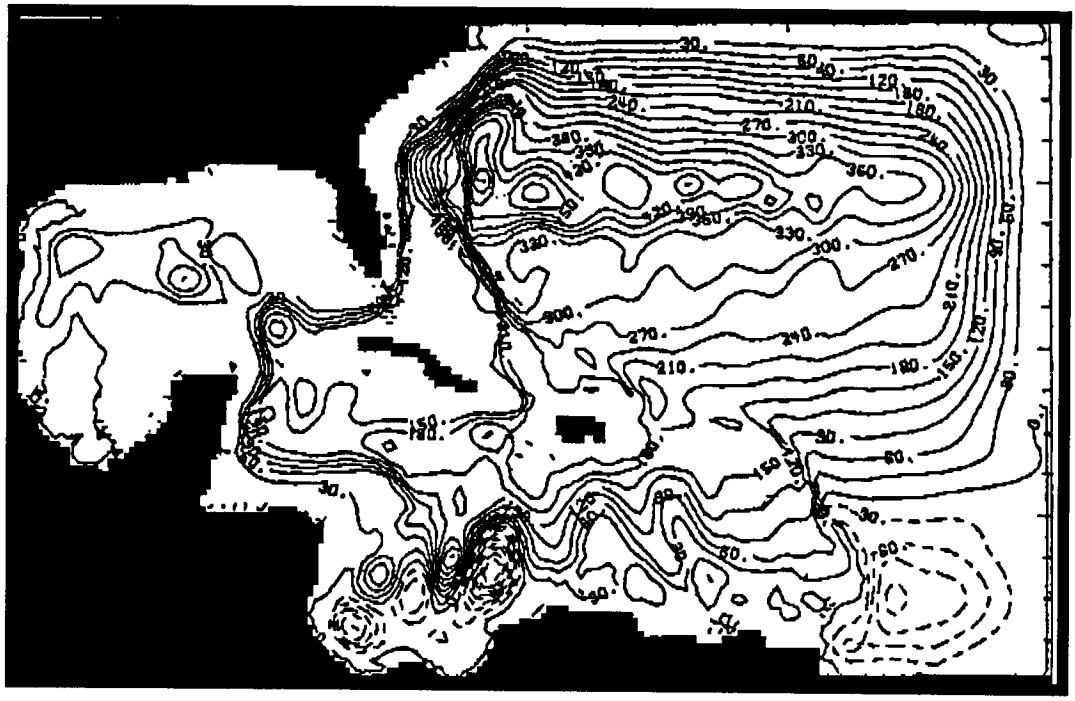

156 weeks

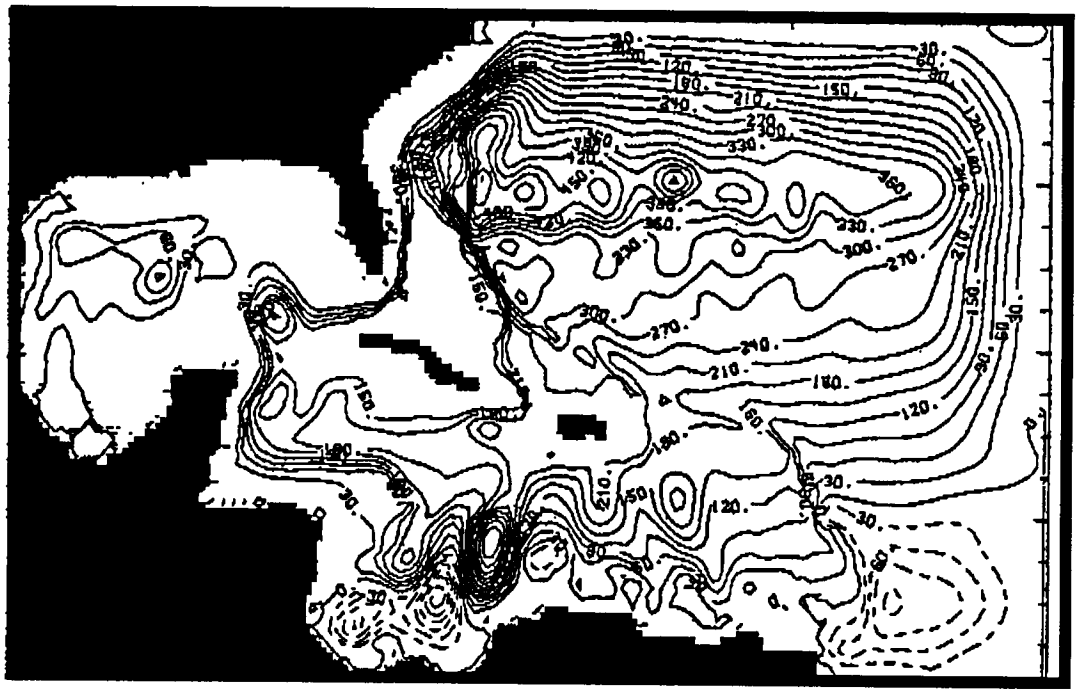

160 weeks

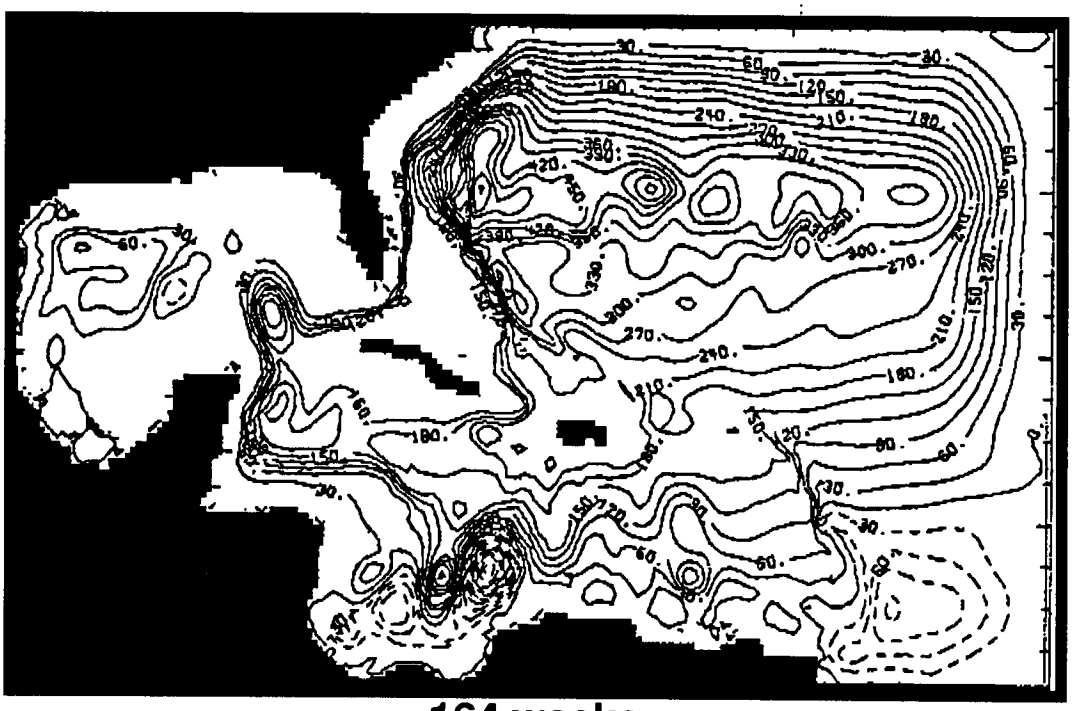

164 weeks

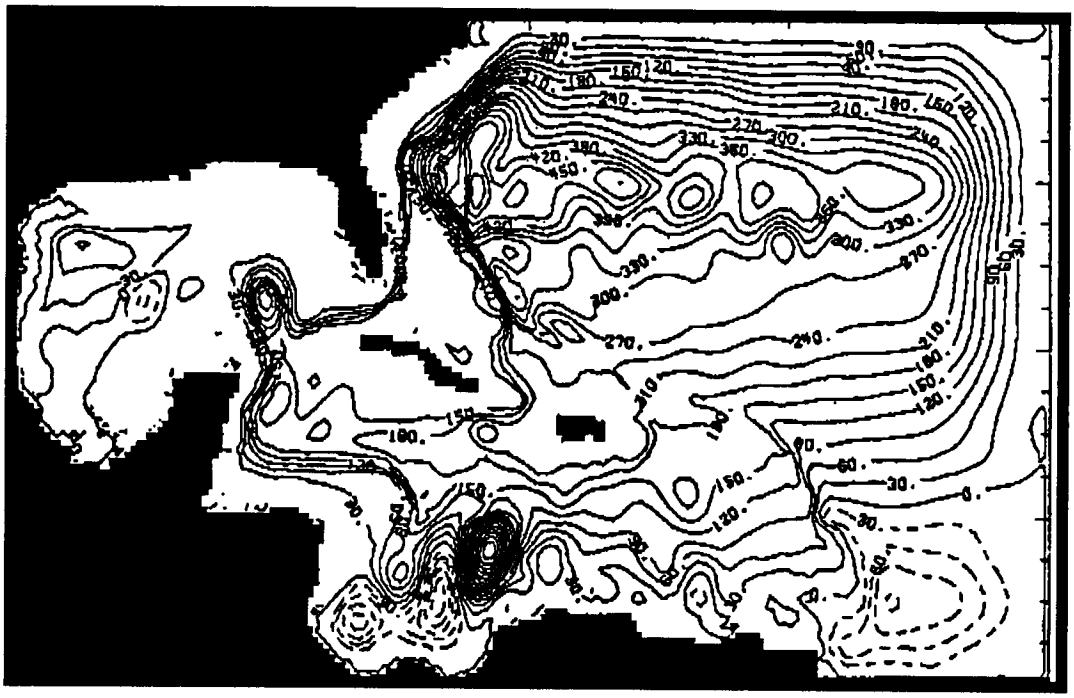

168 weeks

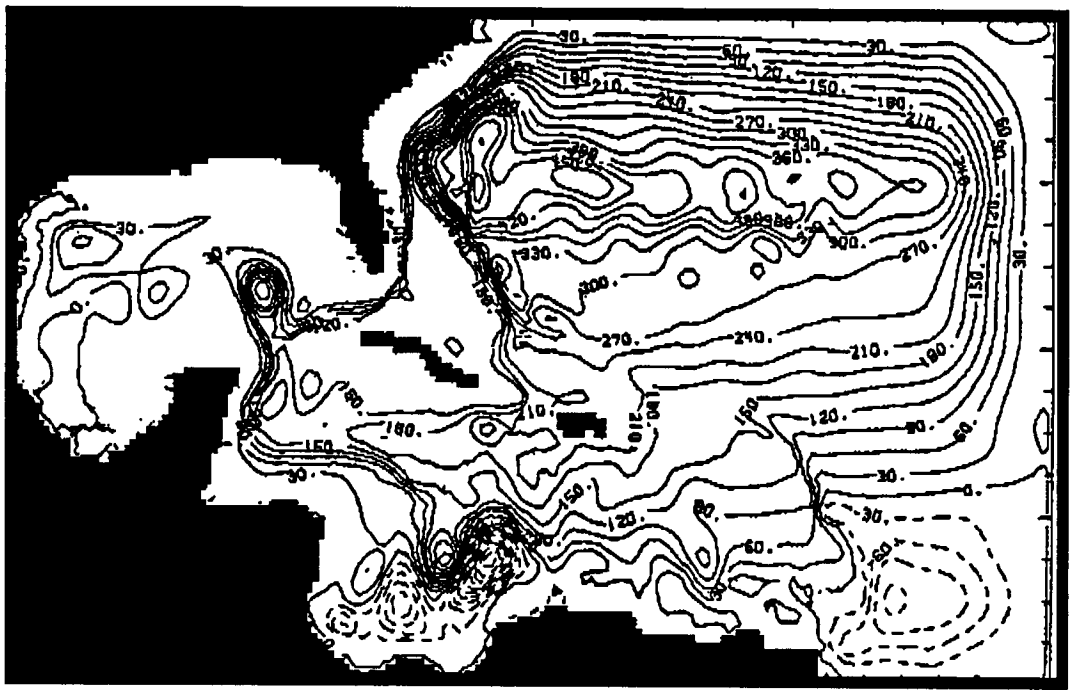

172 weeks

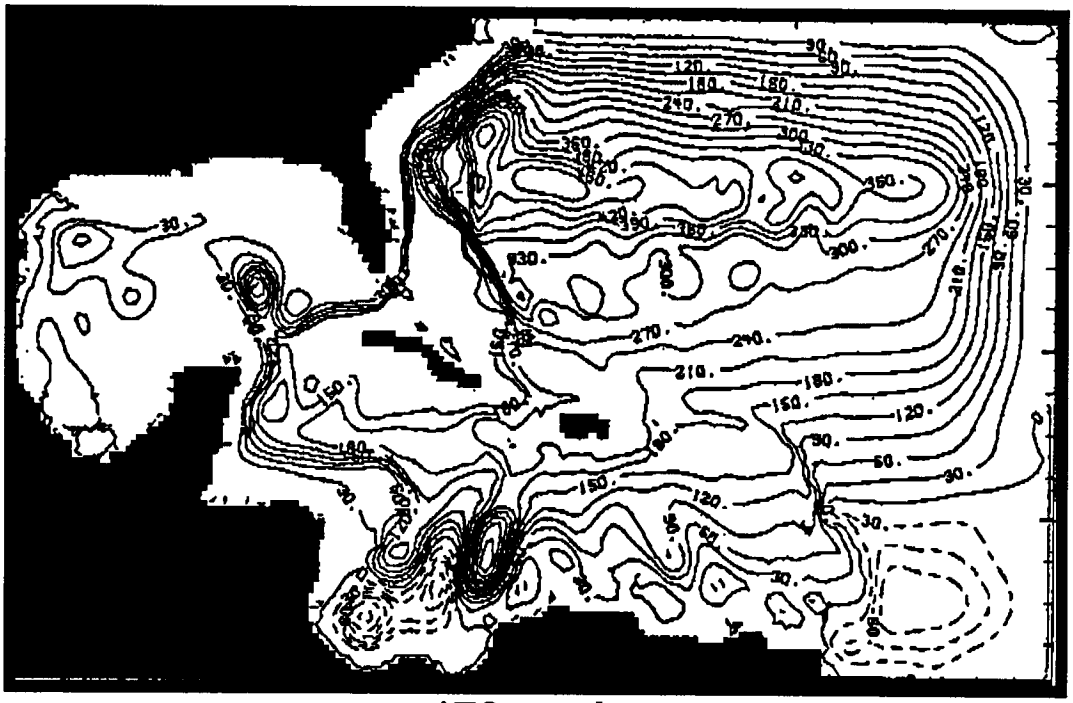

176 weeks

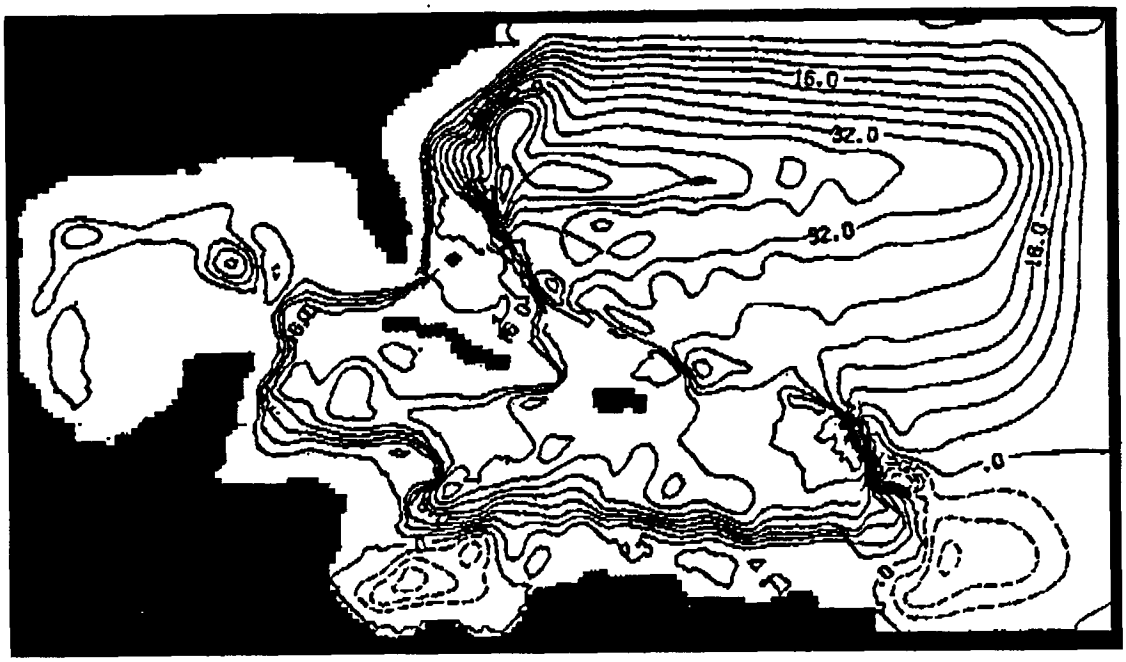

216 weeks

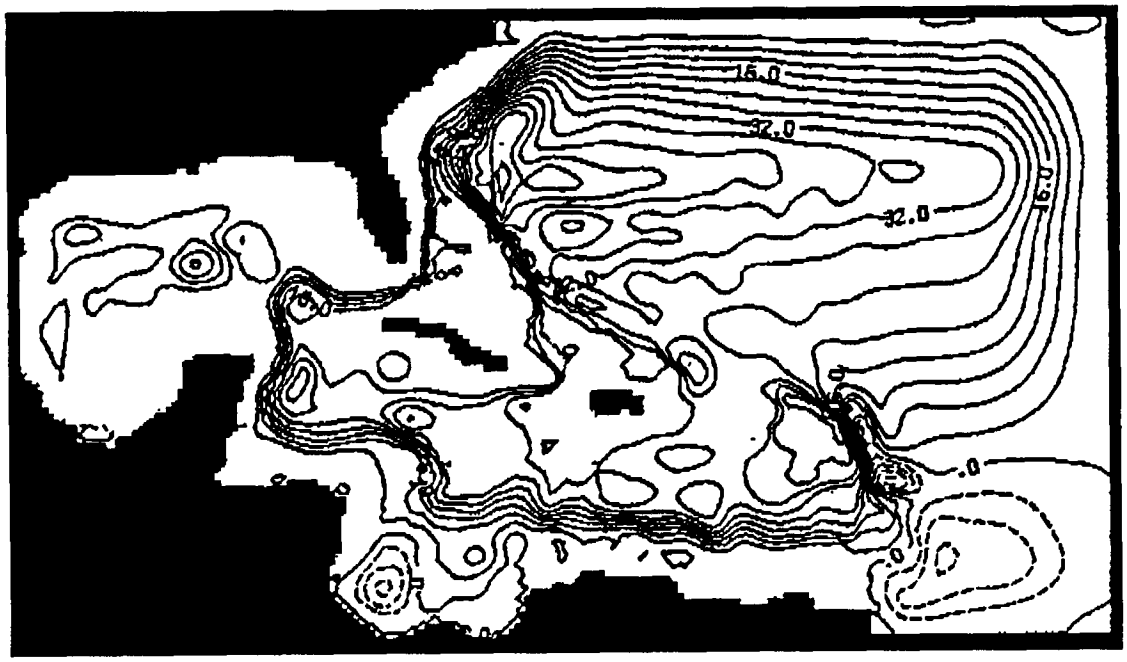

220 weeks

224 weeks

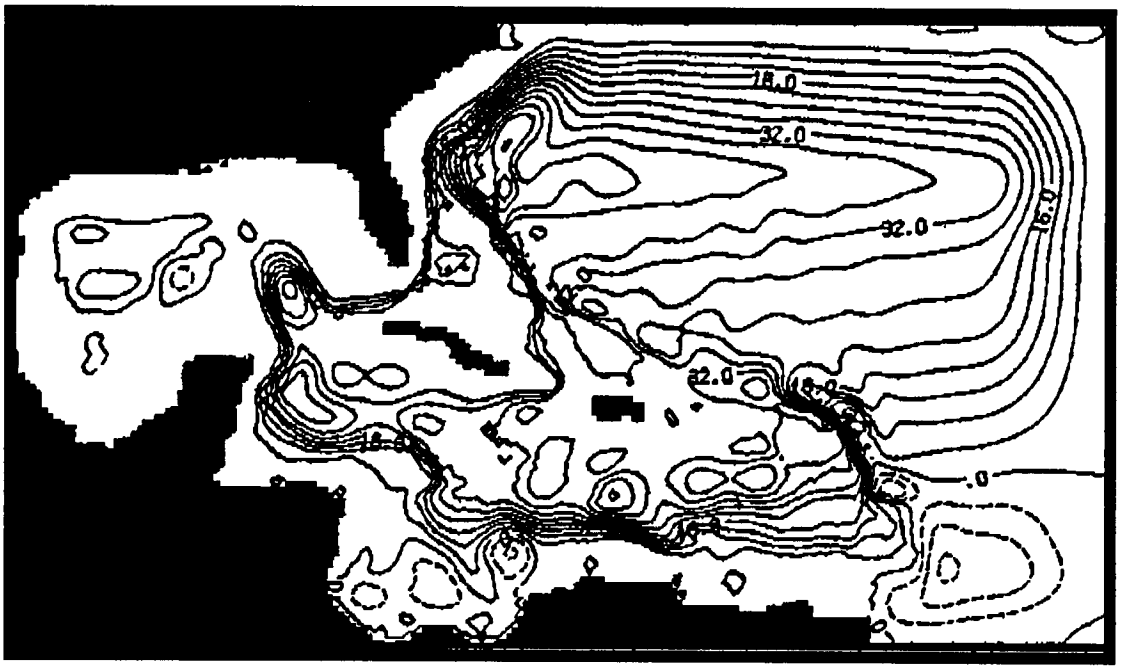

228 weeks

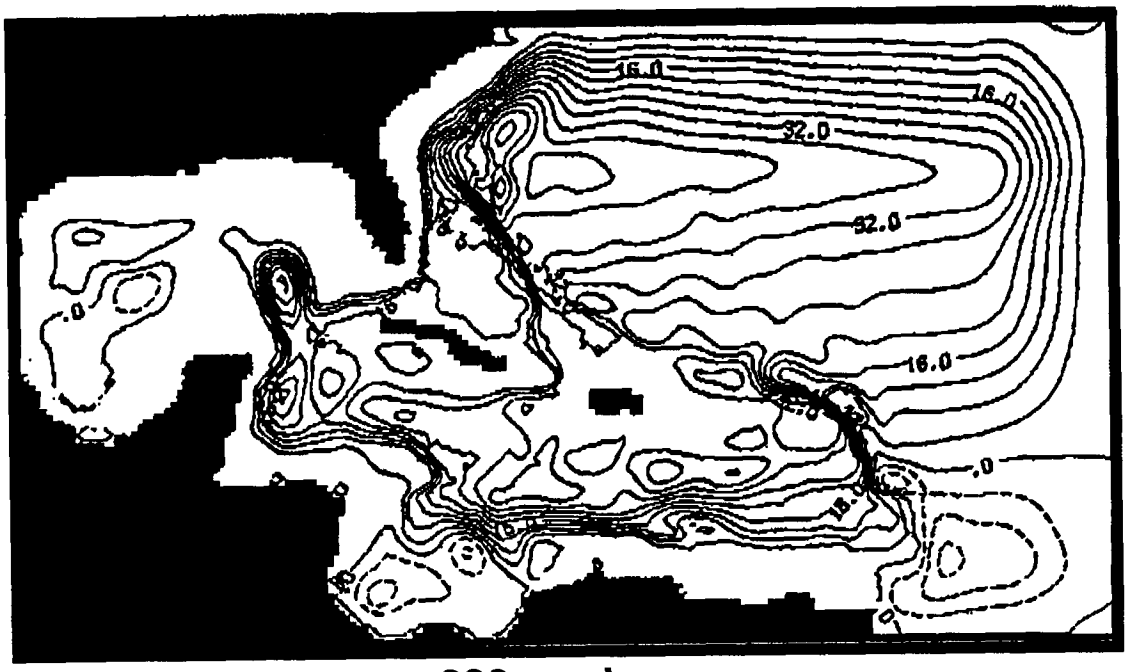

232 weeks

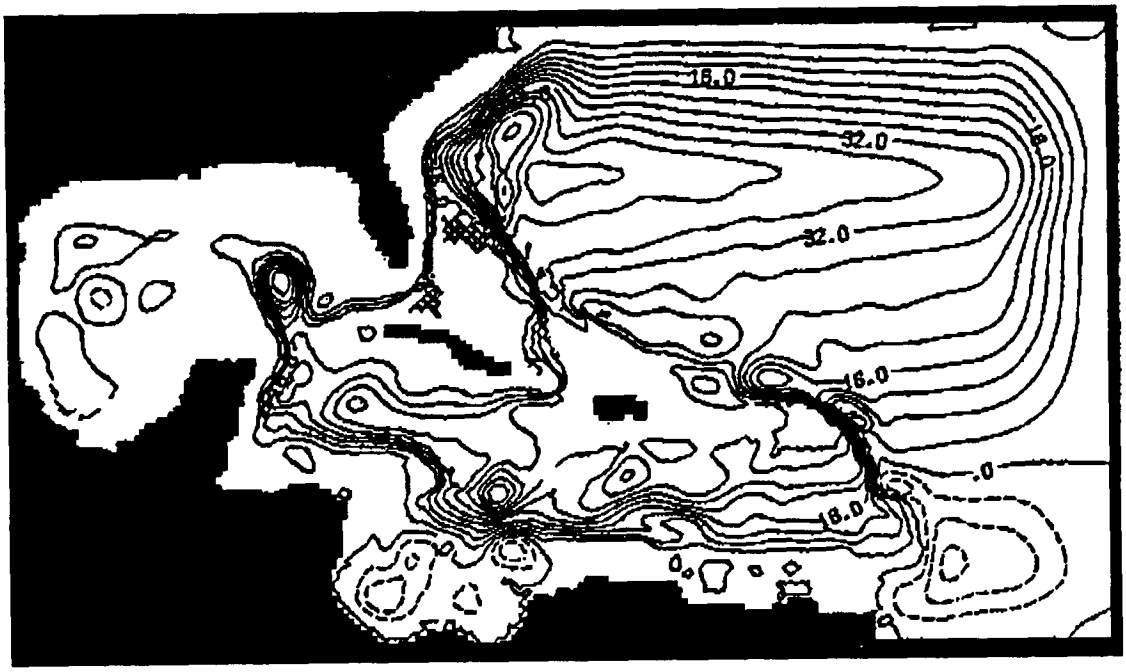

236 weeks

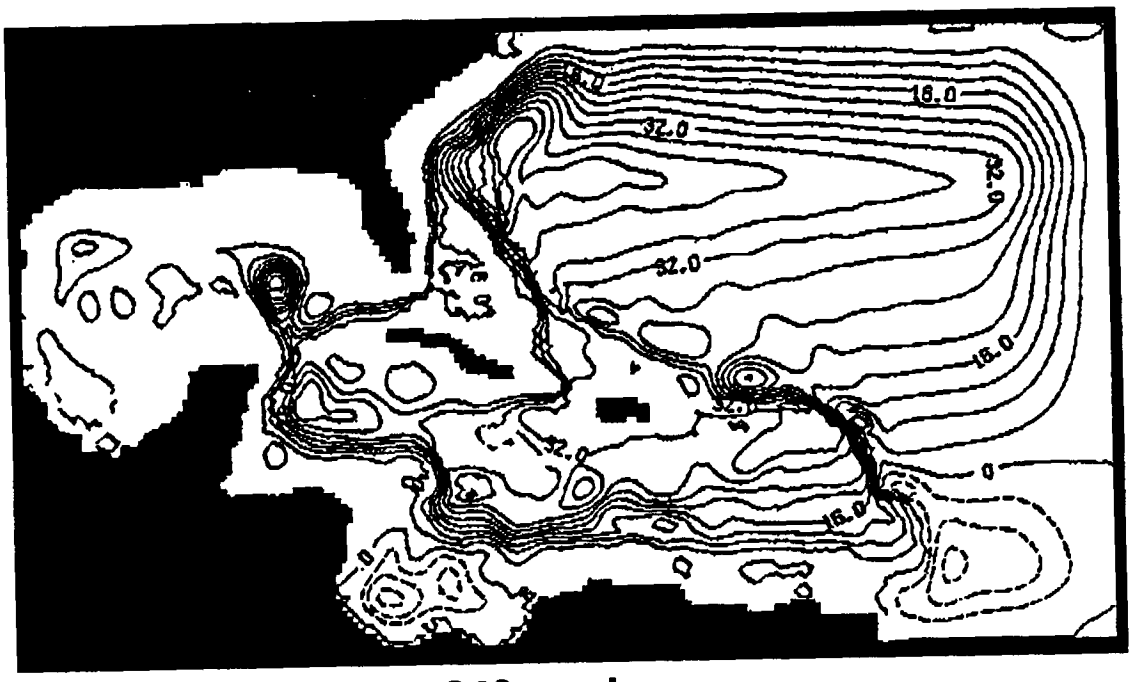

240 weeks

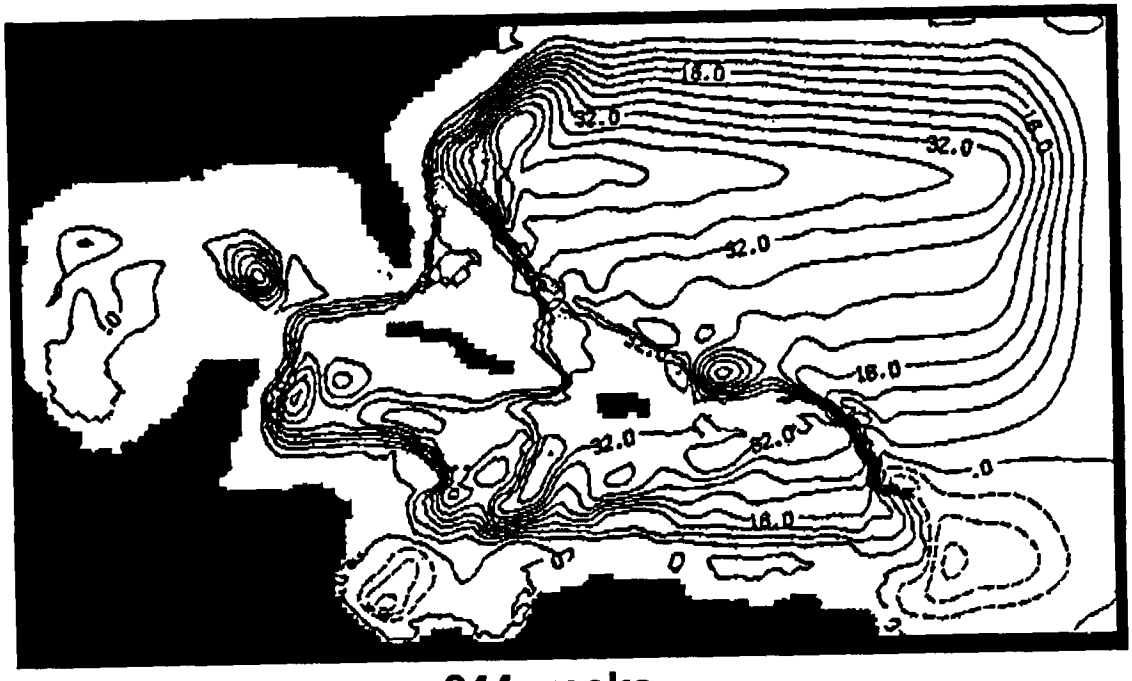

244 weeks

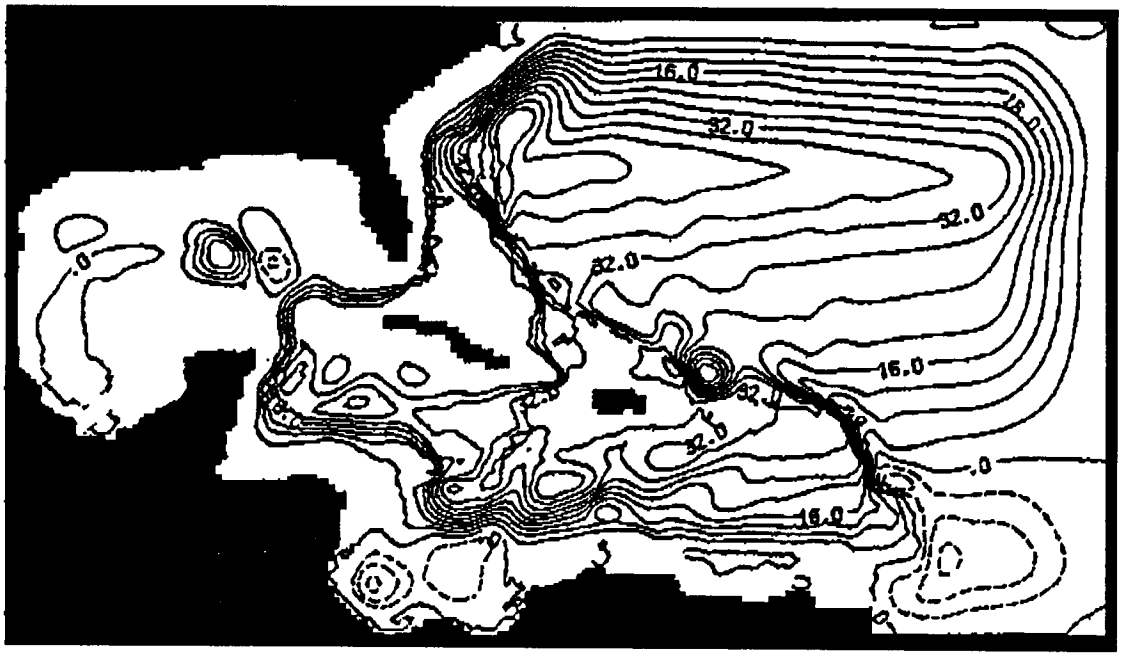

248 weeks

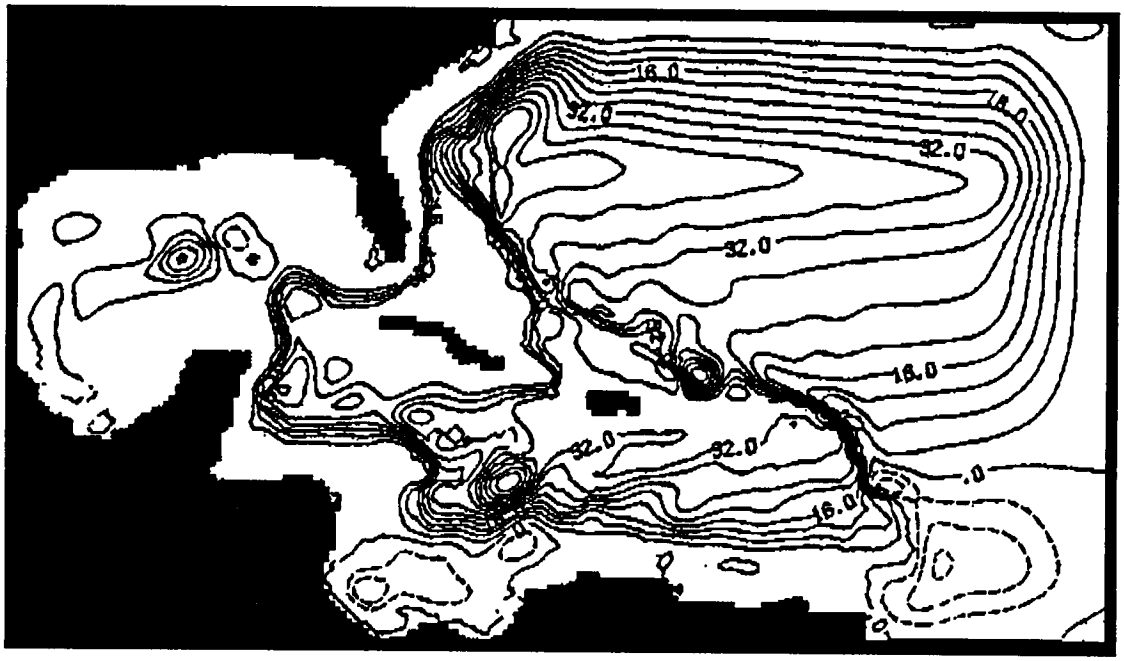

252 weeks

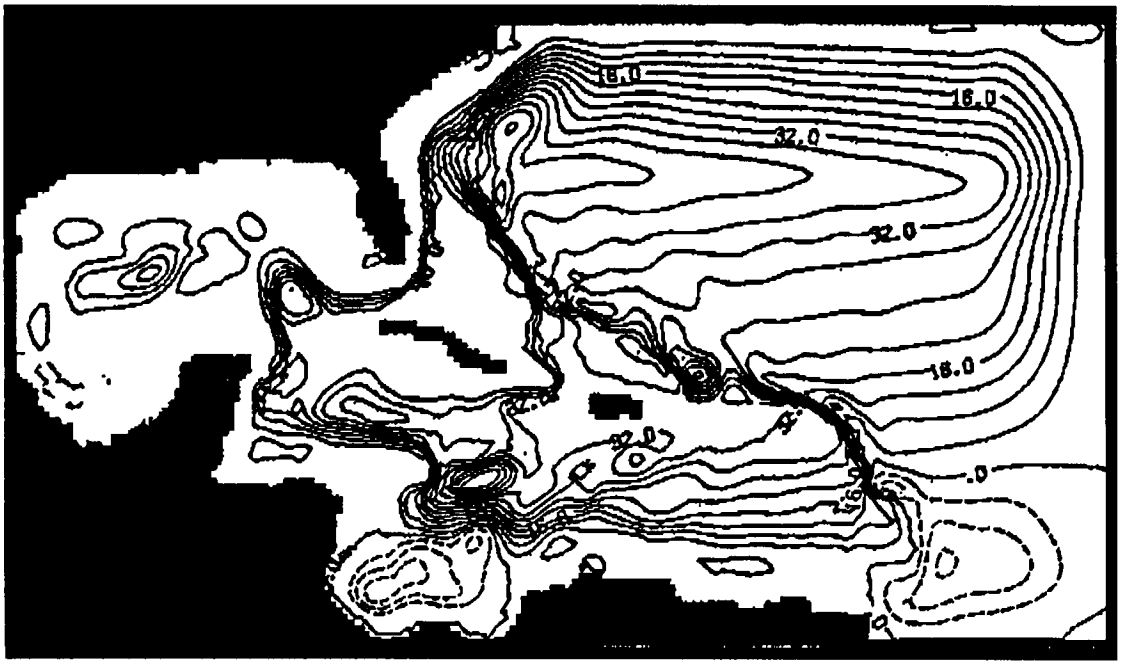

256 weeks

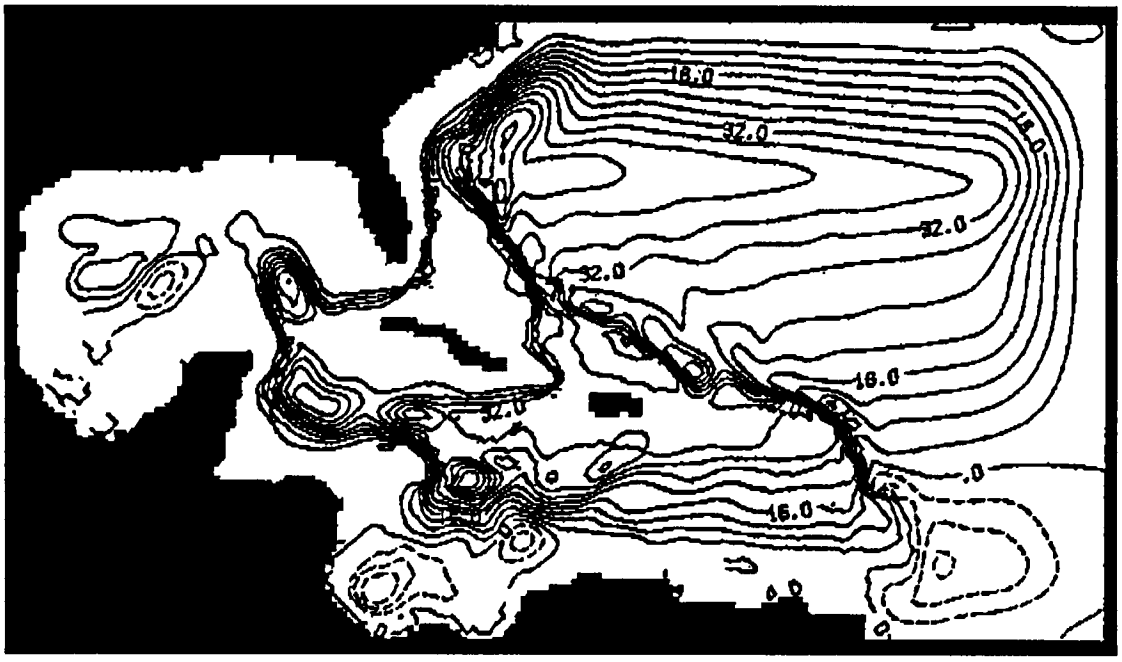

260 weeks

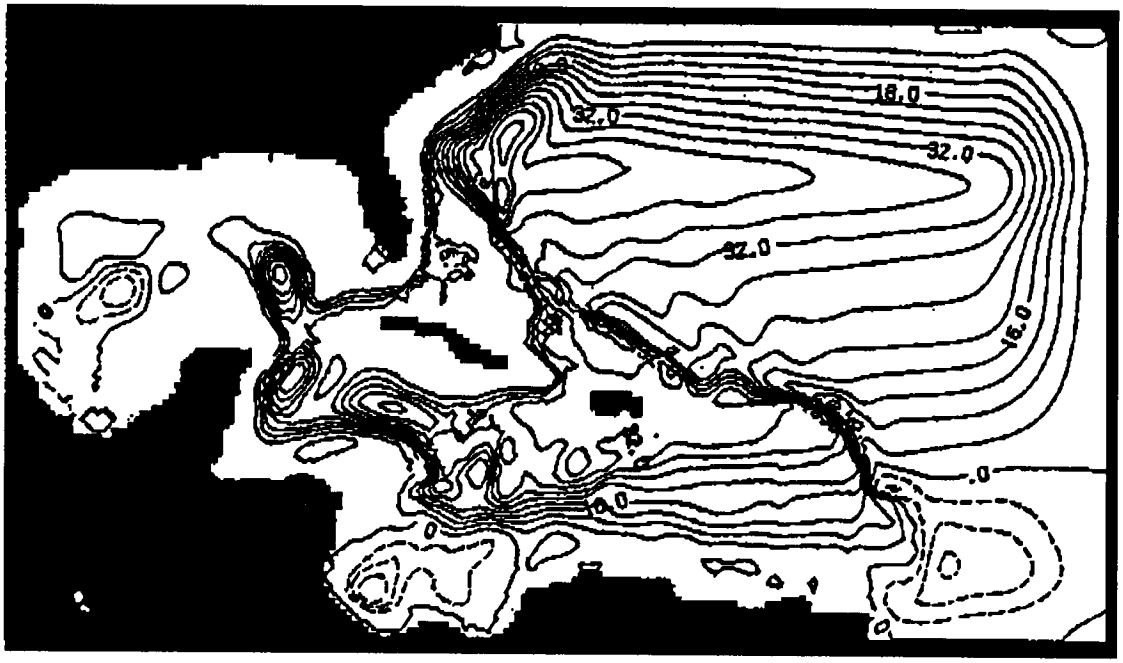

264 weeks

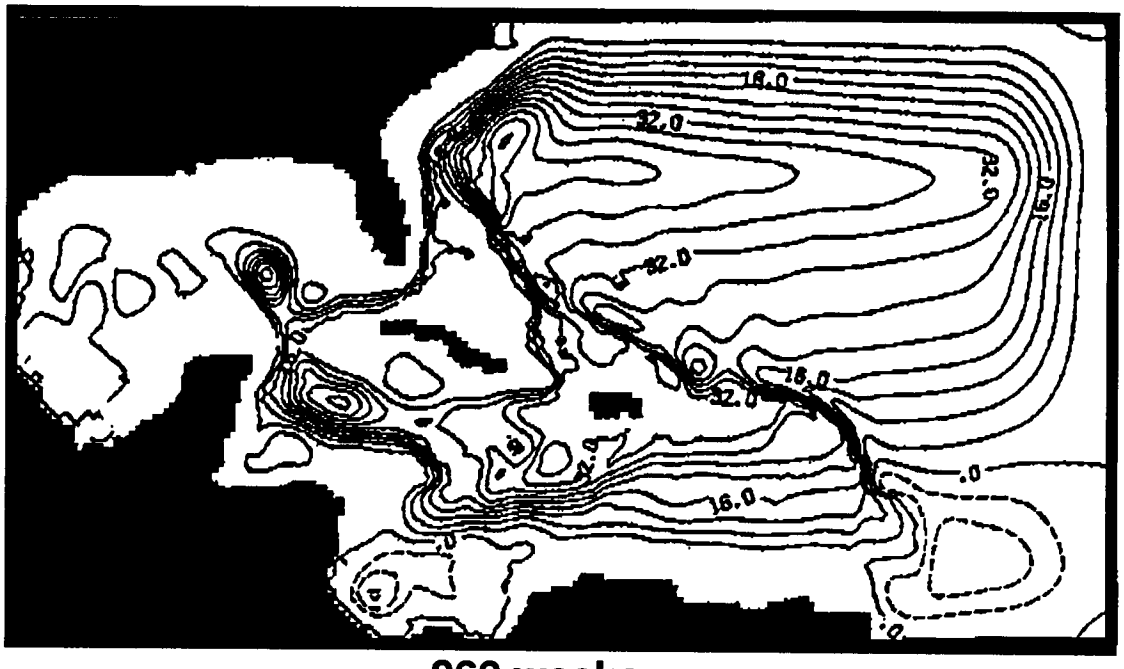

268 weeks

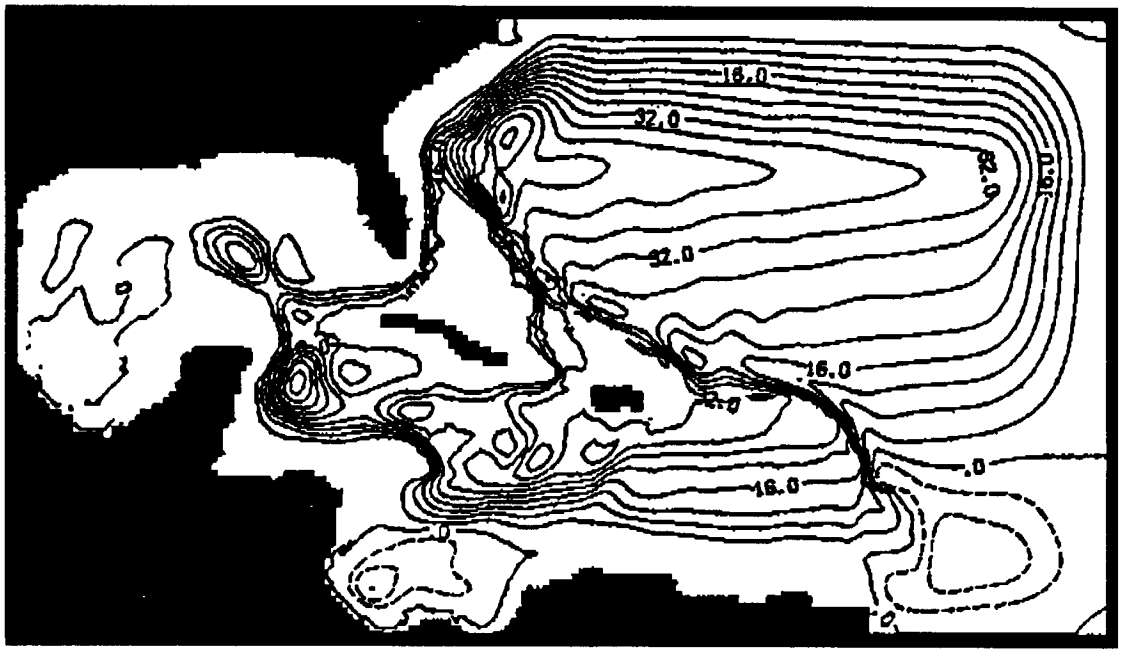

272 weeks

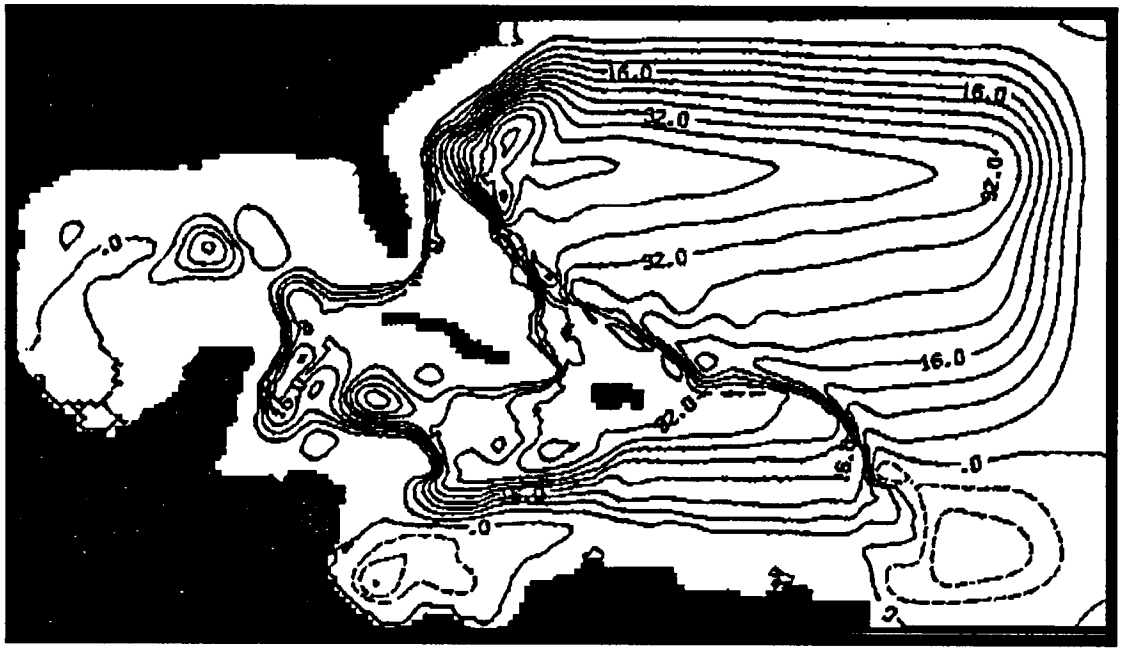

276 weeks

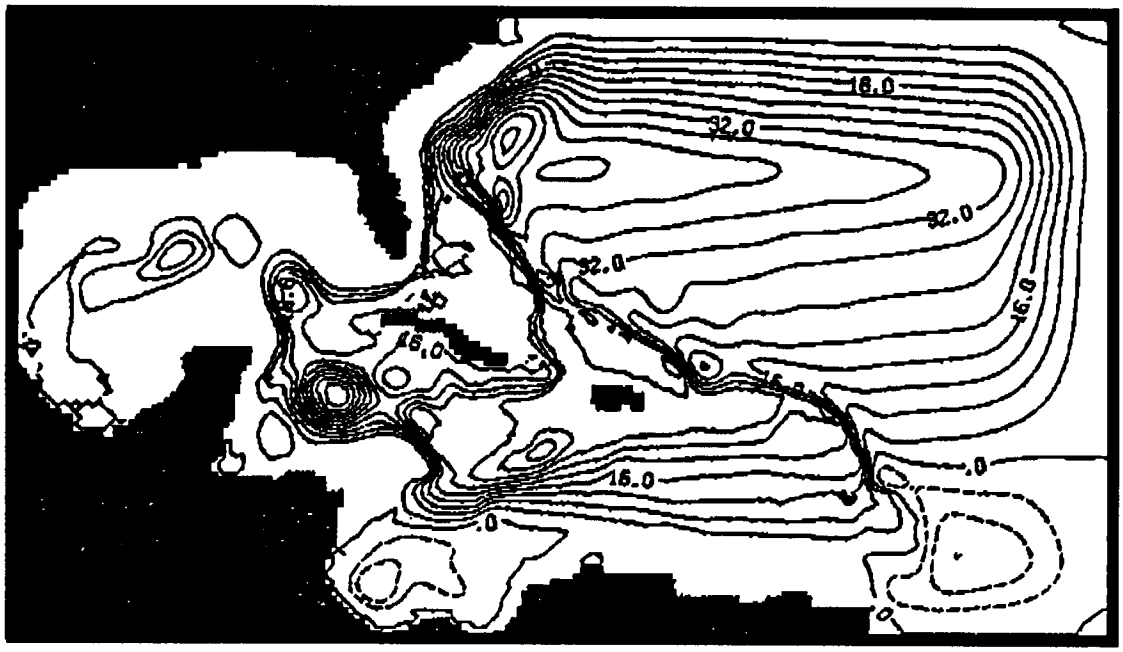

280 weeks

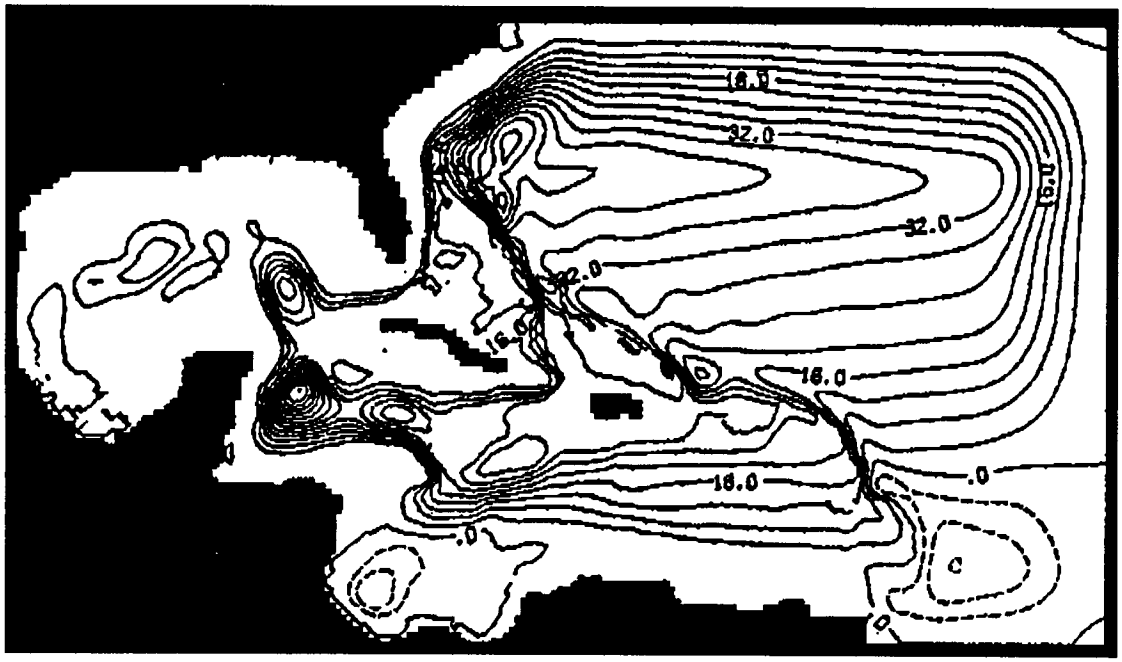

284 weeks

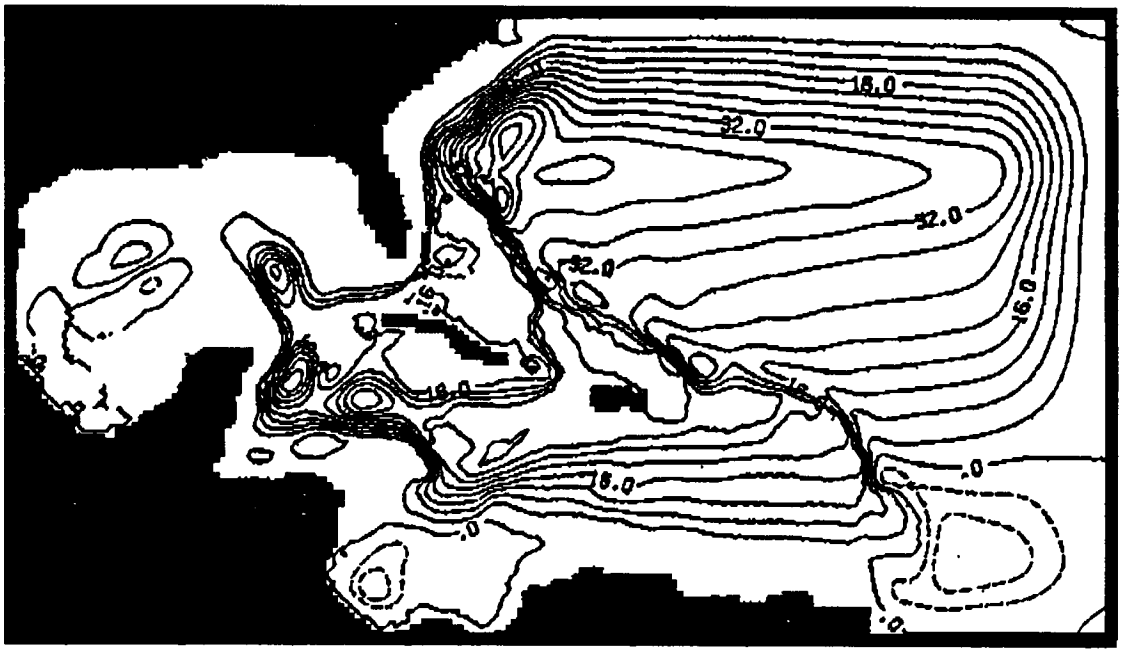

288 weeks

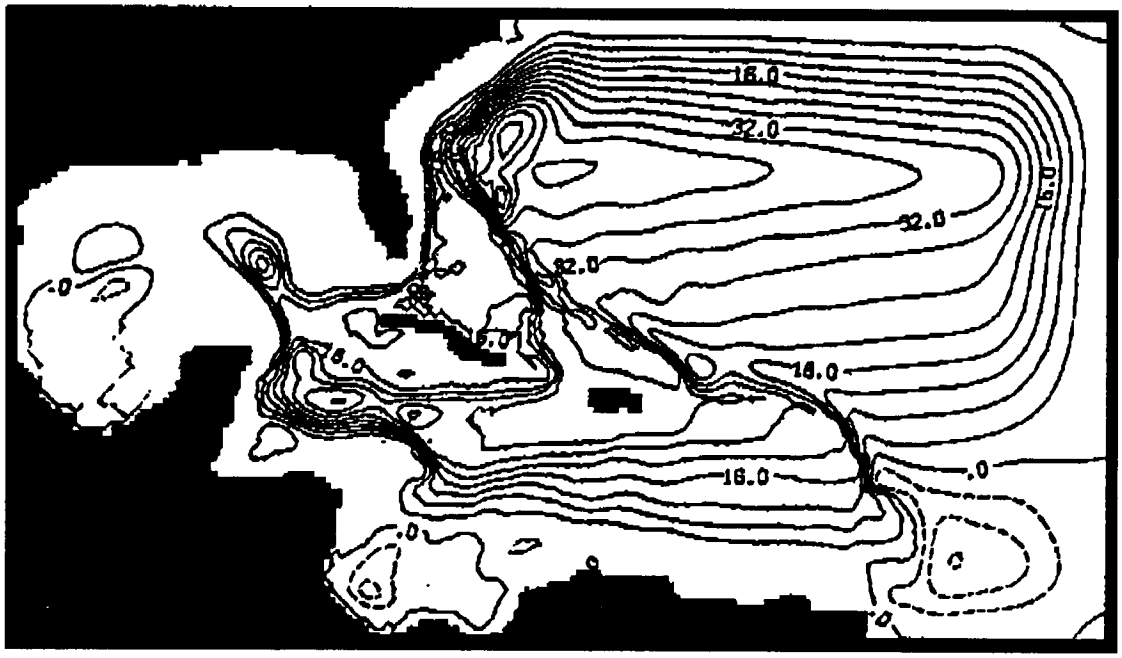

292 weeks

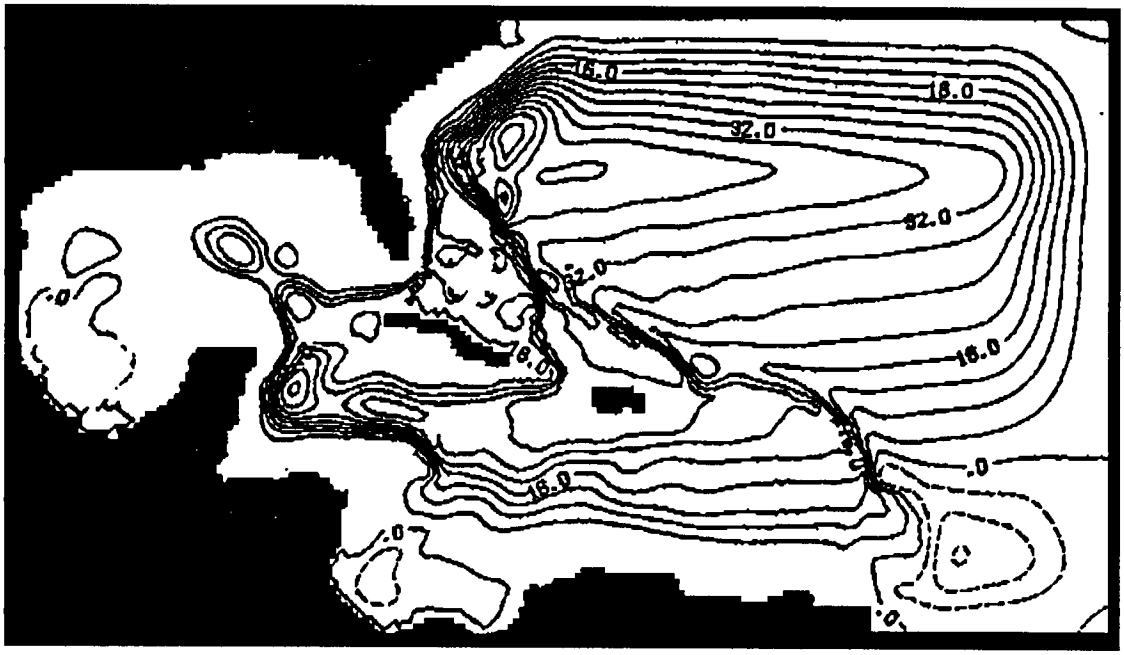

296 weeks

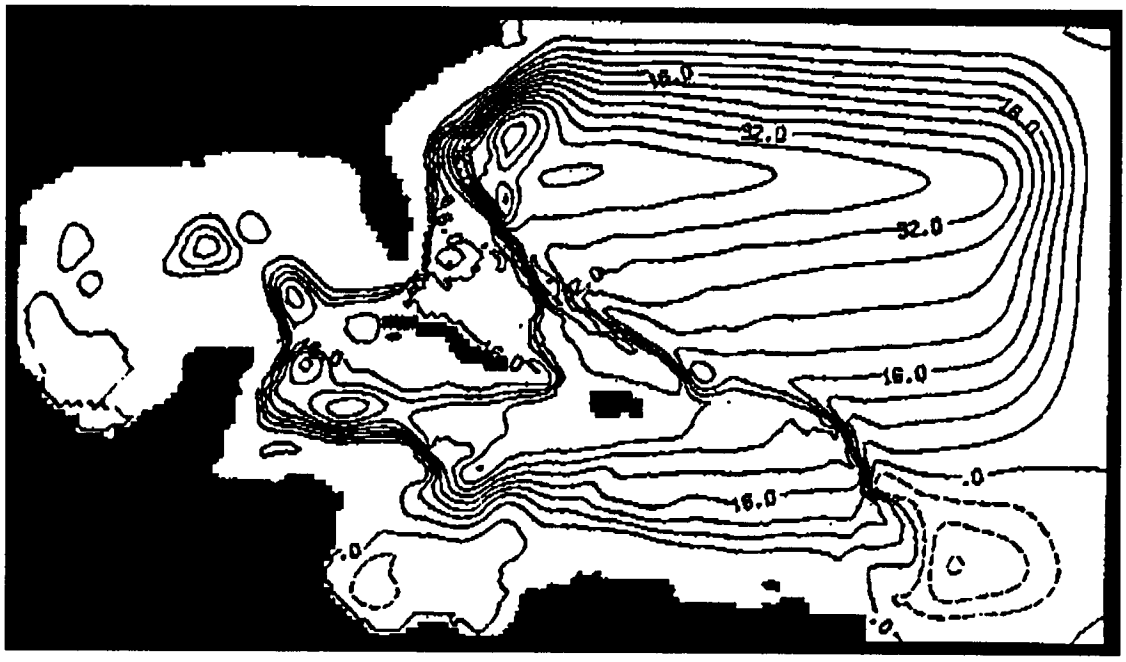

300 weeks

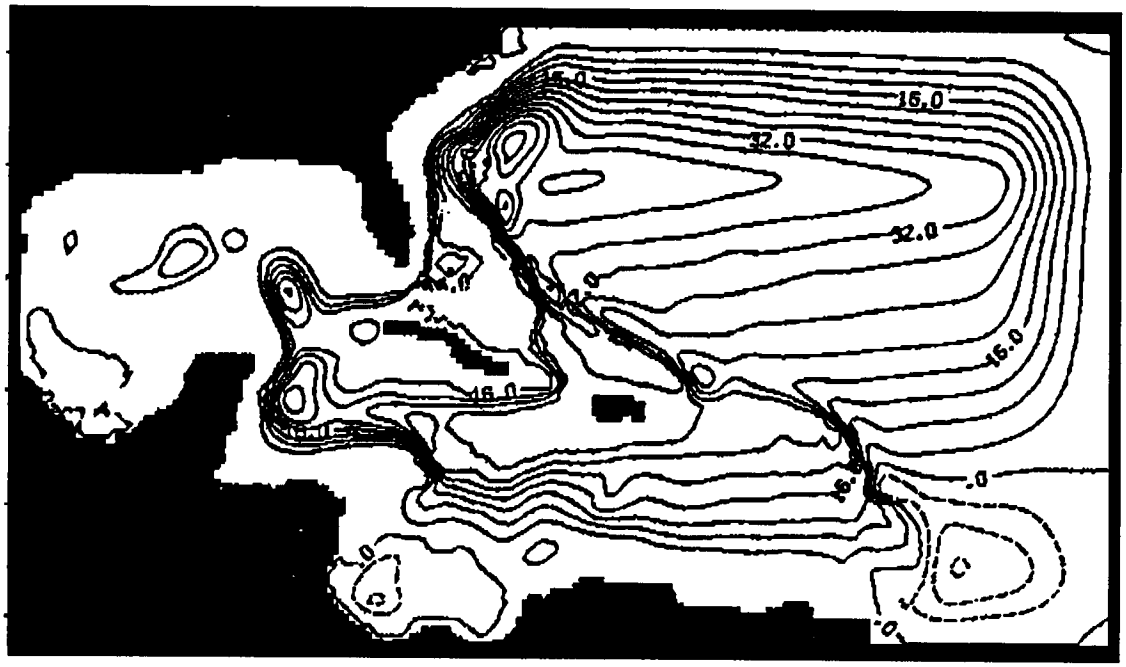

304 weeks

APPENDIX B

CURRENT-METER DATA

In several places in this report we have presented plots of some of the current meter data from the recent MMS programs in the Gulf of Mexico. These valuable data sets have been described in detail elsewhere (SAIC 1986, 1987, Hamilton 1990). We present here several plots (adapted from Hamilton, 1990) to have available a more comprehensive view than could be obtained from the limited subset in the body of the report. The mooring locations are shown in Figure 14. The current-meter velocities have been rotated so that upward is along the local isobaths.

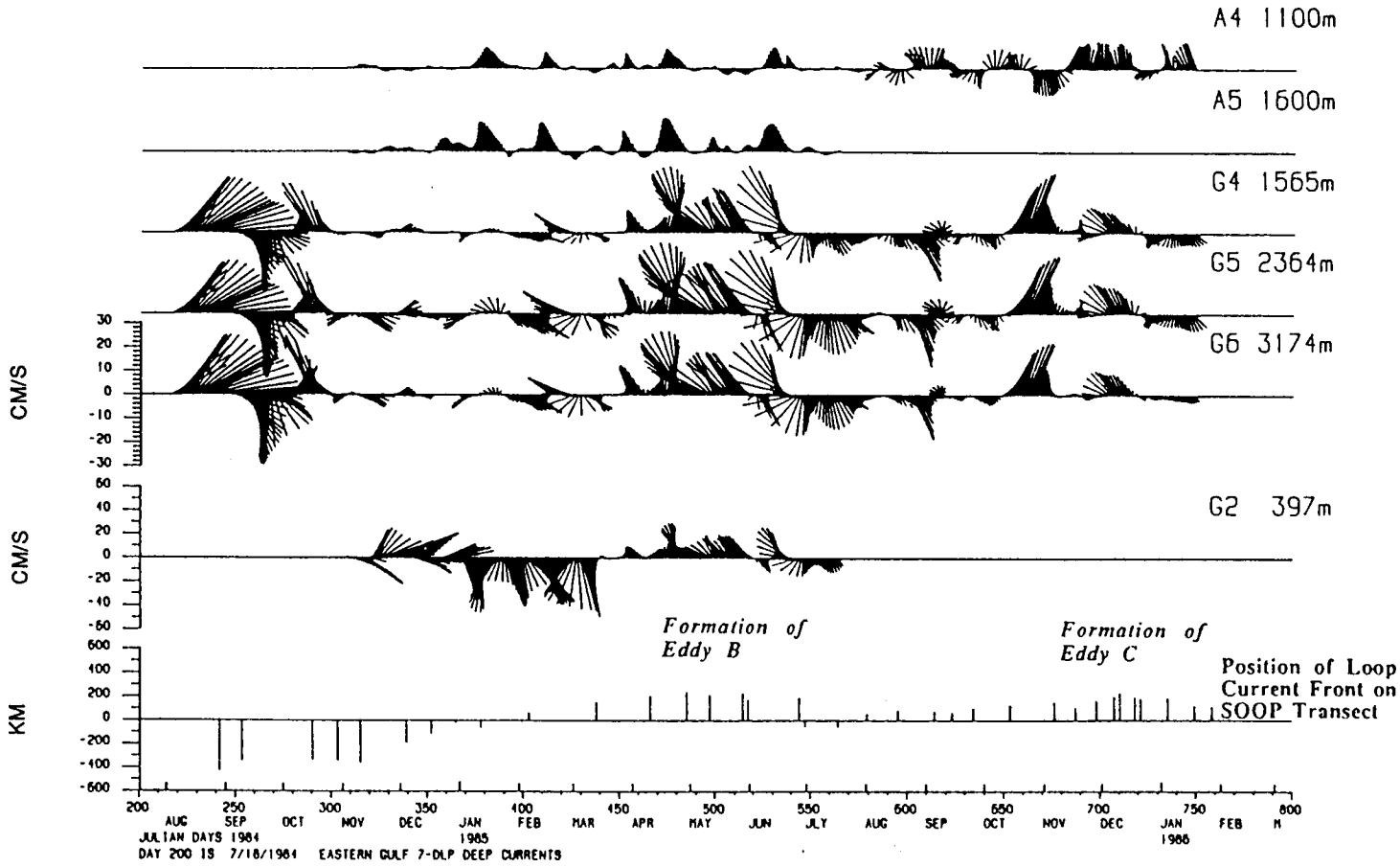

Figure B.1. Data from current meter moorings A and G in the eastern Gulf. The bottom trace shows positions of the Loop Current as inferred from XBT sections along the ship-of-opportunity track shown in Fig. 14.

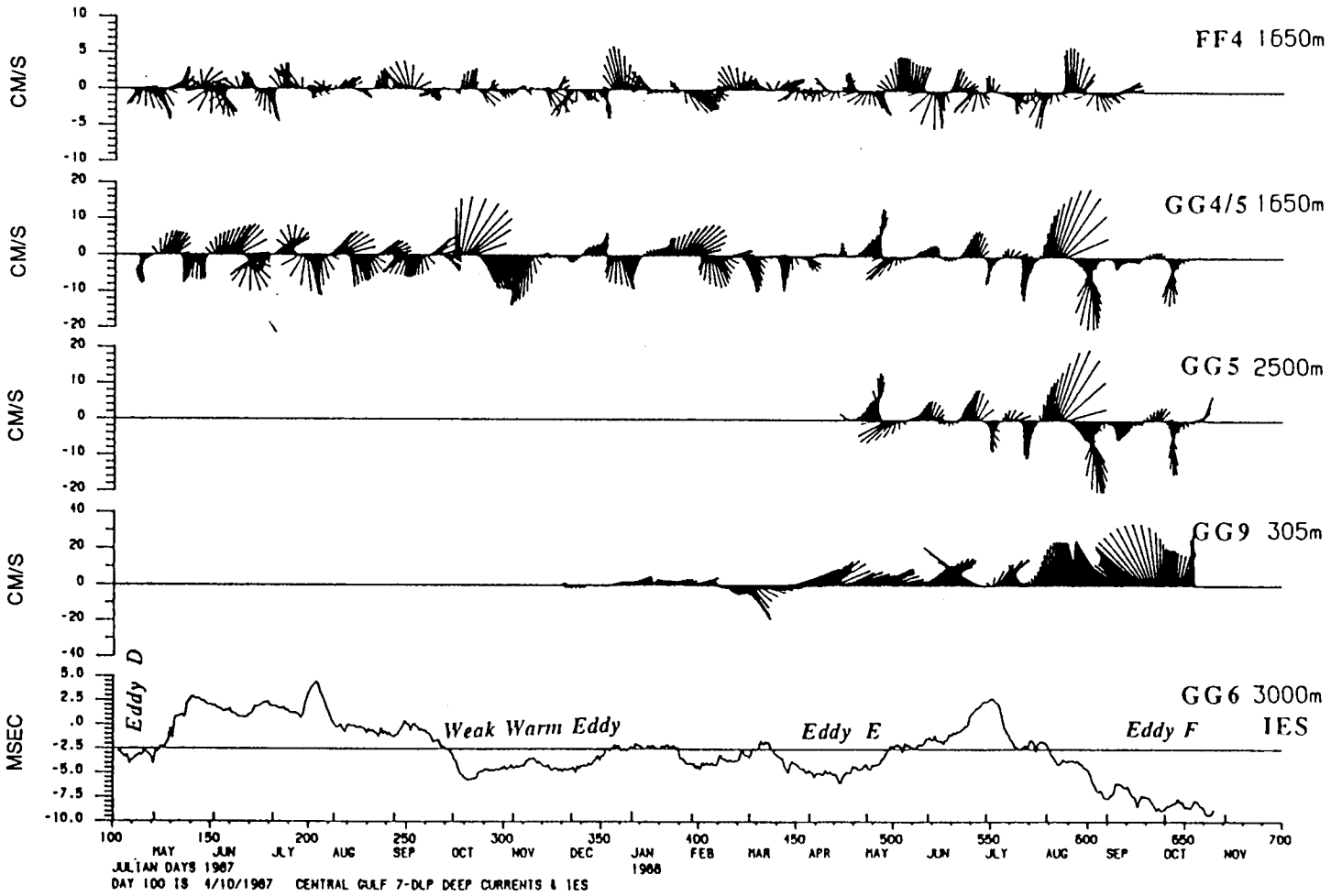

Figure B.2. Data from moorings FF and GG in the central Gulf. The bottom trace shows travel time at an inverted echo sounder (IES) at the bottom of GG.

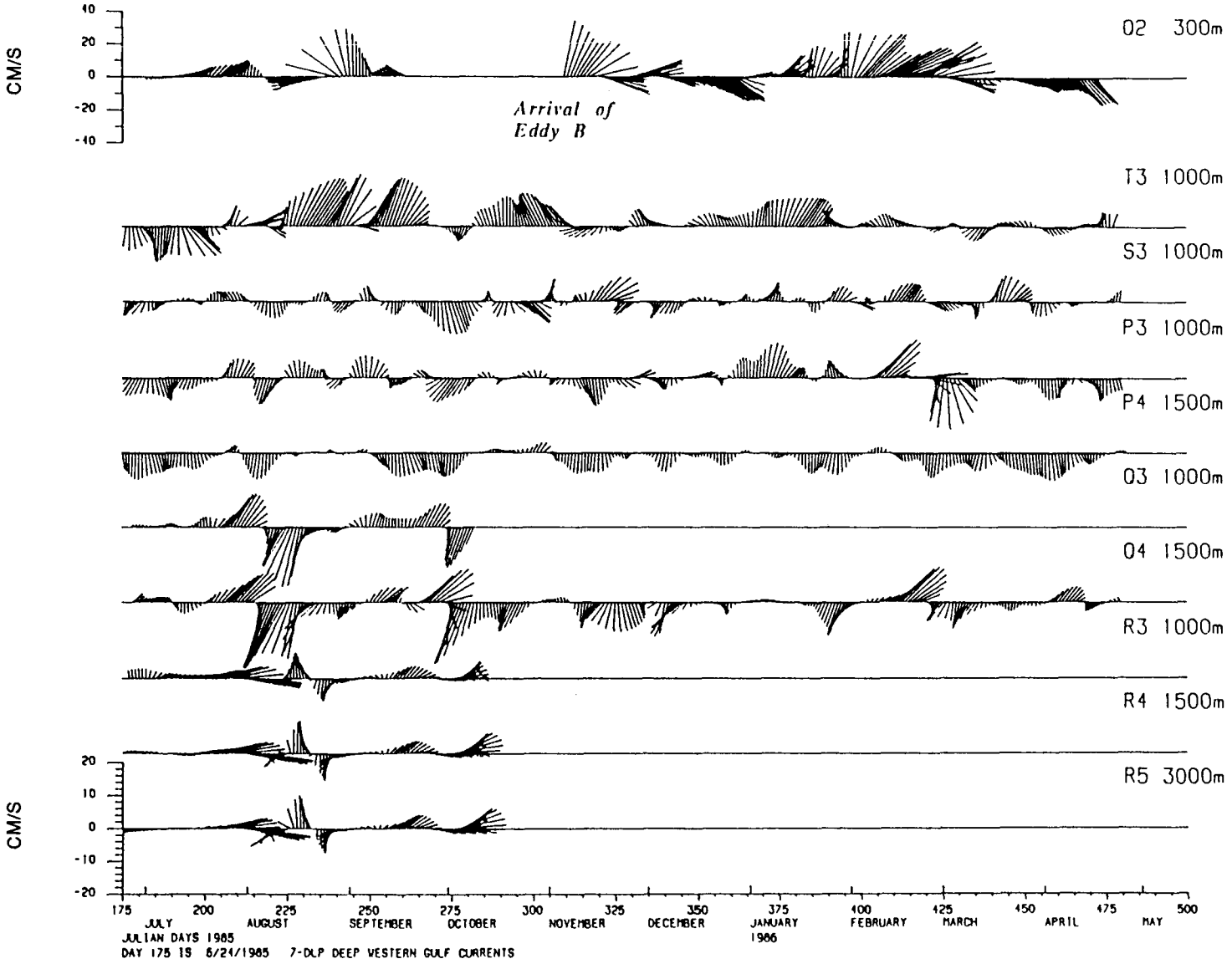

Figure B.3. Data from moorings P, Q, R, S, and T in the western Gulf.

APPENDIX C

VERTICAL CROSS SECTION OF VELOCITY IN YUCATAN

We wish to emphasize that although the flow in the upper levels of the model appears to have come to equilibrium, the deeper levels may not yet have reached equilibrium during these model runs. For completeness, however, Figure C.1 shows a representative velocity cross section in Yucatan Channel. We see the typical region of highest velocities concentrated against the western side. The highest speeds to the south are ~10 cm/sec decreasing to ~2 cm/sec near the bottom. Weak flow to the south occupies the eastern half of the cross section. For comparison, see Figures 7 and 9.

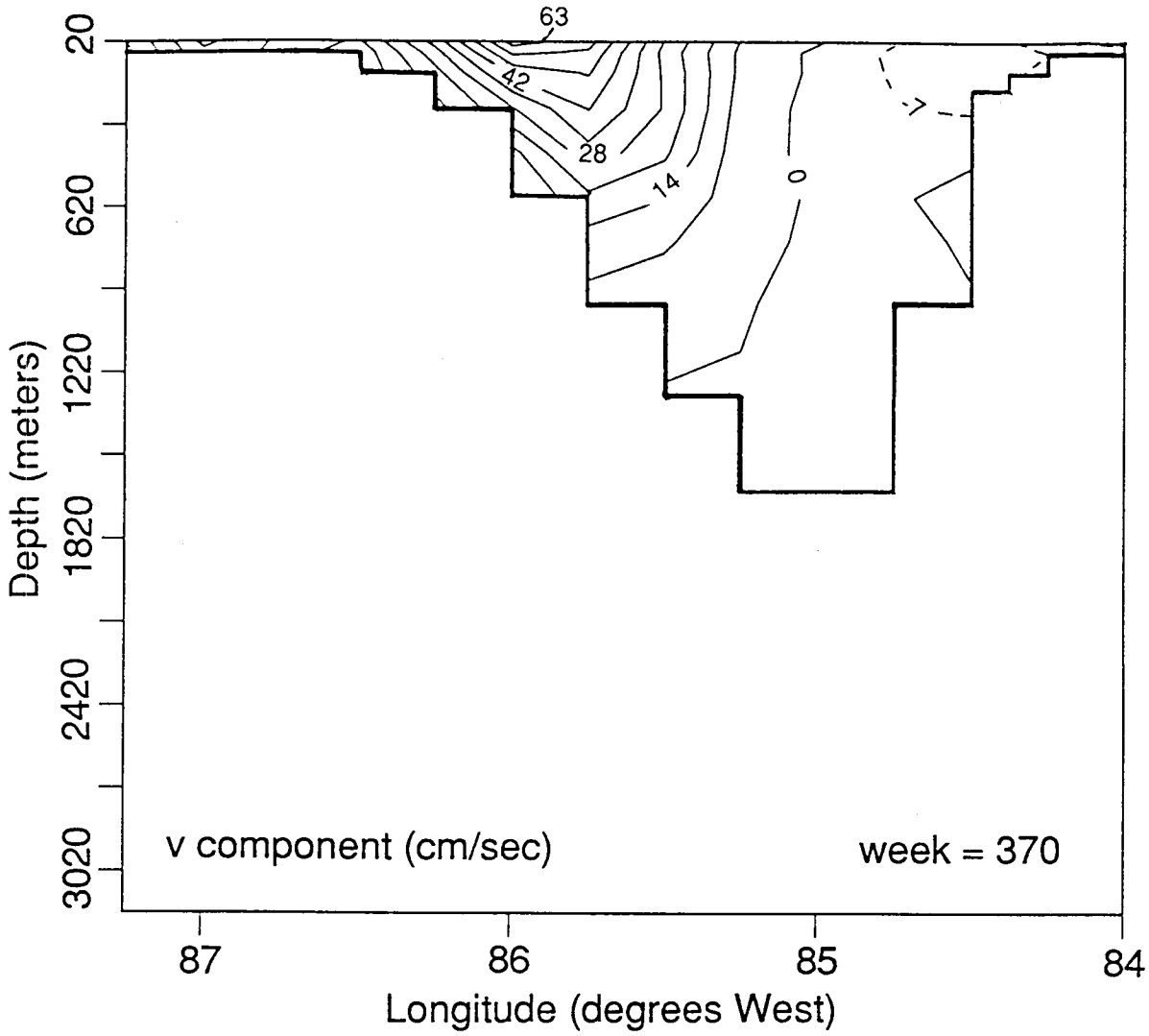

Figure C.1. A vertical cross section of the N-S velocity component in Yucatan Channel at week 370. Southward velocity is contoured with dashes. The contour interval is 7 cm/sec. The flow is to the south in most of the eastern side of the section. The speed near the bottom is ~2 cm/sec in the model (see, e.g., Figure 9).

As the Nation's principal conservation agency, the Department of the Interior has responsibility for most of our nationally owned public lands and natural resources. The includes fostering the wisest use of our land and water resources, protecting our fish and wildlife, preserving the environmental and cultural values of our national parks and historical places, and providing for the enjoyment of life through outdoor recreation. The Department assesses our energy and mineral resources and works to assure that their development is in the best interest of all our people. The Department also has a major responsibility for American Indian reservation communities and for people who live in Island Territories under U.S. Administration.